A comparison of the wound healing dynamics in an acute and newly developed chronic wound model using Neutral endopeptidase, an inhibitor of Substance P.

By

Kiara Boodhoo

Thesis presented in the fulfilment of the requirements for the degree of Master of Science (Physiological Sciences) in the Faculty of Science at Stellenbosch University

Supervisor: Dr Mari van de Vyver

Co-supervisor: Prof Kathy Myburgh

March 2020

Declaration

By submitting this thesis electronically, I declare that the entirety of the work contained therein is my own, original work, that I am the sole author thereof (save to the extent explicitly otherwise stated), that reproduction and publication thereof by Stellenbosch University will not infringe any third party rights and that I have not previously in its entirety or in part submitted it for obtaining any qualification.

Abstract

Chronic wounds affect millions of people with diabetes world-wide. Various diabetic wound healing animal models exist, none of which currently replicate chronic wounds in diabetic patients. Animal models that do not closely resemble human conditions delay application of promising therapeutic strategies in clinical settings. Substance P is a neuropeptide that promotes wound healing by binding to neurokinin-1 receptor initiating the inflammatory process. Neutral endopeptidase (NEP) is a zinc metalloprotease that degrades substance P, thereby hindering the healing process. Increased NEP enzymatic activity is evident in chronic wounds of diabetic patients unlike in current animal models. This study aimed to determine the optimum dose of NEP for injection into wound edges in obese pre-diabetic mice (B6.Cg- Lepob/J, ob/ob) in order to create a chronic non-healing wound. Thereafter, the study investigated wound healing dynamics of this chronic non-healing wound compared to an acute wound treated with saline. In addition to a saline control, three concentrations of NEP [low NEP (0.33 mg/µL), medium NEP (0.68 mg/µL) or high NEP (1.02 mg/µL)] were used to obtain a dose-response curve. NEP activities did not differ between treatment groups however, substance P was lower in the wound areas for high NEP compared to low NEP groups. Therefore, less substance P was present to initiate wound healing with high NEP. MMP-9 was higher with high NEP treatment on day 2 compared to saline, low and medium NEP groups. Similarly, the cytokine profile within pooled samples of day 2 wound fluid was lowest with high NEP treatment. Therefore, high NEP application did mimic some characteristics of a chronic wound during the early stages post wounding, including delayed onset of inflammation. When comparing the healing dynamics of this chronic non-healing wound, induced by high NEP, to an acute wound [wild-type (C57BL/6J) saline-treated mice] that follows the normal progression of healing, the chronic wound displayed delayed wound closure (day 7), significantly greater MMP-9 expression (day 0, 2 and 7) with no formation of granulation tissue, re-epithelization and angiogenesis (day 7). Proteomic analysis of the acute saline-treated and chronic high NEP wounds at day 2 indicated significant differences in expression of proteins such as Stefin-1, Stefin-3, Microtubule-associated protein 1B, Band 4.1-like protein 2, Caveolae-associated protein 1 and Gamma-synuclein. These proteins have not been previously described as involved in wound healing and may be directly involved or have downstream interactions in the wound healing processes. This study identified two proteins previously described as playing a role in wound healing, via their involvement in inflammation (Alpha-1- acid glycoprotein 1) and proliferation and remodelling (Nidogen-1). In conclusion, high NEP administration in the wound boarders of obese pre-

diabetic mice resulted in a chronic wound model that better mimics human diabetic chronic wounds, which could be used to test various treatment strategies. High NEP administration resulted in less wound closure that could be explained by higher MMP-9, lower cytokine content in wound fluid and differences in several proteins identified by proteomic analysis.

Opsomming

Chroniese wonde kom wêreldwyd onder miljoene mense met diabetes voor. Verskeie diermodelle vir diabetiese wondgenesing bestaan, maar geen repliseer tans chroniese wonde onder diabetiese pasiënte nie. Diermodelle wat nie voldoende met mensetoestande ooreenstem nie, belemmer die toepassing van belowende terapeutiese strategieë in kliniese omgewings. Substansie P is 'n neuropeptied wat wondgenesing bevorder deur aan die neurokinien 1-reseptor te bind, wat die inflammatoriese proses in werking stel. Neutrale endopeptidase (NEP) is 'n sinkmetalloprotease wat substansie P degradeer, waardeur die genesingsproses belemmer word. Verhoogde NEP ensimatiese aktiwiteit is sigbaar in chroniese wonde van diabetiese pasiënte, wat nie die geval in huidige diermodelle is nie. Die doel van hierdie studie was om die optimale dosis van NEP vir inspuiting in wondrande van vetsugtige prediabetiese muise (B6.Cg- Lepob/J, ob/ob) te bepaal ten einde 'n chroniese niegenesende wond te skep. Daarna is die wondgenesingsdinamika van hierdie chroniese niegenesende wond met 'n akute wond wat met 'n soutoplossing behandel is, vergelyk. Benewens soutoplossingkontrole is drie konsentrasies van NEP (lae NEP [0.33 mg/µL], middelslag-NEP [0.68 mg/µL] of hoë NEP [1.02 mg/µL]) gebruik om 'n dosisrepsonskromme te verkry. NEP-aktiwiteite het nie onder die behandelingsgroepe verskil nie, maar substansie P was wel laer in die wondareas vir die hoë NEP- vergeleke met die lae NEP-groepe. 'n Kleiner hoeveelheid van substansie P was dus teenwoordig om wondgenesing met hoë NEP in werking te stel. Daar is spesifiek gevind dat MMP-9 hoër was in die hoë NEP- behandelde groep op dag 2, vergeleke met soutoplossing-, lae en middelslag-NEP-groepe. Eweneens was die sitokienprofiel in gemengde monsters van dag 2 se wondvloeistof die laagste met hoë NEP-behandeling. Hoë NEP-toepassing het dus wel enkele eienskappe van 'n chroniese wond in die vroeë fases ná verwonding nageboots, insluitende vertraagde aanvang van inflammasie. Met vergelyking van die genesende dinamika van hierdie chroniese wond, deur hoë NEP geïnduseer, met 'n akute wond (wilde tipe [C57BL/6J] soutoplossingbehandelde muise) het die chroniese wond vertraagde wondgenesing (dag 7) en aanmerklik groter MMP-9-uitdrukking (dag 0, 2 en 7) getoon, met geen vorming van granulasieweefsel, herepitelisasie en angiogenese in die wondarea van die chroniese wond nie (dag 7). Proteomiese analise van die akute soutoplossing- en chroniese hoë NEP-wonde op dag 2 het aanmerklike verskille in uitdrukking van proteïene (Stefin-1, Stefin-3, mikrotubulus-geassosieerde proteïen 1B, band 4.1-agtige proteïen 2, kaveola-geassosieerde proteïen 1 en gamma-sinukleïen) getoon, wat nog nie voorheen met betrekking tot wondgenesing beskryf is nie. Hierdie proteïene is dalk nie direk betrokke nie,

maar het moontlike stroomaf-interaksies in die wondgenesingsproses. Hierdie studie het slegs twee proteïene geïdentifiseer wat volgens die literatuur ’n rol in wondgenesing speel deur hul betrokkenheid by inflammasie (alfa-1-suur glikoproteïen 1) en proliferasie en hermodellering (Nidogen-1). Die gevolgtrekking is dat hoë NEP-toediening in die wondrande van vetsugtige prediabetiese muise ’n wond geskep het wat ’n chroniese wond beter naboots as laer NEP-konsentrasies of soutoplossingtoediening. Hoë NEP-toediening het tot minder wondgenesing gelei, wat die gevolg mag wees van hoër MMP-9, laer sitokien-inhoud in wondvog en verskille in verskeie proteïene wat deur proteomiese analise geïdentifiseer is.

Acknowledgements

This research project was supported by self-initiated research grants awarded by:

Harry Crossley Foundation

National Research Foundation

I was supported by a postgraduate bursary from the **National Research Foundation**.

I am sincerely thankful to the following people without whom this would not have been possible.

Dr Mari van de Vyver (My supervisor): Thank you for being an amazing mentor and providing me with the opportunity to learn and acquire vital research and writing skills. Thank you for the continuous guidance, support and advice throughout my master's research. I have become a better researcher because of it.

Prof. Kathy Myburgh (My co-supervisor): Thank you for your invaluable input and constructive suggestions. You have provided me with the knowledge and advice on how to improve my research and reporting skills.

Dr Maré Vlok: Thank you for your support, guidance and the hot chocolate without which would have made it difficult to overcome the many hurdles faced though protein extractions.

Dr Dalene de Swardt: Thank you for your support and assistance in wound fluid collection. Your friendship and advice throughout have been greatly valued and appreciated.

Prof. William Ferris (Head of Division): For the continuous laughs throughout the office and your uncanny ability to greatly ease anxiety within a room.

Stephen Houghs Lab colleagues: Thank you for the advice, continuous encouragement and helping me through all the ups and downs. Your friendship has made this an unforgettable experience with the many jokes, laughs and funny stories shared.

The FMHS animal research facility: To Mr Noel Markgraaff and Dr Sven Parsons for their continuous assistance and training.

Finally, a special thank you to **Mr Crisenrai R. Boodhoo**, **Mrs Ansuya Boodhoo**, **Mr. Yavan C. Boodhoo** and **Miss Avana Boodhoo** for always believing in me, for always supporting me through the tough times and celebrating with me through all the wins. You have made this experience that much better. Without you this all would not have been possible.

Table of Contents

List of Tables

List of Figures

Abbreviations

°C:	Degrees Celsius
µg:	micro gram
µL:	micro litre
µm:	micrometers
ACN:	Acetonitrile
CCL17/TARC:	Thymus and activation-regulated chemokine
CCL22/MDC:	Macrophage-derived chemokine
CCL24:	Eotaxin-2
CHAPS:	3-[(3-cholamidopropyl) dimethylammonio]-1-propanesulfonate
cm:	centimetre
COX-2:	cyclooxygenase-2;
ECM:	Extracellular matrix
EGF:	Epidermal growth factor
ELISA:	Enzyme-linked immunosorbent assay
ESC:	Epidermal stem cells
EtOH:	Ethanol
FA:	Formaic acid
FGF:	Fibroblast growth factor
g:	grams
GCSF:	Granulocyte colony-stimulating factor
GMCSF:	Granulocyte macrophage colony-stimulating factor
H&E:	Haematoxylin & Eosin
h:	hour
HMEC-1:	Human microvascular endothelial cell.
IFN- γ:	Interferon gamma
IFN-γ:	Interferon gamma

IHC:	Immunohistochemistry
IL:	Interleukin
KC:	Keratinocyte chemoattractant
kV:	Kilo volts
LC MS:	Liquid chromatography–mass spectrometry
m/z:	Mass to charge number of ions ratio
MAPK:	mitogen-activated protein kinase
MCP-1:	Monocyte chemo-attractant protein-1
mg:	milligrams
min:	minutes
MIP:	Macrophage inflammatory protein
MIP-1β:	Macrophages inflammatory protein – 1 Beta
mL:	millilitre
mm:	millimetre
MOPS:	3-(N-morpholino) propanesulfonic acid
MTBE:	Methyl tert-butylether
NADPH:	Reduced nicotinamide adenine dinucleotide phosphate
NEP:	Neutral endopeptidase
NF-κB:	nuclear factor kappa-light-chain-enhancer of activated B cells
NGF:	nerve growth factor
NKR-1:	Neurokinin-1 receptor
nL:	nanolitre
nm:	nanometre
OD:	optical density
PDGF:	Platelet derived growth factor
PEG:	Polyethylene glycol
pmol:	picomole

PMSF:	Phenylmethylsulfonyl fluoride
ppm:	Parts per million
qRT-PCR:	quantitative real-time reverse-transcriptase polymerase chain reaction
RANTES:	Regulated on Activation, Normal T Cell Expressed and Secreted
RFU:	relative fluorescent units
ROI:	Region of interest
ROS:	Reactive oxygen species
SAP:	Self-assembled peptides
sec:	seconds
SKP:	Skin derived precursors
SP:	Substance P necrosis factor-α
SP1:	Specificity protein 1
STAT6:	Signal transducer and activator of transcription 6
STZ:	Streptozotocin
T2DM:	Type 2 Diabetes Mellitus
TCEP:	Tris(2-carboxyethyl) phosphine
TEAB:	Mriethylammonium bicarbonate
TFA:	Trifluoroacetic acid
TGF- β:	Transforming growth factor beta
TIMP:	Tissue inhibitor of metallo-protease
TMT:	Tandem mass tag
TNF-α:	Tumour necrosis factor alpha
VEGF:	Vascular endothelial growth factor
WT:	wild type
α-SMA:	Alpha smooth muscle actin

Chapter 1 : Introduction

Wound healing plays a vital role in maintaining the integrity of tissue following injury or during disease (Shaw and Martin, 2009). It consists of four major phases namely haemostasis (phase 1), inflammation (phase 2), proliferation (phase 3) and remodelling (phase 4) (Eming et al., 2007) *(refer to chapter 2, section 2.1)*. These stages do not always occur distinctively but involves the coordination and activation of various cell types and signalling pathways to maintain the integrity of the tissue (Gurtner et al., 2008). This ensures the rapid repair of the wound whilst utilizing the least amount of energy. The wound healing process is however hindered in diseases such as Type 2 Diabetes Mellitus (T2DM) due to its deviant pathology. The pathogenesis of uncontrolled T2DM involves persistent hyperglycaemia (elevated blood glucose levels) resulting in the accumulation of advanced glycation end-products (AGEs) (glycosylated proteins and lipids) (Singh et al., 2014, Vlassara and Uribarri, 2014). Consequently, oxidative stress is increased and a chronic low grade self-perpetuating pro-inflammatory state develops (Goh and Cooper, 2008, Zhong et al., 2017, Lasselin and Capuron, 2014, Pradhan et al., 2009). Together, this toxic microenvironment leads to tissue damage and cellular dysfunction and is the underlying cause for co-morbidities such as retinopathy and non-healing wounds (also known as diabetic foot ulcers) (Zhao et al., 2016).

Given the complex nature of non-healing diabetic wounds, there are currently no effective treatment strategies, making it a global economic burden. In 2017, approximately 8.8% of the world's population was affected by diabetes and this percentage is projected to increase to 9.9% by the year 2045 (Cho et al., 2018). The prevalence of diabetic foot ulcers in diabetic patients is approximately 6.6% (Zhang et al., 2016). A different study found that due to the lack of effective treatment options the recurrence rate of diabetic wounds is 22.1% (Fu et al., 2019). This problem is further exacerbated and perpetuated by the lack of appropriate animal models to test novel therapeutic strategies. There is thus the need for an animal model that replicates the microenvironment within diabetic wounds as observed in the clinical setting. A better understanding of the complex nature of these wounds will furthermore aid in the development of more effective treatments.

In diabetic patients, pathogenesis-induced neuropathy is one of the leading causes for the development of non-healing wounds (Pradhan et al., 2009). It is characterized by the insufficient production of neuropeptides such as substance P and the over production of Neutral endopeptidase (NEP), an enzyme that degrades substance P (Olerud et al., 1999, Antezana et al., 2002). Substance P is secreted by sensory nerves and inflammatory cells (macrophages and eosinophils) (O'Connor et al., 2004). It functions via it's receptor,

neurokinin-1 receptor (NKR-1), and has been shown to promote the wound healing process in both diabetic and non-diabetic skin wounds by initiating the second phase of healing, namely inflammation (Leal et al., 2015). Overproduction of the cell surface enzyme NEP, that degrades substance P, therefore hinders the onset of the healing process (Olerud et al., 1999).

In a patient-based study, Antezana et al. (2002) observed an increase in NEP enzymatic activity in the ulcer margins (wound edges) of diabetic patients (~ 14 fold) compared to non-diabetic controls, suggesting its role in chronic diabetic wounds. The relevance of this study has been confirmed by various research groups over the following decade. *In vitro* models that mimic this effect have been developed by exposing normal endothelial cells to high glucose (Wang et al., 2009). Raised NEP levels are not characteristic of wounds in current diabetic animal models; this suggests that the animal models do not accurately reflect the *in vivo* human scenario, which could in turn negatively impact appropriate drug development. The main purpose of this research project was thus to utilize NEP enzyme activity to develop a mouse chronic wound model that more closely mimics diabetic foot ulcers in patients and to compare the protein profile of acute versus chronic wounds during the early stages of healing.

Chapter 2 : Literature Review

2.1 Overview of the wound healing process

Cutaneous wound healing is an essential process for maintaining tissue homeostasis and preserving its physiological function. It is a very complex and coordinated process that involves the activation and inactivation of the immune system, various intra- and extra-cellular components, signalling pathways and paracrine factors (Gurtner et al., 2008). Healing occurs in four very specific phases *(sections 2.1.1-2.1.4)* and dysregulation thereof can cause wounds to become chronic with debilitating consequences for patients.

2.1.1 Phase 1: Haemostasis

Haemostasis is the first stage to occur immediately after injury. It is characterized by 3 components i.e. vasoconstriction, platelet plug formation and coagulation. The vasoconstriction stage involves the contraction of smooth muscles in the blood vessel walls to prevent excessive blood loss (Young and McNaught, 2011). This stage is followed by platelet plug formation which is mediated by the interaction of platelets, the vessel walls and adhesion proteins (such as integrins, glycoproteins and cadherins) (Xu et al., 2016). Platelets recognise the exposed fibrous matrix and the vascular endothelial cell lining in the injured area. As a result, they become activated to trigger the secretion of clotting factors such as thrombin and fibrin (Sira and Eyre, 2016). The downstream blood clotting cascade plays a crucial role in platelet plug formation (Periayah et al., 2017). The fibrin matrix within the platelet plug serves as a scaffold for infiltrating immune cells during the second phase of healing (Zilberman, 2011). In a review Young and McNaught (2011) discussed the role that platelets play in stimulating angiogenesis via the secretion of platelet derived growth factor (PDGF), transforming growth factor β (TGF-β) and fibroblast growth factor (FGF) in the subsequent proliferative stage of healing (phase 3).

2.1.2 Phase 2: Inflammatory immune response

Inflammation occurs in the first 72 hours (3-days) post injury and involves the infiltration of a variety of immune cells (neutrophils, monocytes/macrophages and lymphocytes) into the wounded area. Phagocytic neutrophils start infiltration immediately post injury and remain within the wounded area for the first 48 hours. They function to phagocytose and de-granulate tissue debris and bacteria through the secretion of reactive oxygen species (ROS)

and antimicrobial proteases (neutrophil elastase, cathepsin G and proteinase-3) whilst proteolytic enzymes [matrix metalloprotease (MMP)-2 and MMP-9] degrade non-viable collagen tissue (Zhao et al., 2016, Larouche et al., 2018, Stapels et al., 2015). Neutrophils subsequently undergo apoptosis or are removed from the injured area through macrophage-mediated phagocytosis (Young and McNaught, 2011).

Coinciding with neutrophil infiltration, monocytes and tissue resident macrophages with a pro-inflammatory phenotype (M1) fill the wounded area between 24-72 hours (day 1-3) post injury (see the wound area of Figure 2.1). The infiltrating monocytes differentiate into M1 macrophages and together with tissue-resident monocytes that mature into macrophages, both contribute to phagocytosis, presentation of antigens (to trigger a T- lymphocyte immune response) and secrete a variety of chemokines and cytokines (see the dermal layer of Figure 2.1) (Fujiwara and Kobayashi, 2005). The release of tumour necrosis factor-α (TNF-α), interleukin (IL)-1, IL-6, IL-8 and IL-12 by M1 macrophages improves vascular permeability and together with chemokines [thymus and activation-regulated chemokine (CCL17/TARC), macrophage-derived chemokine (CCL22/MDC) and CCL24/Eotaxin-2], increase the influx of inflammatory cells into the wounded area (Owen and Mohamadzadeh, 2013).

Once the wound is clear of debris and bacteria the macrophage population shifts its phenotype to have a predominantly anti-inflammatory (M2) function. This phenotype switch is a crucial step in wound healing, since it facilitates the transition from the destructive pro-inflammatory phase (phase 2) to the growth promoting proliferative phase (phase 3) of healing. The M2 macrophages secrete anti-inflammatory cytokines (IL-10, IL-13 and IL-8) and chemokines [monocyte chemo-attractant protein-1 (MCP-1), macrophages inflammatory protein – 1 beta (MIP-1β/ CCL4) and Regulated on Activation, Normal T Cell Expressed and Secreted (RANTES)] to inhibit the inflammatory response and growth promoting factors [vascular endothelial growth factor (VEGF), TGF-β, epidermal growth factor (EGF), FGF and PDGF] to initiate regeneration by augmenting granulation tissue formation and stimulating angiogenesis (Young and McNaught, 2011, Atri et al., 2018).

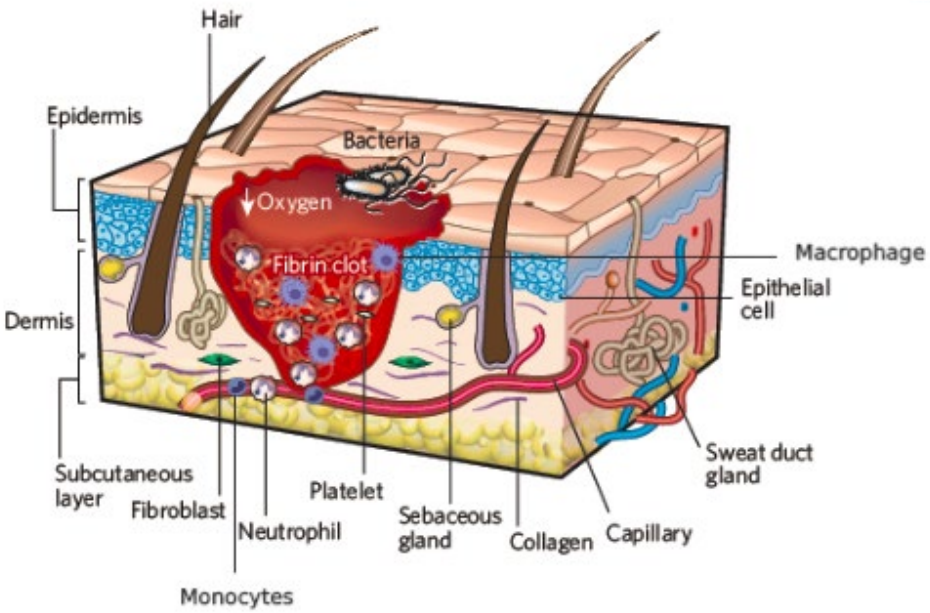

Figure 2.1. Haemostasis and inflammatory phases of wound healing. Haemostasis and inflammation are the first two phases of healing to occur and last for the first 72 hours post injury. In the haemostasis stage (phase 1) a platelet plug forms, vasocontraction and coagulation occurs to prevent blood loss. The inflammation stage (phase 2) is facilitated by the infiltration of various immune cells and functions to phagocytose cellular debris and foreign particles within the wound. Image adapted from Gurtner et al. (2008).

2.1.3 Phase 3: Proliferation

Proliferation, alternatively referred to as the proliferative phase of healing, occurs between 2 and 10 days post injury and is characterized by several concurrent processes namely, angiogenesis, collagen deposition, granulation tissue formation and re-epithelisation (wound closure, refer to Fig. 2.2) (Li et al., 2007). This phase therefore involves the action of numerous cell types (keratinocytes, epithelial cells, fibroblasts, endothelial cells, stem/progenitor cells) and is mediated by the increased secretion of growth promoting factors such as VEGF, TGF-β and EGF.

Upon stimulation by macrophage-derived growth factors and cytokines such as IL-1, TGF-β, EDGF and PDGF, tissue resident fibroblasts proliferate and migrate to the wound edges before differentiating into myofibroblasts (Kalluri and Zeisberg, 2006). Myofibroblasts express α-smooth muscle actin (α-SMA) that gives them the ability to physically contract and by doing so assist in decreasing the wound size. Following contraction, the wound area undergoes re-epithelialization for complete wound closure to occur (Bhowmick et al., 2004). Activated fibroblasts also secrete collagen, fibronectin and other matrix proteins that result in the formation of granulation tissue which replaces the fibrin matrix of the platelet plug

(Gurtner et al., 2008). The interactions between the fibroblasts and myofibroblasts are essential in the secretion of collagen III to form new extracellular matrix (ECM) within the wounded area. At the same time, angiogenesis that is mediated by the action of endothelial progenitor cells restore the capillary network within the granulation tissue. Together, these cell interactions form the basis for keratinocytes to migrate and proliferate to re-establish the epithelium (Gonzalez et al., 2016).

All the cells involved in the proliferative phase of the healing process are located within the granulation tissue at this point. These reparative cellular mediators must then either mature, migrate out of the wounded area or undergo apoptosis to allow for tissue remodelling to occur.

Below is an illustration of the proliferative phase of healing process (Fig. 2.2). Take note the main proliferative cells are epithelial cells that migrate in order to close the wound site.

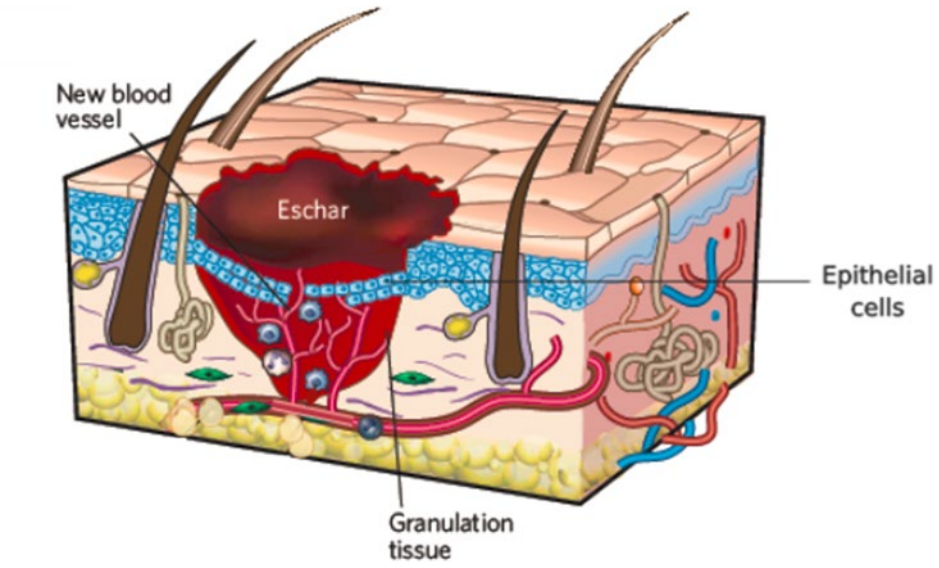

Figure 2.2. Proliferative stage of wound healing. The proliferative stage of wound healing (phase 3) occurs between 2 to 10 days post wounding and involves angiogenesis, collagen deposition, granulation tissue formation and re-epithelisation. Image adapted from Gurtner et al. (2008).

2.1.4 Phase 4: Tissue remodelling

Tissue remodelling occurs after complete wound closure at about 2 weeks post injury and can continue for up to a year (Velnar et al., 2009). During this process, the collagen III within the ECM is degraded by MMPs and is replaced with collagen I that is secreted by fibroblasts (Zhao et al., 2016). This remodelling of the granulation tissue restores the functional capacity of the tissue and/or result in scar formation (Fig. 2.3).

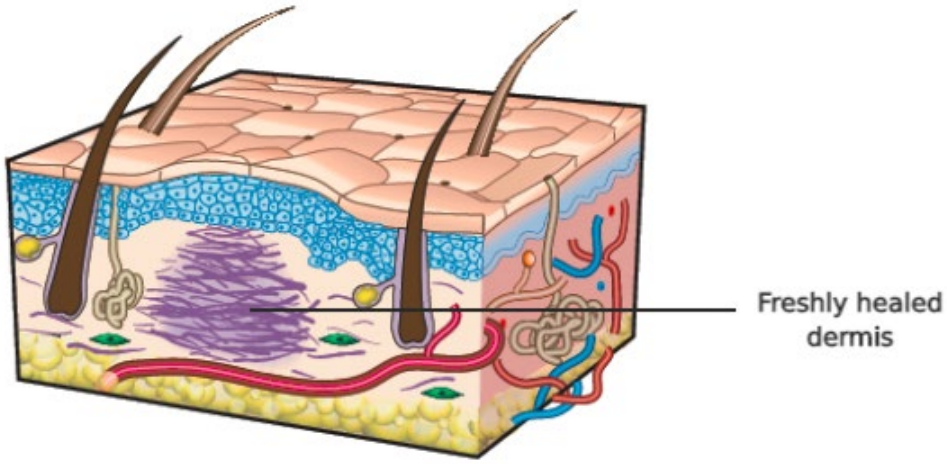

Figure 2.3. Remodelling stage of wound healing. Remodelling (phase 4) occurs between 2 weeks and a year post wounding. During this stage of healing collagen III is replaced with collagen I via MMP degradation to restore the structural and functional integrity of the tissue. Image adapted from Gurtner et al. (2008).

Below is a detailed overview of the paracrine factors and their downstream signalling pathways involved in each of the phases of healing (Table 2.1). Studies have shown that in diabetic patients there is a disruption and dysregulation in the progression of inflammation to proliferation which can cause a wound to become chronic and subsequently inhibit the 4 phases of healing, leading to chronic wounds. However, the study of this disruption in animal models mostly rely on acute wounds.

Table 2.1: Paracrine Factors involved in wound healing

	Secreted by	Phase in wound healing	Function	Signalling pathway
Platelet derived growth factor (PDGF)	Platelets	Haemostasis	• Stimulates proliferation of smooth muscle cells and fibroblasts. • Promotes angiogenesis (Diegelmann and Evans, 2004). • Collagenase production.	• Functions via PDGF receptor (PDGFR) α and β.(Canalis, 2008).
Interleukin 1 (IL-1)	M1 macrophages	Immune response	• Promotes expression of IL-6, IL-8, MCP-1, COX-2 (Weber et al., 2010).	• Functions via IL1 Receptor (IL-1R).
Interleukin 6 (IL-6)	M1 macrophages	Immune response	• Regulation of angiogenesis and deposition of collagen (Lin et al., 2003). • Proliferation of neutrophils, B cells and T cells.	• Functions via IL6 Receptor (IL-6R).
Interleukin 8 (IL-8)	M1 macrophages	Immune response	• Migration and activation of neutrophils (Bickel, 1993).	• Functions via IL-8 Receptor α and IL-8 Receptor β(Ben-Baruch et al., 1995).
Interleukin 12 (IL-12)	M1 macrophages	Immune response	• Inhibition of angiogenesis. • Promotes secretion of IF-γ. • Macrophage chemotaxis. • Up regulation of MMP 9 (Matias et al., 2011).	• Functions via IL-12 Receptor (IL-12R).
Interleukin 4 (IL-4)	Type 2 T-Helper cells, neutrophils, eosinophils, mast cells.	Immune response	• Upregulates collagen I synthesis. • Anti-inflammatory macrophage polarization. • Promotes synthesis of fibrin (Larouche et al., 2018).	• Functions by activating SP1, NF-κB, and STAT6 pathways to promote Collagen I synthesis (Bou-Gharios et al., 2020).
Tumour necrosis factor-α (TNF-α)	Platelets, M1 macrophages	Immune response Proliferation	• Stimulates synthesis of collagen and MMPs.(Mast and Schultz, 1996). • Promotes proliferation of fibroblasts.	• Functions via TNF-R1p55, TNF-R2p75 receptors which in turn activates the (NF)-κB transcription and MAPK pathways (Cho et al., 2007).

	Secreted by	Phase in wound healing	Function	Signalling pathway
Transforming growth factor β (TGF β)	Platelets M2 macrophages T-Lymphocytes	Immune response Proliferation	• Macrophage attractant. • Stimulates macrophages to secrete FGF, PDGF, TNFα and IL-1. • Initiates fibroblasts and keratinocytes. chemotaxis.(Diegelmann and Evans, 2004). • Promotes migration of fibroblasts and keratinocytes. • Wound closure. • Stimulates TIMP. • Establishment of Collagen matrix (Young and McNaught, 2011).	• Function via TβR I and TβR II which in turn activates Smad transcription signalling pathway (Finnson et al., 2013).
Epidermal growth factor (EGF)	Platelets, macrophages and epithelial cells	Proliferation	• Formation of granulation tissue. • Proliferation and migration of epithelial cells, keratinocytes and fibroblasts.	• Functions via Epidermal growth factor receptor (EGFR) (Bodnar, 2013).
Vascular Endothelial growth factor (VEGF)	M2 macrophages, keratinocytes, fibroblasts and endothelial cells	Proliferation	• Mediates angiogenesis. • Promotes proliferation and migration of endothelial cells (Li et al., 2007). • Collagen deposition. • Epithelialization (Bao et al., 2009).	• Function via Flt-1 (VEGFR-1) and KDR (VEGFR-2) receptors found on the blood vessels and surface of endothelial cells (Bao et al., 2009).
Fibroblast growth factor (FGF)	M2 macrophages, endothelial cells	Proliferation	• Stimulates angiogenesis. • Proliferation of fibroblasts. • Deposition of collagen matrix. • Wound contraction.	• Function via Fibroblast growth factor receptors (FGFR) which in turn activates the STAT signalling pathway (Ornitz and Itoh, 2015).

Footnotes: The table indicates the origin, function and some of the potential downstream signalling pathways of the most prominent cytokines involved in wound healing. **Abbr:** PDGF, Platelet derived growth factor; IL, Interleukin; COX-2: cyclooxygenase-2; MCP-1, Monocyte chemoattractant protein-1; SP1, Specificity protein 1; NF-κB, nuclear factor kappa-light-chain-enhancer of activated B cells; TIMP, Tissue inhibitor of metallo-protease; MMP, Matrix metalloprotease; IFN-γ, Interferon gamma; STAT6, Signal transducer and activator of transcription 6; MAPK, mitogen-activated protein kinase; TNF-α, Tumour necrosis factor-α; FGF, Fibroblast growth factor; EGF, Epidermal growth factor; VEGF, Vascular endothelial growth factor.

2.2 Overview of chronic wounds

Chronic wounds are injuries that are unable to heal in a timely manner and often occur due to an underlying pathological condition. Depending on the underlying cause, chronic wounds are subdivided into three main classes i.e. leg ulcers (associated with venous disease), pressure ulcers (associated with prolonged bed rest) and diabetic foot ulcers (associated with uncontrolled hyperglycaemia). Of these, diabetic foot ulcers are the most common, very difficult to treat and often necessitate amputation (Alexiadou and Doupis, 2012, Lepäntalo et al., 2011). It therefore places a socio-economic burden on the patients and enormous financial strain on health care systems worldwide (Frykberg and Banks, 2015).

Acute wounds involve the co-ordinated activation of several different cell types by paracrine factors to progress through all the stages of wound healing (Fig. 2.4 A). In chronic wounds, the onset of the inflammatory phase is initially delayed but once it commences, inflammation is persistent and the wound is unable to progress into the proliferative and remodelling phases of healing (Landén et al., 2016). The continued presence of pro-inflammatory cytokines and destructive immune cells has numerous deleterious effects such as ECM degradation and impaired cellular migration/proliferation (Fig. 2.4 B) (Larouche et al., 2018).

Inflammation is a vital process during wound healing that prepares the injured area for regeneration by preventing infection and removing cellular debris, however prolonged inflammation causes tissue damage. The accumulation of macrophages (M1) and neutrophils causes an increase in secretion of pro-inflammatory cytokines (Table 2.1) and chemokines that recruit even more immune cells. The increase in infiltration of immune cells cause excessive ROS production within the wounded area leading to destruction of cellular membranes, ECM components and can cause the onset of early senescence in cellular mediators of regeneration (Demidova-Rice et al., 2012). Tissue destruction is also caused by an increase in the secretion of serine proteases such as MMPs and neutrophil elastase, whilst tissue inhibiting metalloproteases (TIMPs) are downregulated (McCarty and Percival, 2013). This results in a) the degradation of various growth factors (TGF-β and PDGF) and ECM components, b) reduction of fibroblast proliferation, c) a decrease in cell migratory ability and d) reduced collagen secretion (Zhao et al., 2016). Consequently, the debris from the degradation of ECM components attracts more immune cells that release additional pro-inflammatory cytokines, thus generating a self-perpetuating pro-inflammatory cycle and ultimately a non-healing wound develops.

Persistent inflammation and also bacterial infection are well-known phenomenon in chronic wounds during the late stages of healing (day 7 onwards) (Fig. 2.4 B)(Zhao et al., 2016, Frykberg, 1998). At this time a greater infiltration of neutrophils and monocytes is evident with subsequent increase in the cytokine and growth factor milieu (Larouche et al., 2018). However, little is known about the differences between acute and chronic wounds in the early stages (days 1-2) post injury. Thus, identifying the dysregulation early could greatly inform potential therapeutic strategies.

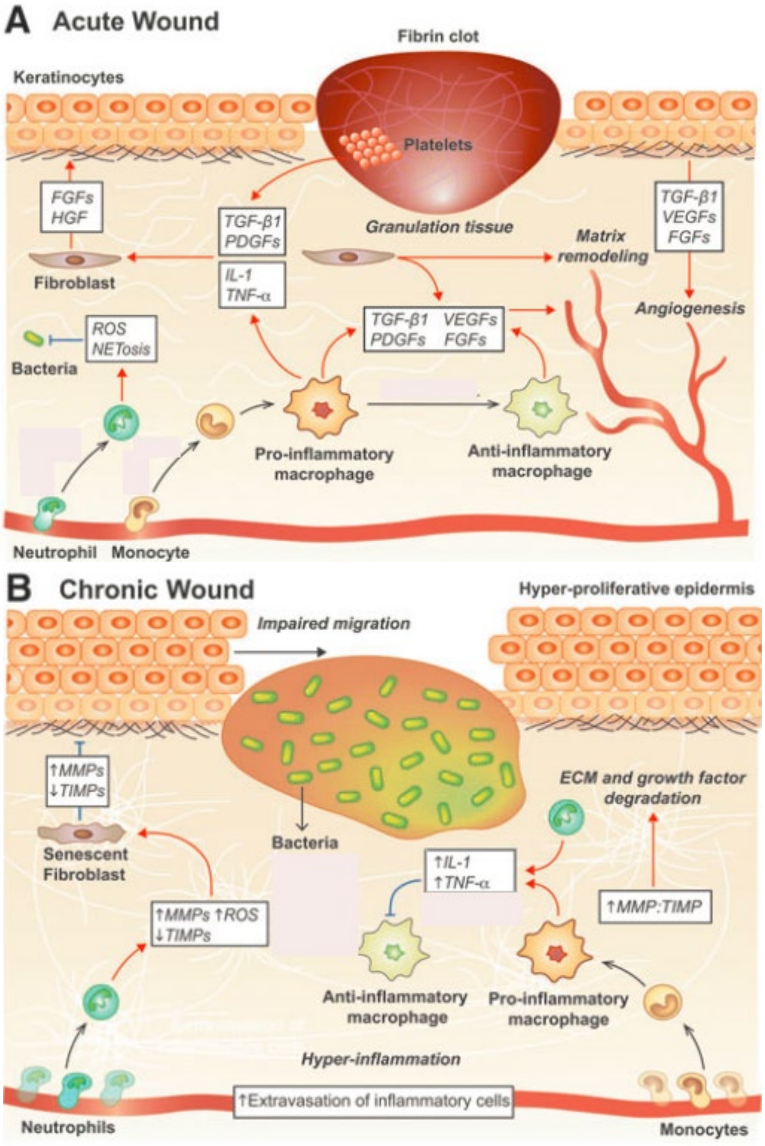

Figure 2.4. Illustration of the various pathways, growth factors and cytokines involved in an acute and chronic wound. A) Acute wounds involve the co-ordination and activation of several different cell types and progresses through all stages of wound healing i.e. haemostasis, inflammation, proliferation and remodelling. Platelets fill the wound area and secrete TGF-β1 and PDGF which promote angiogenesis and activate fibroblasts to proliferate. Neutrophils and monocytes infiltrate. Neutrophil phagocytose debris and bacteria, degrades them via secretion of ROS and anti-microbial proteases. Monocytes differentiate into M1 proinflammatory macrophages and secrete IL-1, TNF-α, TGF-β1, VEGF, PDGF and FGF, which promotes fibroblast activation and angiogenesis. Activated fibroblasts secrete collagen, fibronectin and other matrix proteins that result in the formation of granulation tissue. **B)** Chronic wounds are unable to progress from inflammatory phase of wound healing into the proliferative and remodelling phases resulting in a build-up of pro-inflammatory cytokines, MMPs and ROS which has numerous deleterious effects such as ECM degradation, impaired cell migration and proliferation. Image adapted from Larouche et al. (2018).

2.2.1 Neuropathy as underlying cause for non-healing diabetic wounds

Prior to the development of a diabetic foot ulcer, the pathogenesis of T2DM induces lower limb ischemia and neuropathy (Frykberg, 1998). The dysregulation of glucose metabolism (hyperglycaemia) and subsequent accumulation of AGEs leads to the hyper-glycosylation of tissues for long periods of time, which in turn causes oxidative stress-associated cellular damage (Wieman, 2005).

Normal wound healing requires the production of low levels of ROS by nicotinamide adenine dinucleotide phosphate (NADPH) oxidase enzymes (Jiang et al., 2011). ROS plays a role in both the destruction of invading bacteria through inflammatory cell recruitment and cell signalling via promoting angiogenesis and the proliferation and migration of fibroblasts and keratinocytes (Hoffmann and Griffiths, 2018). In T2DM, hyperglycaemia and increased glycolysis cause a build-up in the mitochondrial electron transport chain. This increases superoxide production and consequently ROS levels become excessive. The oxidative dysregulation results in peroxidation of DNA, lipids and proteins leading to cellular apoptosis or senescence (Han et al., 2013, Cano Sanchez et al., 2018).

The peripheral microvascular and nervous systems are particularly sensitive to this destructive microenvironment. The high levels of oxidative stress contribute to diabetic neuropathy through the build-up of free radicals within the neurons leading to cell death (Vincent et al., 2004). This causes decreased sensation and movement, initially affecting the longer nerve fibres within the lower limbs. With the onset and progression of neuropathy there is a decrease in the production of neuropeptides such as substance P.

Neuropeptides are released by nerves and inflammatory cells in response to environmental stressors (injury) and their main function is immune regulation (Pradhan et al., 2009). Of particular relevance to this study, is the role that substance P plays in initiating the wound healing cascade *(refer to section 2.2.2 below)* and that the dysregulation thereof is associated with the overproduction of NEP (enzyme that degrades substance P). Antezana et al. (2002) conducted a study to assess NEP activity in T2DM patients with neuropathy and chronic wounds. The authors observed higher NEP activity in the ulcer margins of chronic wounds in diabetic patients (47.54±17.18 pmol MNA per h per µg) compared to the skin of healthy controls (3.42±1.84 pmol MNA per h per µg) and suggested that diabetic patients have a reduced neuroinflammatory function that leads to impaired healing.

2.2.2 Role of Substance P and Neutral Endopeptidase in wound healing

Substance P is an 11 amino acid long tachykinin neuropeptide (Arg-Pro-Lys-Pro-Gln-Gln-Phe-Phe-Gly-Leu-Met-NH2) encoded by the TAC1 gene and is secreted by sensory nerve fibres during injury (Fig. 2.5) (Leal et al., 2015). It is responsible for the pain sensation experienced during wounding (Um et al., 2017) and plays a role in initiating the healing cascade (Pradhan et al., 2009). Substance P functions via its G-protein coupled receptor, NKR-1, located on the surface of fibroblasts, keratinocytes, immune, endothelial, epithelial and smooth muscle cells (Mashaghi et al., 2016, Liu et al., 2006).

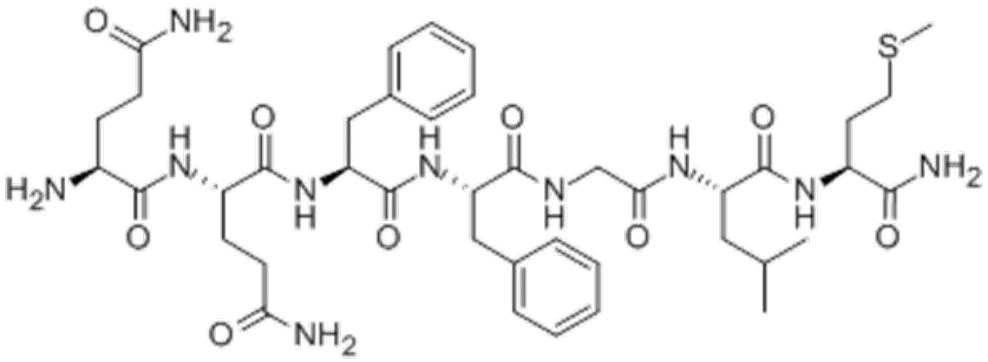

Figure 2.5. Amino acid structure of Substance P. Substance P is an 11 amino acid long hydrophobic neuropeptide found in the central nervous system and is responsible for assisting in the wound healing process by binding with high affinity to its receptor Neurokinin 1 receptor (NKR-1).

In response to injury, substance P binds to its receptor and mediates wound healing through a series of downstream signalling events depending on the target cell type. Endothelial cells respond to substance P by acting as attractants and upregulate the infiltration of leukocytes to the injured area (Pernow, 1983). Subsequently, substance P promotes vasodilation and cell adhesion between leukocytes and endothelial cells. The generation of the endothelial cell adhesions creates a platform for infiltrating immune cells (Pradhan et al., 2009). These leukocytes release pro-inflammatory cytokines. Substance P has also been shown to stimulate the secretion of IL-1β, IL-2, IL-6, IL-8 and TNF-α by T-lymphocytes, macrophages and neutrophils (Delgado et al., 2003) and by doing so acts as a chemoattractant for additional neutrophils, lymphocytes, monocytes and fibroblasts (Pradhan et al., 2011). .

Chronic diabetic wounds display reduced expression of substance P due to the lack of nerves in diabetic patients compared to non-diabetic patients in addition to the overproduction of NEP (Scott et al., 2008). The use of substance P as a potential therapeutic

agent for the treatment of chronic wounds has therefore been investigated in various models (Table 2.2*)*.

In animal models of delayed healing where type1 diabetes mellitus (T1DM) is induced by administering either streptozotocin (STZ) or alloxan monohydrate to destroy pancreatic function (Lukačínová et al., 2013), topical application of substance P onto the wounded areas has shown promising results (Table 2.2). In STZ-induced diabetic Wistar rats, substance P treatment resulted in decreased wound closure time, decreased MMP-9 expression, increased release of growth promoting factors such as VEGF, TGF-β1, IL-10, improved proliferation of fibroblasts, increased angiogenesis and greater collagen deposition (Kant et al., 2013, Kant et al., 2015, Kant et al., 2017). In a STZ-induced diabetic mouse model, substance P has also been shown to improve corneal epithelial wound healing, mitochondrial function and it increased ROS scavenging capacity (Yang et al., 2014).

Similarly, in T2DM animal models (db/db mice, T2DM and Goto-Kakizaki rats) substance P treatment significantly improved wound healing. In db/db wound models, substance P treatment promoted angiogenesis, cell proliferation, improved wound closure time, re-epithelialisation, nerve fibre density, collagen deposition and increased inflammatory cell density (Um et al., 2017, Younan et al., 2010, Scott et al., 2008, Gibran et al., 2002). These findings are supported by *ex vivo* studies utilizing dermal fibroblasts isolated from db/db mice to investigate the effect of substance P. Jung et al. (2016) demonstrated that substance P treatment increased fibroblast proliferation, VEGF expression, angiogenesis promoting factors and could thus function to improve wound contraction (Jung et al., 2016). In a similar study, the co-culture of dermal db/db fibroblasts and bone marrow-derived macrophages in the presence of substance P resulted in M2 polarization of macrophages, improved fibroblast migration and induced cytokine release from macrophages and fibroblasts (Ni et al., 2016).

Taken together, these studies emphasise the role and importance of substance P in wounding healing (Table 2.2). Substance P has been shown to increase angiogenesis, fibroblast proliferation and migration, increase the secretion of VEGF, TGF-β, pro-inflammatory cytokines, induce polarization of macrophages to M2 phenotype, improve wound closure and improve collagen deposition during the different stages of healing. Hence a decrease in its expression during distress (injury) results in severe impairment in the progression of healing, as is seen in chronic diabetic ulcerations.

Table 2.2: Substance P in human diabetic wounds and animal models

Wound model	Method/treatment	Outcomes	references
Animal models			
T1DM			
streptozotocin-induced diabetic Wistar rats	Topical application of 400 µL of SP (10^{-6}M)	Wound closure by day 14. Increased levels of IL-10, VEGF and TGF-β. Decreased expression of MMP-9, IL-1β and TNF-α.	(Kant et al., 2015)
streptozotocin-induced diabetic Wistar rats	SP (0.5 × 10^{-6}M) + curcumin (0.15%) were topically applied once daily for 19 days	SP + curcumin combination on excision skin wound accelerated the wound healing. Wound closure was observed in day 19.	(Kant et al., 2017)
streptozotocin-induced diabetic Wistar rats	Topical application of SP solution (10^{-7}M)	Wound closure by day 14. Increased levels of VEGF and TGF-β. Improved fibroblast proliferation with collagen deposition and angiogenesis.	(Kant et al., 2013)
streptozotocin-induced diabetic Wistar rats	self-assembled peptides (SAPs)+ SP 200:7 (vol/vol)	SAP +SP combination on excision skin wound accelerated the wound healing enhanced collagen deposition, and increased angiogenesis. Wound closure was observed after 3 weeks.	(Kim et al., 2018)
streptozotocin-induced diabetic ICR male mice	Treatment with SP (5 nmol/kg)	Decreased chronic inflammation, induced angiogenesis.	(Park et al., 2016)
alloxan monohydrate - induced diabetic New Zealand White rabbits	qRT-PCR to quantitate and compare levels of peripheral cytokine (IL-6 and IL-8) and neuropeptide (SP).	Increased gene expression of IL-6 and IL-8 and a decrease in SP precursor. Observed a dysregulation of neuropeptide expression (SP) and suppressed inflammatory response.	(Pradhan et al., 2011)
streptozotocin-induced diabetic C57BL/6J WT mice	Treatment with 32 µg per 90 µL of SP	WT diabetic mice had reduced SP expression. Treatment with SP induced an acute inflammatory response causing wound to move into proliferative phase II of healing, activation of macrophages to M2 phenotype, reduced MMP-9 expression and wound closure was observed at day 10.	(Leal et al., 2015)
streptozotocin-induced diabetic C57BL/6 male mice	topical SP application, 5 µL SP (1 mmol/L) on the corneal surface	Promoted corneal epithelial wound healing, improved mitochondrial function and increased ROS scavenging capacity.	(Yang et al., 2014)
BALB/C-nu (nude mice)	Treated with Skin-derived precursors (SKPs)	SKPs promoted wound healing via cell proliferation, nerve fiber regeneration and the release of neuropeptides (SP).	(Shu et al., 2015)
Sprague-Dawley rats	Treatment of SP (10^{-7}) mol/L combined with epidermal stem cells (ESC) injected into wound margins and middle of wound.	Wound closure observed on day 14. Improved collagen deposition and nerve regeneration.	(Zhu et al., 2012)
Sprague-Dawley rats	Treatment with epidermal stem cells and substance P	Wound closure observed at 14 days and increased nerve regeneration and wound healing.	(Zhu et al., 2016)

Wound model	Method/treatment	Outcomes	references
T2DM			
type 2 diabetic mice (db/db mice)	SP injection (10 nM/kg, subcutaneously)	Enhanced angiogenesis, increased cell proliferation. Observed the same wound closure after 7 days.	(Um et al., 2017)
type 2 diabetic Goto-Kakizaki (GK) male rats	changes in expression of neuro- and angiotrophic mediators and receptors in intact and healing Achilles tendon via (qRT-PCR)	NGF (upregulates SP expression) was down regulated resulting in diabetic rats causing a decrease neuropeptide expression (SP) and angiogenesis.	(Ahmed et al., 2017)
Dermal fibroblasts from db/db mice co-cultured with bone marrow-derived macrophages	Cells were treated with SP (10 nM)	Promoted the migration of fibroblasts, M2 macrophage polarization and release of pro-inflammatory cytokines by fibroblasts and macrophages.	(Ni et al., 2016)
Dermal fibroblasts from db/db mice	Treatment with SP (100nM)	Increased proliferation of fibroblasts, increased expression of VEGF – increase in angiogenesis promoting factors and wound contraction.	(Jung et al., 2016)
type 2 diabetic mice (db/db mice)	Vacuum-assisted closure device	An increase in epidermal and dermal nerve fibre density and SP expression.	(Younan et al., 2010)
type 2 diabetic mice (db/db mice)	Topical application of 10^{-9} M SP	Increased early inflammatory cell density.	(Scott et al., 2008)
type 2 diabetic mice (db/db mice)	Treatment with polyethylene glycol (PEG) and SP 10^{-9} M	SP promoted re-epithelialization. Wound closure observed by day 45.	(Gibran et al., 2002)
Human Models			
Human microvascular endothelial cells (HMEC-1)	HMEC-1 cells treated with 10^{-4} mol/L SP followed by treatment with high levels of glucose and fatty acids (observed in DMII) to assess migration and proliferation	SP treated cells without glucose and fatty acid treatment had increased levels of proliferation. The glucose and fatty acid treatment group showed significant impairment in cell migratory ability.	(Wang et al., 2009)

Abbreviations: SP, Substance P; IL, Interleukin; MMP-9, Matrix metalloprotease-9;TNF-α, Tumour necrosis factor-α; TGF-β: Transformation growth factor beta; SAP, self-assembled peptides; qRT-PCR, quantitative real-time reverse-transcriptase polymerase chain reaction; NGF, nerve growth factor; VEGF, Vascular endothelial growth factor; WT, wild type and ROS, reactive oxygen species; ESC: Epidermal stem cells; SKP: Skin derived precursors; PEG: Polyethylene glycol; HMEC-1, Human microvascular endothelial cell.

2.2.3 Dysregulation of NEP in non-healing diabetic wounds.

NEP is a thermolysin-like zinc metalloprotease that plays an essential role in the regulation of peptide signalling on the cell surface. It is located on the membrane of the same cells that express the NKR-1 receptor such as fibroblasts, keratinocytes, immune, endothelial, epithelial and smooth muscle cells and is anchored to the cell membrane via its hydrophobic amino acid chain with its active site facing the extracellular space (Antezana et al., 2002).

NEP assists in various peptide metabolic regulatory processes in the cardiovascular, immune, inflammatory and nervous systems (Turner et al., 2001). These peptides include chemotactic peptides, enkephalins, natriuretic peptides and tachykinins (e.g. substance P). NEP regulates the expression of substance P by degrading it thereby hindering its biological function (Olerud et al., 1999). Once substance P binds to NEP, it competes with the NKR-1 receptor, substance P is then hydrolysed at the amino terminal between Gln^6 – Phe^7, Phe^7 – Phe^8 or Gly^9 – Leu^{10} residues to produce several degradation products (Figure 2.6) (Skidgel et al., 1984).

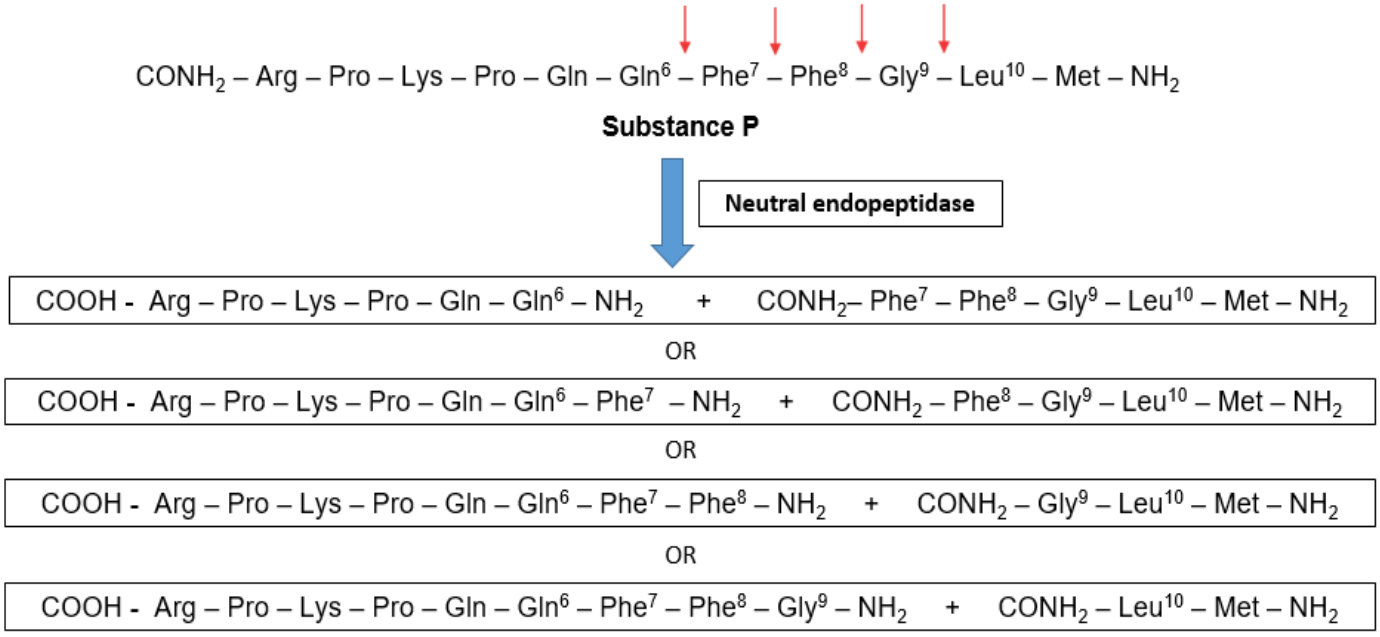

Figure 2.6. Hydrolysis of hydrophobic residue Substance P by Neutral endopeptidase. Substance P is cleaved by NEP at the amino terminal between Gln6 – Phe7, Phe7 – Phe8 and Gly9 – Leu10 residues (Skidgel et al., 1984).

The overexpression of NEP in chronic diabetic wounds is thought to be a contributing factor that prevents healing due to its high binding affinity to substance P. There are many studies that support this hypothesis (Table 2.3).

Diabetic (db/db) mice have been shown to have a 3 fold higher NEP enzyme activity than control mice (Spenny et al., 2002), and a significant increase in corneal wound healing has been demonstrated in NEP $^{-/-}$ mice compared to wild-type controls (Genova et al., 2018). Burssens et al. (2005), indicated that treatment of wounded Achilles Tendons in rats with substance P and a NEP inhibitor, increased fibroblast proliferation, angiogenesis and collagen deposition. Thus, providing further evidence for the role of NEP in delayed healing in animal models.

In a cell culture model, Muangman et al. (2003) showed that in the presence of high levels of glucose and fatty acids (as is the case in T2DM), NEP activity was increased in human microvascular endothelial cells (HMEC-1) and that treatment with vitamins were able to significantly reduce NEP enzyme activity. In patients (without neuropathy and diabetes mellitus), the assessment of NEP activity in acute wounds, unwounded skin and human derived skin cells indicated that NEP was expressed more in the migrating epithelial wound edges and first presented in the wound 6 hours post wounding (Olerud et al., 1999).

Taken together, these studies reaffirm the importance of NEP regulation in wound healing and suggest that excessive NEP activity can lead to severe impairments in the healing process. NEP is thus an excellent candidate to use in designing a chronic wound model that mimics the clinical characteristics of diabetic wounds more closely.

Table 2.3: Neutral endopeptidase in wound healing

Wound model	Method/treatment	Outcomes	references
Animal models			
type 2 diabetic mice (db/db mice)	NEP enzymatic activity assay Treatment with NEP inhibitor (thiorophan 25µM)	Significantly higher activity (20.6pmol MNA/hr/µg) in skin of db/db mice compared to non-diabetic mice (7.96pmol MNA/hr/µg) Wound closure observed at day 18.	(Spenny et al., 2002)
NEP-deficient ($NEP^{-/-}$) mice	Alkali burn model of corneal injury	Corneal wound healing was significantly increased in $NEP^{-/-}$ mice compared to the controls.	(Genova et al., 2018)
Sprague-Dawley rats	Two treatments to wounded Achilles Tendon: SP 10^{-6} mol/kg body weight + NEP inhibitor or SP 10^{-6} mol/kg body weight + inhibitor	Both treatments increased fibroblast proliferation, angiogenesis and collagen orientation.	(Burssens et al., 2005)
Human Models			
Diabetic patients undergoing lower extremity amputation.	NEP enzymatic activity assay.	NEP activity in the ulcer margins of diabetic patients was 47.54717.18 pmol MNA per h per mg which was 15.22 times higher than the control skin from patients without diabetes.	(Antezana et al., 2002)
Human microvascular endothelial cells (HMEC-1)	Cells were first treated with high levels of glucose and fatty acids followed by treatment with Vitamins E and C	NEP enzyme activity was upregulated in cells treated with high levels of glucose and fatty acids. Treatment with the vitamins blocked upregulation of NEP by glucose and fatty acids, NEP enzyme activity was significantly reduced.	(Muangman et al., 2003)
Human microvascular endothelial cells (HMEC-1)	Cells were first treated with high levels of glucose and fatty acids followed by treatment with Vitamins E and C and *N*-acetylcysteine	NEP gene expression was upregulated when cells were treated with high levels of glucose and fatty acids. Treatment with the vitamins blocked upregulation of NEP by glucose and fatty acids.	(Muangman et al., 2005)
Human subjects without neuropathy and diabetes mellitus	NEP expression in wounded, unwounded skin and human derived skin cells	NEP present 6 hours after wounding. NEP was expressed more in the migrating epithelial wound edges. NEP activity was detected in keratinocytes derived from human skin.	(Olerud et al., 1999)

Footnote: The table above contains animal and human diabetic wound models that either use or show the effect/ importance of NEP on wound healing. **Abbr:** NEP, Neutral endopeptidase; SP, Substance P; HMEC-1, Human microvascular endothelial cells.

2.3 Current animal models: non-healing diabetic wounds

There are currently various diabetic wound models that are commonly used such as the Rabbit ear ulcer model (Leal et al., 2015), the STZ-induced diabetic rat model (Kant et al., 2015) and various mouse models (Healthy control C57Bl/6J mice fed a high fat diet, NONcNZ010, db/db, ob/ob mice and STZ-induced diabetic mice) (Table 2.4). Each of these models have advantages and disadvantages as summarized in Table 2.4.

For a diabetic wound model, it is essential that the animal itself has a similar pathological profile and phenotype to T2DM patients. The NONcNZ010, db/db and ob/ob mice are therefore the most popular mouse strains used for diabetic wound studies and are readily available and supplied by Jacksons laboratories (Nunan et al., 2014, Elliot et al., 2018). NONcNZ010 are polygenic, insulin resistant mice with morbid obesity (Leiter et al., 2013). Fang et al. (2010) indicated that impaired healing of splinted wounds was evident in NONcNZ010 mice. This model has however sexual bias when it comes to diabetes and obesity development (Leiter et al., 2013). Db/db mice are diabetic leptin receptor deficient mice and become noticeably obese after 3 weeks of age. The db/db mice display delayed wound healing, increased metabolic efficiency, excessive hunger (constant eating), increased thirst and higher plasma insulin levels (Coleman, 1978). The one disadvantage of the db/db model is that these animals are born diabetic and therefore do not follow the same disease progression into diabetes as in human patients. The ob/ob mouse strain first become obese, insulin resistant and then develops T2DM, which is a similar progressive diabetic phenotype observed in human patients in a clinical setting.

The ob/ob mice are pre-diabetic leptin deficient mice. The ob/ob mice exhibit obesity, delayed wound healing, insulin intolerance, hyperglycaemia, excessive hunger and increased thirst (Coleman, 1978). Both the db/db and ob/ob strains are reproductively impaired and hence difficult to breed (Leiter et al., 2013). Nonetheless, these two strains are some of the most commonly used strains to study diabetic wounds (Elliot et al., 2018).

Table 2.4: Advantages and limitations of Diabetic wound models in animals

Chronic wound Model	Description	Advantages	Limitations
Rabbit ear ulcer model	Induces ischemic full thickness wounds by suturing and cutting of blood supply to wounded part of ear.	• Low cytokine concentration post wounding. • High M1/M2 ratio. • Efficient in testing of pharmological agents. • Cheap to maintain. • Reproduce quickly.	• Genetic variability between rabbit and humans. • Induction of neuropathy is due to ischemia and not diabetes.
Streptozotocin-induced diabetic rats' model	Induces diabetes by administration of streptozotocin which kills off pancreatic β cells.	• Successful induction of diabetes. • Cheap to maintain. • Reproduce quickly.	• Anatomical differences between Rat and human skin.
NONcNZ010 mice	Insulin resistant mice with morbid obesity.	• Successful impairment of wound healing.	• Sexual bias.
Db/db mice	Diabetic and leptin receptor deficient mice usually used in combination with additional factors that assist in delayed healing.	• Cheap to maintain. • Reproduce quickly. • Easy to handle. • Impaired wound healing.	• Difficult to breed due to sub-fertility. • Develop diabetes spontaneously. • Do not have the same progression into diabetes that we see in human patients.
Ob/ob Mice	Pre-diabetic Leptin deficient mice usually used in combination with additional factors that assist in delayed healing.	• Cheap to maintain. • Reproduce quickly. • Easy to handle. • Shares exact phenotype of the development of diabetes as seen in patients. • Impaired wound healing.	• Difficult to breed due to sub-fertility.
Healthy control C57Bl/6J mice High fat diet model	Healthy control mice fed a high fat diet to induce a diabetes-obesity syndrome.	• Cheap to maintain. • Reproduce quickly • Slight delay in healing. • Pro-longed inflammation	• Does not develop chronic inflammatory state.

Footnote: The table above contains the advantages and limitations of diabetic animal wound models. Selected references using each chronic wound model (Leiter et al., 2013, Nunan et al., 2014, Elliot et al., 2018, Kant et al., 2015, Leal et al., 2015).

Although these particular strains (db/db and ob/ob) exhibit delayed wound healing, they do not display the increased NEP levels observed in a chronic diabetic wound causing many therapeutic strategies that are successful in substandard animal models to fail in the clinical setting. There is thus a need for a chronic wound model that is able to overcome these limitations to assess the efficacy of new potential therapies.

Chapter 3 : Aims and Objectives

It was hypothesised that administration of NEP to the margins of full-thickness excisional wounds, induced in obese pre-diabetic mice (B6.Cg-Lep^{ob}/J, ob/ob), would impair healing to such an extent that a chronic wound develops which resembles the phenotype of diabetic ulcers in the clinical setting.

The aims and objectives of this study therefore included the following:

Aim 1: Determine the optimum dose of NEP to be injected into the wound edges in an obese pre-diabetic mouse model (B6.Cg-Lep^{ob}/J, ob/ob) of delayed healing to create a chronic non-healing wound.

Objective 1.1: Assess NEP enzyme activity (kinetic profile) within the wound tissue during the first 2 days post wounding following injection of various NEP concentrations.

Objective 1.2: Assess substance P expression within the wounded area and edges (immunohistochemistry) during the first 2 days post wounding following injection of various NEP concentrations.

Objective 1.3: Assess MMP-9 expression in the wound tissue (enzyme-linked immunosorbent assay) during the first 2 days post wounding following injection of various NEP concentrations.

Objective 1.4: Harvest and collect wound fluid on day 2 post wounding following injection of various NEP concentrations and determine the cytokine profile (multiplex bead array) within wound fluid.

Aim 2: Investigate and compare the wound healing dynamics of a chronic non-healing wound in obese pre-diabetic mice (B6.Cg-Lepob/J, ob/ob), using the optimum NEP dosage injected into the wound edges, to an acute wound in wild-type mice (C57BL/6J) with saline treatment.

Objective 2.1: Compare the macroscopic wound closure of the newly developed chronic wound model with an acute wound model over a period of 7 days.

Objective 2.2: Compare the wound healing parameters of acute and chronic wounds by assessing granulation tissue formation, re-epithelialisation, cellularity and angiogenesis over a period of 7 days (histological analysis).

Objective 2.3: Compare MMP-9 expression (enzyme-linked immunosorbent assay) within wound tissue of acute and chronic wounds over a period of 7 days.

Aim 3: Investigate if there are differences in the protein profile of acute and chronic wounds during the early stages of wound healing.

Objective 3.1: Compare the protein profile of acute and chronic wound tissue 2 days post wounding using proteomics (mass spectrometry).

Chapter 4 : Materials and Methods

4.1 Ethics Approval statement

This study was approved by the animal research ethics committee at Stellenbosch University (SU-ACUD17-00016, 30 June 2017) and complied with the South African Animal Protection Act (Act no 71, 1962). All experimental procedures were conducted according to the ethical guidelines and principles of the declaration of Helsinki. The surgical procedures were performed only after authorization was granted by the South African Veterinary Council (SAVC). Refer to *Appendix A* for the ethical approval letters and proof of SAVC authorization.

4.2 Overview of study design

This study involved the induction of full-thickness dorsal excisional wounds on wild-type (C57BL/6J) and obese pre-diabetic (B6.Cg-Lepob/J, ob/ob) mice and was therefore classified as a high-risk study. Animal welfare was the main priority during the study and all relevant measures were taken to ensure that the animals did not suffer or experience any unnecessary pain and discomfort. Refer to *Appendix B* for the animal welfare monitoring sheet template and to Figure. 4.1 below for an overview of the study design. The specific treatment groups and detailed methodology are described in *sections 4.4-4.10*. All animal work, sample collection, processing and storage was conducted by Ms Boodhoo. Histological processing and staining (Masson trichrome stain, Haematoxylin stain and Immunohistochemistry for substance P) was performed by the Histology Lab, Department of Anatomy, Stellenbosch University. The microscopy and analysis of histology was done by Ms Boodhoo herself. All protein extractions and proteomic work was done by Ms. Boodhoo with the assistance of the Central Analytical Facility (CAF).

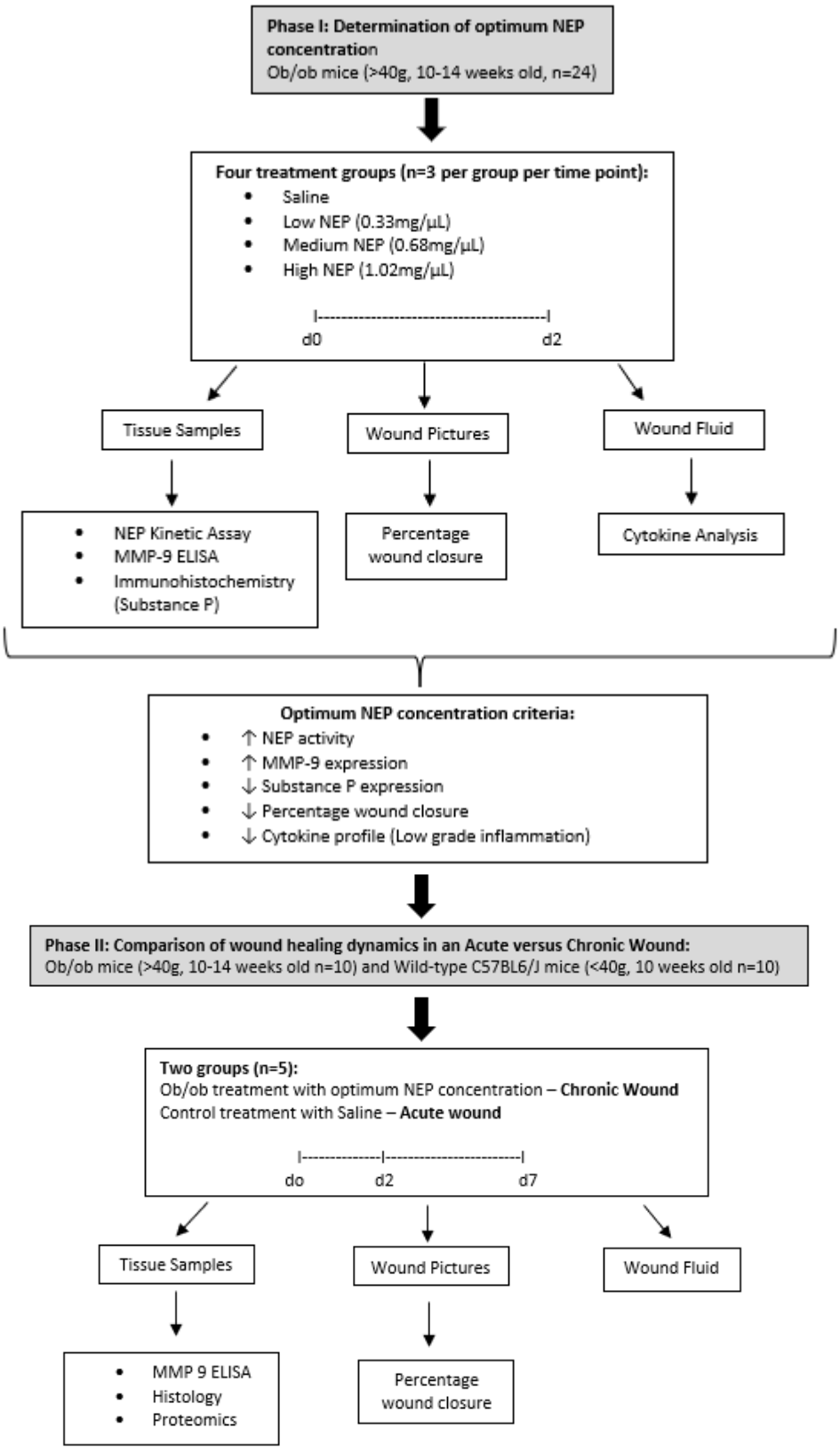

Figure 4.1. Study design. Phase I: Determination of the optimum concentration of NEP. B6.Cg-lepob/J (ob/ob) (>40 g) mice were wounded and treated with either Saline, low NEP (0.33 mg/µL), medium NEP (0.68 mg/µL) or high NEP (1.02 mg/µL) immediately post wounding. Phase II: Comparison of the wound healing dynamics in Acute (wild-type C57BL6/J mice with saline treatment) versus the newly developed Chronic (B6.Cg-lepob/J (ob/ob) mice with optimum NEP treatment) wounds. Tissue samples were collected on days 0, 2 and 7 post wounding and wound fluid collected on days 2 and 7 post wounding.

4.3 Animal housing & husbandry

The animal research facility (Care and Use of Laboratory animals) at the Faculty of Medicine and Health Sciences (FMHS), Stellenbosch University, is equipped for the housing and husbandry of a variety of animal species and complies with accepted standards for the use of animals in research and teaching as reflected in the South African National Standards 10386: 2008. The wild-type mice (C57BL/6J) were housed in this facility under standard conditions (12h light / 12h dark cycle at a controlled temperature of 21°C). The obese pre-diabetic (B6.Cg-Lep^{ob}/J, ob/ob) mice were however not very active, and breeding was slow at 21°C; the temperature was therefore increased to 24°C which improved breeding outcomes. Animals had free access to drinking water and chow (Rat and Mouse Breeder Feed, Animal Specialties, Pty, Ltd., Klapmuts, SA).

4.4 Procedures performed on the animals

4.4.1 Induction of full thickness excisional wounds.

Mice (a total of n=33 ob/ob; n=15 wild-type in Phase I and II) were weighed and anesthetized via an open system inhalation chamber (Fig. 4.2 A) using Isoflurane gas (3% for induction and 2% for maintenance) (Safeline Pharmaceuticals, South Africa). Dorsal hair was shaved, and the skin cleaned with povidone-iodine (Mundipharma, South Africa) prior to making two identical contra-lateral full-thickness skin excisions (Fig. 4.2 B-C). Excisional wounds were made by applying outward retraction of the skin using sterile forceps and the skin cut using sharp surgical scissors (Chen et al., 2013). Wounds (1 cm below the base of the skull and 1 cm on either side of the midline) were approximately 6 mm^2 in diameter and included removing of the underlying layers (panniculus carnosus) to achieve a full-thickness wound. Immediately after wounding, local anaesthetic, 7mg/kg lignocaine (2%) (Bodene, South Africa) was injected around the wound edges. Pain management was maintained for a period of 3 days by administering 300 mg/kg acetaminophen (Paracetamol 120 mg, South Africa) in the drinking water. Both excisional wounds were covered by a vapor-permeable polyurethane film (Hydro-film, Paul Hartmann AG, Germany). After recovery from the anaesthesia, mice were individually housed for a maximum period of 7 days and were monitored closely for signs of distress and pain to ensure the welfare of the animals. Refer to *Appendix B* for the animal welfare monitoring sheet template.

During the optimization of the procedures it became clear that the obese pre-diabetic mice (B6.cg-lepob/J, ob/ob, >40 g, 10-14 weeks old) react adversely to the anaesthesia upon

prolonged exposure (>10 min) and as consequence suffered from heart and respiratory failure. This is consistent with other reports in the literature (Gargiulo et al., 2012). To avoid this complication, mice were thus shaved and wounded on separate days in order to reduce the required time period under anaesthesia.

Immediately post wounding, NEP (150 µL) was injected subcutaneously around the wound edges as indicated by the arrows in Figure 4.2 C. The ob/ob mice (n=24) were grouped into one of four treatment groups

- Saline (control) (n=3 per time point)
- Low NEP (0.33 mg/µL; enzyme activity:50 pmol/hour/ug) (n=3 per time point)
- Medium NEP (0.68 mg/µL; enzyme activity:100 pmol/hour/ug) (n=3 per time point)
- High NEP (1.02 mg/µL; enzyme activity:150 pmol/hour/ug) (n=3 per time point)

The lowest concentration of NEP corresponds to the enzyme activity of NEP previously observed in the ulcer margins of diabetic patients by Antenzana et al. (2002). A dose response was however required, since mice have a higher metabolic turnover compared to humans.

A)

B)

C)

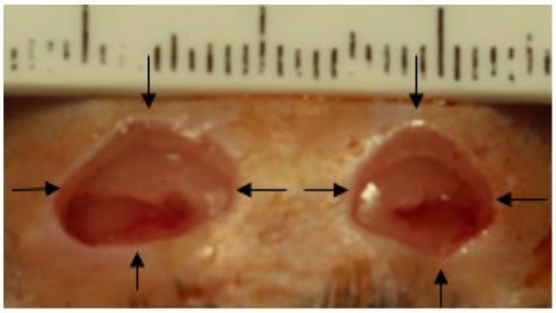

Figure 4.2. Representative images of the wounding procedure. **A)** Open system inhalation chamber used to anesthetize animals. **B)** Illustration of shaved mouse with bilateral full thickness excisional wounds on the dorsal surface. **C)** Full thickness excisional wounds (day 0). The arrow heads indicate points around the wound edges where subcutaneous NEP treatment was administered.

4.4.2 Wound images and collection of wound fluid

Images of the wounds were taken from directly above at three different time points (day 0, 2 and 7) post wounding using a Canon digital camera (EOS 600D, Canon Inc., Taiwan). A ruler was placed horizontally along the wound edges in order to have a point of reference (scale = 1 cm) for assessment of macroscopic wound closure.

Immediately prior to taking the wound images, wound fluid was collected using the needle puncture technique. The vapor-permeable polyurethane wound dressing was removed and 100 µL of saline solution injected into the wound edges using a needle (25-30G, BD Micro-Fine™ Plus, USA) and re-collected after approximately 30 sec. Dried wound exudate visible on the vapor-permeable polyurethane film was also collected using sterile tweezers and dissolved in the saline solution. The collected wound fluid was stored in Eppendorf tubes at -80º C for subsequent analysis. Prior to analysis, wound fluid was pooled together for each treatment group to ensure an adequate volume was available for analysis.

4.4.3 Animal Euthanasia

The wounded mice (n=34 ob/ob; n=10 wild-type) were euthanized on either day 0 and 2 in phase 1 or on day 0, 2 and 7 in phase 2 (Fig. 4.1). At the respective time points, all animals were anesthetized via an open system inhalation chamber using Isoflurane gas (3% for induction) and euthanized using cervical dislocation. The procedure was performed by a trained para veterinarian according to the SAVC guidelines.

4.4.4 Harvesting of tissue and storage

Immediately following sacrifice, the wounded tissue including a 5 mm margin was excised and processed for storage as follows: One half of each wound was snap frozen in liquid nitrogen (N_2) and stored at -80^{o}C. These samples were used for protein extraction to assess MMP-9 expression, NEP enzymatic activity and the protein profile within the wounded tissue. The other half of each wound was fixed in 10% buffered formalin solution (10 mL 37% formaldehyde solution, 0.8 g NaCl, 0.4 g Potassium phosphate monobasic, 0.65 g Potassium phosphate dibasic and 90 mL distilled water at pH 6.8) and embedded in paraffin wax for histological processing. Histological processing (*section 4.9*) and Figure 4.3 below for an illustration of how the wounds were divided for processing.

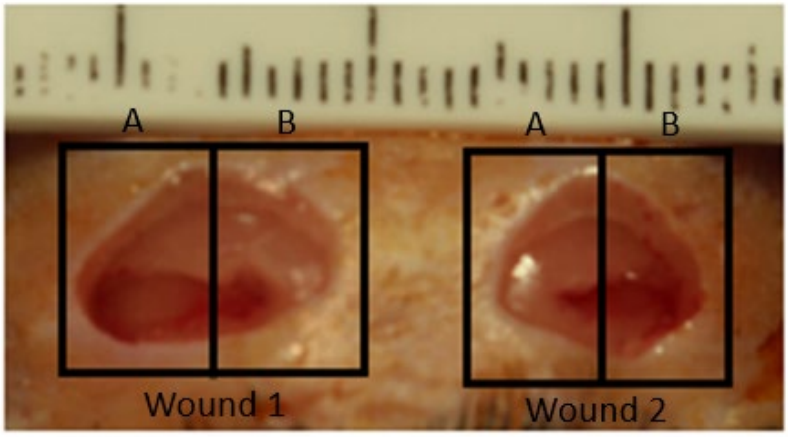

Figure 4.3. Bilateral wounds on the dorsal surface of an obese mouse on day 0. The blocks surrounding the wound 1 and 2 indicates how both wounds were excised and halved into sections A and B. Section A for both wounds 1 and 2 were stored in 10% buffered formalin and section B for both wounds 1 and 2 were snap frozen in liquid nitrogen and stored at -80ºC.

4.5 Determination of macroscopic wound size

The surface area (mm^2) for each wound was determined using Image J software (version 1.46, NIH.gov, USA). Images were opened in Image J and the scale set according to the point of reference on each image. The *straight-line* tool was used to measure the number of pixels per 1 cm and the image scale set according to this measured distance. The *free hand tool* was used to trace around the wound edges and the surface area for each wound determined. Percentage wound closure over time was calculated using the following formula:

$$\% \text{ Wound closure} = \frac{\text{Wound area (day 0)} - \text{Wound area (day x)}}{\text{Wound area (day 0)}} \text{ X } 100$$

4.6 Analysis of wound fluid

Wound fluid collected on day 2 was analysed using the Bio-Plex Pro™ Mouse 23-plex bead-array assay (M60009RDPD, Bio-Rad, USA) as per manufacturer's instructions.

Principle of the assay: This assay is a sandwich immunoassay that uses magnetic beads (Fluorescently dyed microspheres). The magnetic beads use antibodies that are directed against specific targets that are covalently bound to internally dyed beads. This permits for the distinction between various targets based on the colour emitted allowing the assessment of multiple cytokines/ targets within one given sample.

Assay procedure: All assay components were supplied by the manufacturer and brought to room temperature before use. Beads (x 1 working solution of 50 µL) were added to each well and the plate incubated at room temperature with gentle agitation for 30 min after which it was washed twice with 100 µL wash buffer per well. Serial dilutions of known standards, a blank (background control) and the wound fluid samples (50 µL each) were loaded in duplicate wells of the 96 well plate. The plate was then incubated at room temperature with gentle agitation for 30 min followed by a washing step (three times with 100 µL wash buffer per well). Detection antibody (1 x working solution, 25 µL) was added to each well and incubated at room temperature for 30 min with gentle agitation followed by another washing step (three times with 100 µL wash buffer per well). Streptavidin PE (50 µL) was then added to each well and incubated at room temperature for 10 min with gentle agitation. The plate was then washed again three times with 100 µL wash buffer per well. The beads within the plate, were then resuspended in 125 µL of assay buffer per well and the plate incubated at room temperature for 30 sec with gentle agitation. The plate was then read using a Luminex Bio-Plex 200 System (Bio-Rad; USA) at Low PMT, RP1 settings. All washing steps were performed using the automated plate washer (Bio-PlexTM Pro Wash Station; Bio-Rad, USA). Refer to *Appendix C* for the standard curves for all 23 cytokines assessed.

4.7 NEP kinetic assay

The enzymatic activity of NEP within the wound tissue was assessed using the Neutral endopeptidase Kinetic assay (K487-100, Bio vision, USA) according to the manufacturer's instructions.

Principle of assay: This assay is based on the ability of NEP to cleave a synthetic substrate (Abz-based peptide) that is specific to NEP to produce a fluorescent product. This free fluorophore once cleaved can then be quantified using a fluorescent microplate reader via the following reaction:

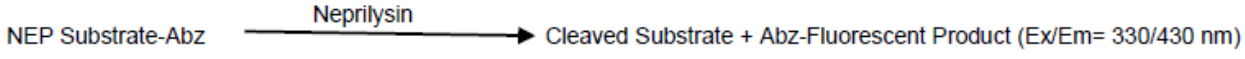

Assay procedure: Snap frozen tissue samples were homogenized in liquid nitrogen using a mortar and pestle and 100mg of each sample was weighed out into labelled Eppendorf tubes. Neutral endopeptidase Assay buffer (400 µL) containing 1 mM PMSF (1083709100, Sigma Aldrich, South Africa) and 10 µg/mL Aprotinin (A1153-5MG, Sigma Aldrich, South Africa) were added to each sample and incubated for 10 min on ice. Samples were then

centrifuged at 4°C for 10 min at 12 000 x g. The supernatant was collected and stored at -20°C for use in the kinetic assay. The protein concentration within each sample was determined using a NanoDrop™ 2000/2000c (Thermo fisher scientific, USA) (260/280 nm).

The known NEP standards (0, 200, 400, 600, 800 and 1000 pmol/well), a positive control (NEP) and the extracted protein (6 µg) from each sample were loaded into duplicate wells of a 96 well plate. A background control for each sample was also run in duplicate (i.e. samples that did not receive the NEP substrate). The excitation and emission filters used to measure substrate development during the kinetic assay were 355 nm and 460 nm. Fluorescent intensity was measured at 10 min intervals over the course of 2 h (120 min) using a fluorometric multiplate reader (Fig. 4.4 A) (FLUOstar Omega, BMG LABTECH, Germany).

End point (120 min) data analysis was performed as follows: The standard curve at 120 min (end point) was plotted on a graph with known NEP activity (pmol) of the standards on the x-axis and fluorescent intensity (RFU) on the y-axis (Fig. 4.4 B) to obtain the slope of the curve (ΔRFU/pmol)**.** For each sample, the background reading was subtracted from the corresponding sample fluorescent reading at each time point to calculate the ΔRFU. The NEP activity for each sample was calculated using the following formula:

$$\textbf{Sample NEP Activity} = B/(\Delta t \times V) \times D = \text{pmol/min/mL} = \mu\text{U/mL}$$

Key:

B = Abz from Standard Curve (pmol)

Δ**t** = Reaction time (min)

V = Sample volume added into the reaction well (mL)

D = Sample Dilution Factor (D = 1 when samples are undiluted)

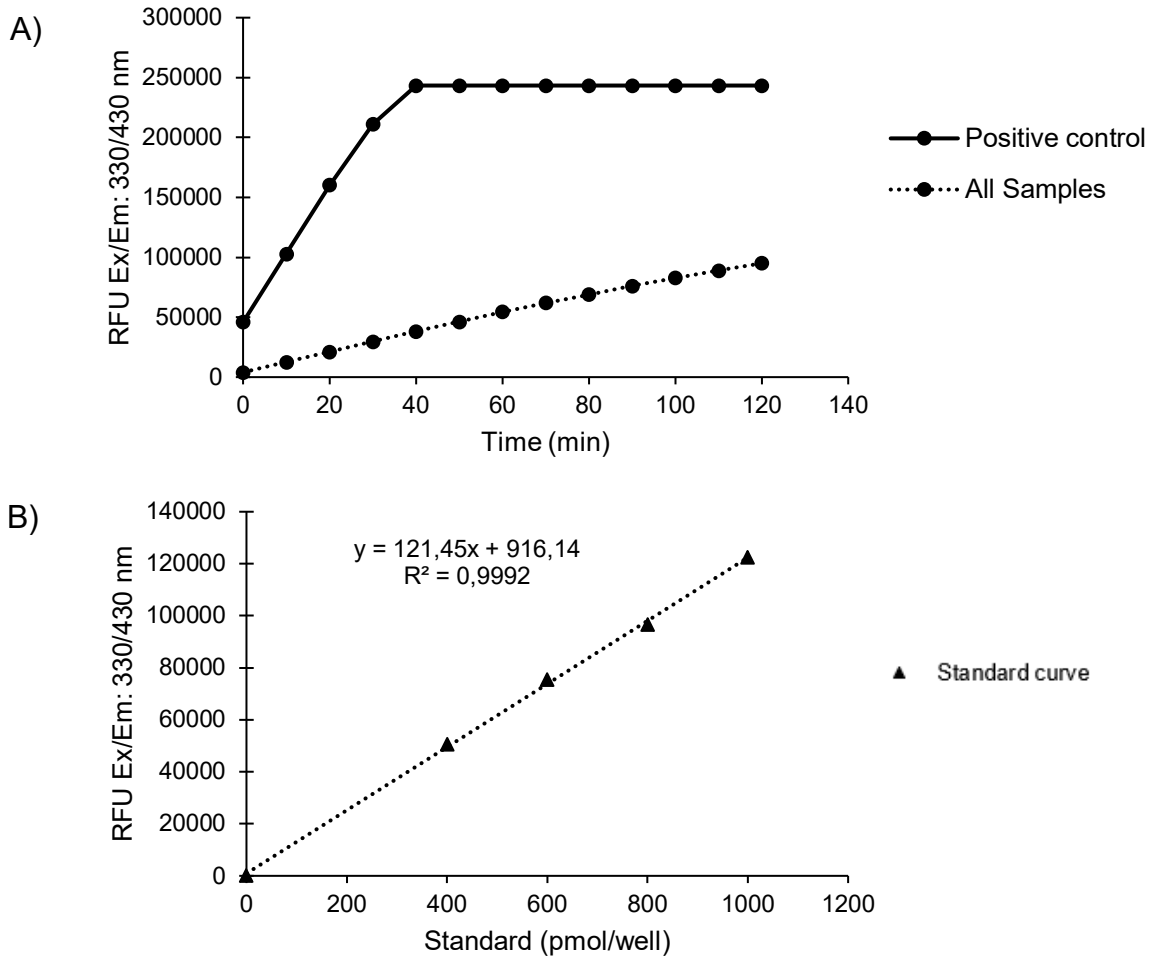

Figure 4.4. NEP Kinetic assay. A) NEP enzyme activity over time illustrating the increase in fluorescent intensity over time for the positive control+ and wound tissue samples. **B)** Standard curve illustrating the quantification of NEP activity (0, 200, 400, 600, 800 and 1000 pmol/well) according to the fluorescent Ex/Em: 330/430 nm readings at the 120 min end point.

4.8 MMP-9 ELISA

A sandwich MMP-9 ELISA (Enzyme-linked immunosorbent assay) kit (AB100732, Abcam, United Kingdom) was used to analyse the samples as per the manufacturer's instructions. Extracted protein samples that were prepared for the NEP kinetic assay were also used in this assay.

Principle of the test: The sandwich ELISA kit consists of a 96 well plate precoated with an antibody specific to MMP-9. Once the samples are loaded onto the ELISA plate, MMP-9 binds to the target specific antibody forming an antigen-antibody complex. A secondary antibody conjugated to an enzyme then binds to the antigen-antibody complex. A substrate is then added and reacts with the secondary antibody's conjugated enzyme to form a coloured detectable product.

Procedure: The known recombinant MMP-9 standard was serial diluted to produce a dilution gradient ranging between 0 and 25 000 pg/mL. The standards and samples (100 µL) were loaded into duplicate wells of the 96 well plate and incubated at 37˚C for 1 h 30 min. Following incubation, the samples and standards were aspirated from each well and Biotinylated anti-Mouse MMP-9 working solution (100 µL per well) added to the plate and incubated at 37˚C for 1 h. This was followed by washing the plate three times at room temperature with 350 µL wash buffer per well for 2 min. HRP-Streptavidin 1 x working solution (100 µL per well) was added to the plate and incubated at 37˚C for 30 min followed by five washing steps (350 µL wells per well). TMB One-Step Substrate Reagent (90 µL per well) was added to the plate and incubated at 37˚C for 15 min to allow for the colour (blue) to develop in direct proportion to the amount of bound MMP-9 within each sample. The reaction was stopped by adding stop solution (50 µL per well) to the plate (colour changes from blue to yellow) and the absorbance was read immediately at 450 nm using a micro-plate reader (Multiskan GO 1.00.40, THERMO-Scientific Group, USA). Due to a technical error, the standard curve failed to produce any colour, but the assay was successful for all the samples analysed. The results are therefore presented as Absorbance/ Optical density (OD) at 450 nm (*Chapter 5*).

4.9 Histology and Immunohistochemistry.

4.9.1 Tissue Processing & Paraffin wax embedding.

Tissue samples preserved in a 10% buffered Formalin solution (10mL 37% formaldehyde solution, 0.8 g NaCl, 0.4 g Potassium phosphate monobasic, 0.65 g Potassium phosphate dibasic and 90 mL distilled water at pH 6.8) were processed within 2 weeks of harvest. Samples were transferred into labelled embedding cassettes and dehydrated in a series of 70% Ethanol (EtOH) (30 min x1 repeats), 96% EtOH (30 min x2 repeats) and 99.9% EtOH (30 min x4 repeats). The dehydration steps were followed by Xylene (Kimix, South Afica) (30 min x2 repeats) and paraffin wax (SMM group, China) (60 min x 3 repeats).

Tissue samples were removed from the cassettes, carefully orientated with the wound edge placed face down on a metal embedding mould and covered with melted Paraffin wax (SMM group, China) at 60°C (Leica EG1160 embedder, USA). The embedded samples were labelled and placed on a cold surface to allow the wax to set. Serial microtome sections (5 µm) were made (Leica RM 2125 RT microtome, USA) and mounted onto labelled glass slides, coated with poly-L-lysine (Leica Bond^{TM} plus, USA).

4.9.2 Haematoxylin & Eosin stain (histology)

Wound tissue sections were stained for H&E to assess histological parameters (granulation tissue formation, angiogenesis, epithelialization and cellularity) using the Leica Auto Stainer XL. Haematoxylin is a blue nuclear stain and Eosin is a pink/ red stain that stains cytoplasm (light pink), collagen (pink), muscle (pink) and erythrocytes (red).

Staining procedure: Tissue sections were incubated at 60°C for 2 min prior to deparaffinization (Xylene, 5 min x2 repeats). This was followed by a series of dehydration steps using 99% EtOH (2 min), 96% EtOH (2 min) and 70% EtOH (2 min). Tissue sections were then dipped in tap water (2 min) followed by staining with Haematoxylin stain (Kimix, South Africa) (8 min) at room temperature. Tissue sections were then rinsed in running water for 5 min to wash off excessive Haematoxylin staining solution before counter staining with Eosin (Kimix, South Africa) (4 min) at room temperature. Excessive Eosin staining solution was then rinsed off for 1 min using running tap water. Finally, the tissue sections were fixed with 70% EtOH (30 sec), 96% EtOH (30 sec) and 99% EtOH (30 sec) and the slides left to dry before mounting with coverslips using DPX mounting media (Sigma Aldrich, South Africa). Refer to Figure 4.5 A for a representative image of H&E staining.

4.9.3 Image acquisition, data analysis and quantification

The H&E stained tissue sections were used to quantify histological parameters such as granulation tissue formation, epithelialization and cellularity. Tile scan images of the entire section were taken at 10x magnification using the Zeiss Axio Vision microscope (Zeiss Axio Observer 7 Inverted microscope, Zeiss, Germany) (Fig. 4.5 A). Assessment of the histological parameters was performed using Image J software (version 1.46, NIH.gov, USA).

Images were opened in Image J. The *straight-line* tool was then used to measure the number of pixels that equates to 1 µm on the scale bar. This measured distance was then used to set the image scale. To determine the epithelial thickness (µm), the *straight-line* tool was used to measure distance by drawing 3 parallel lines through the thickness of the epithelium at both the wound edges and the newly formed epithelium within the wounded area (Fig. 4.5 B). Similarly, the thickness of granulation tissue (µm) was determined by drawing 5 parallel lines through the granulation tissue within the wounded area (Fig. 4.5 B).

The cellularity of the granulation tissue was determined by assessing the percentage area within the granulation tissue that stained positive for nuclei (blue). The image was converted

to an 8-bit grey scale and a region of interest (ROI) was drawn surrounding the granulation tissue within the wounded area by using the *polygon selection tool*. The threshold was then adjusted to select all the blue stained cell nuclei as indicated in red in Figure 4.5 C. The percentage surface area within the granulation tissue (ROI) that represents nuclei were then measured as indication of cellularity.

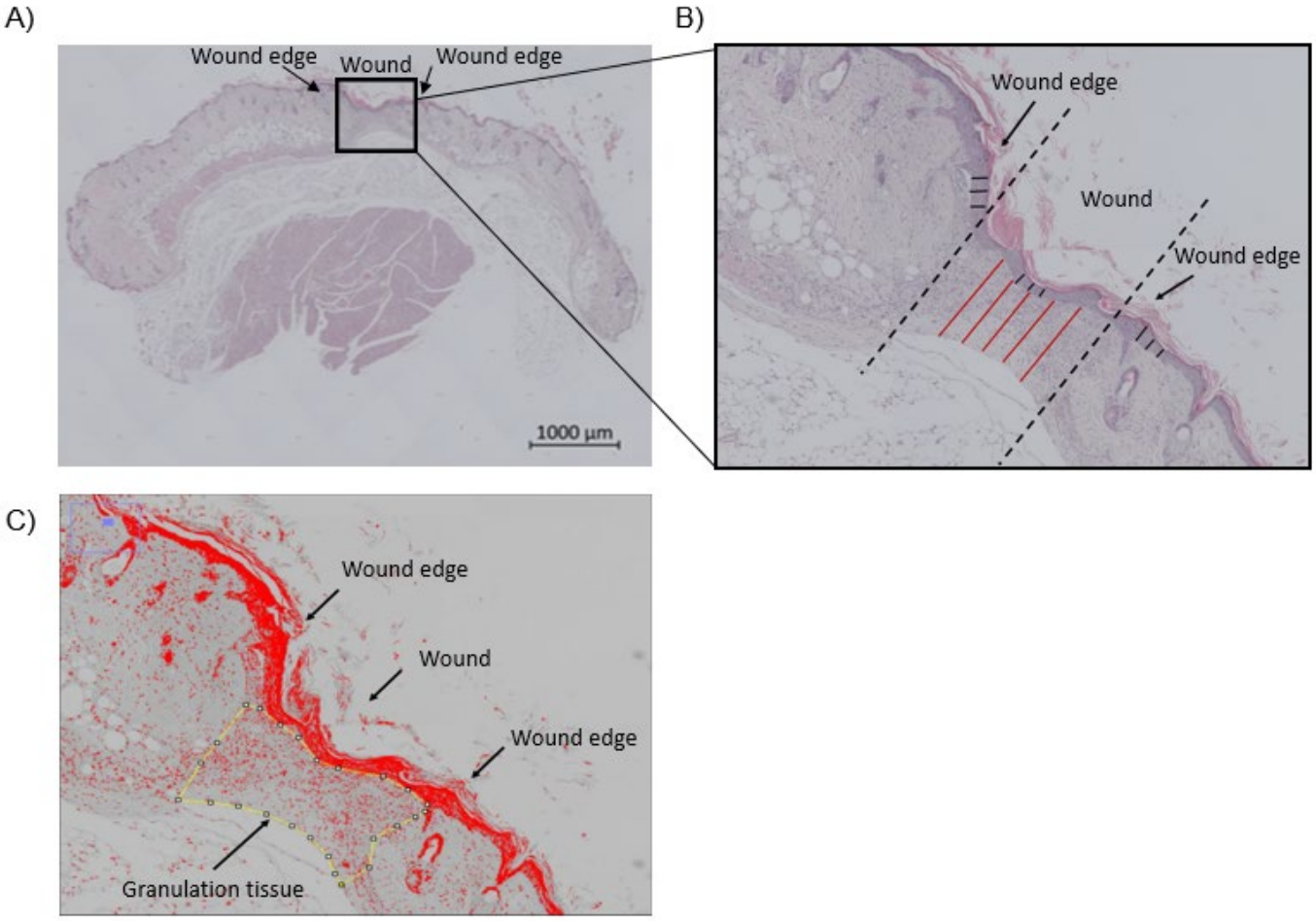

Figure 4.5. Representative images indicating identification of specific wound areas. A) Representative image of H&E staining indicating the wound edges and wounded area of an acute wound 7 days post wounding. **B)** Magnification of wound area illustrating the areas measured to assess epithelial thickness (µm) (black solid lines) and granulation tissue thickness (µm) (red lines). **C)** Illustration of the region of interest (ROI) (yellow outline) identified as granulation tissue within the wounded area. The threshold was set to identify the blue stained nuclei within the ROI. Image analysis was performed using Image J software.

4.9.4 Masson Trichrome Stain (histology)

Wound tissue sections were stained for Masson's trichrome to assess scar formation, vascularization and collagen deposition. Masson trichrome stains collagen blue, nuclei black and the muscle, cytoplasm and keratin red.

Staining procedure: Wound tissue sections were stained using the Leica Auto Stainer XL as follows: Tissue sections were placed in an oven at 60°C for 2 min followed by

deparaffinisation and dehydration as described in *section 4.9.2*. Samples were then dipped in tap water for 2 min and stained with Haematoxylin for 5 min. Samples were then placed in a filtered working solution of fuchsine ponceau-orange G (Sigma Aldrich, South Africa) for 5-30 min before rinsing them in 0.2% Acetic Acid water. This was followed by a 5% phosphotungstic acid (Kimix, South Africa) solution for 5 min. Tissue sections were then stained with methanol green (Sigma Aldrich, South Africa) for 5 to 20 min and rinsed twice in 0.2% acetic acid water. Finally, the tissue sections were fixed with 70% EtOH (30 sec), 96% EtOH (30 sec) and 99% EtOH (30 sec) and the slides left to dry before mounting with coverslips using DPX mounting media (Sigma Aldrich, South Africa).

4.9.4.1 Image acquisition, data analysis and quantification*:*

Tile scan images were taken of the entire Masson's trichrome stained tissue sections at 10x magnification using the Zeiss Axio Vision microscope (Zeiss Axio Observer 7 Inverted microscope, Zeiss, Germany). Refer to Figure 4.6 A for a representative image of Masson's trichrome staining. Assessment of the histological parameters was performed using Image J software (version 1.46, NIH.gov, USA). Images were opened in Image J. The *straight-line* tool was then used to measure the number of pixels that equates to 1 cm on the scale bar. This measured distance was then used to set the image scale.

The Masson trichrome stained tissue sections were used to visualize collagen deposition within the wounded area and to count the number of blood vessels formed within the wound edges and wounded area (Fig. 4.6 B).

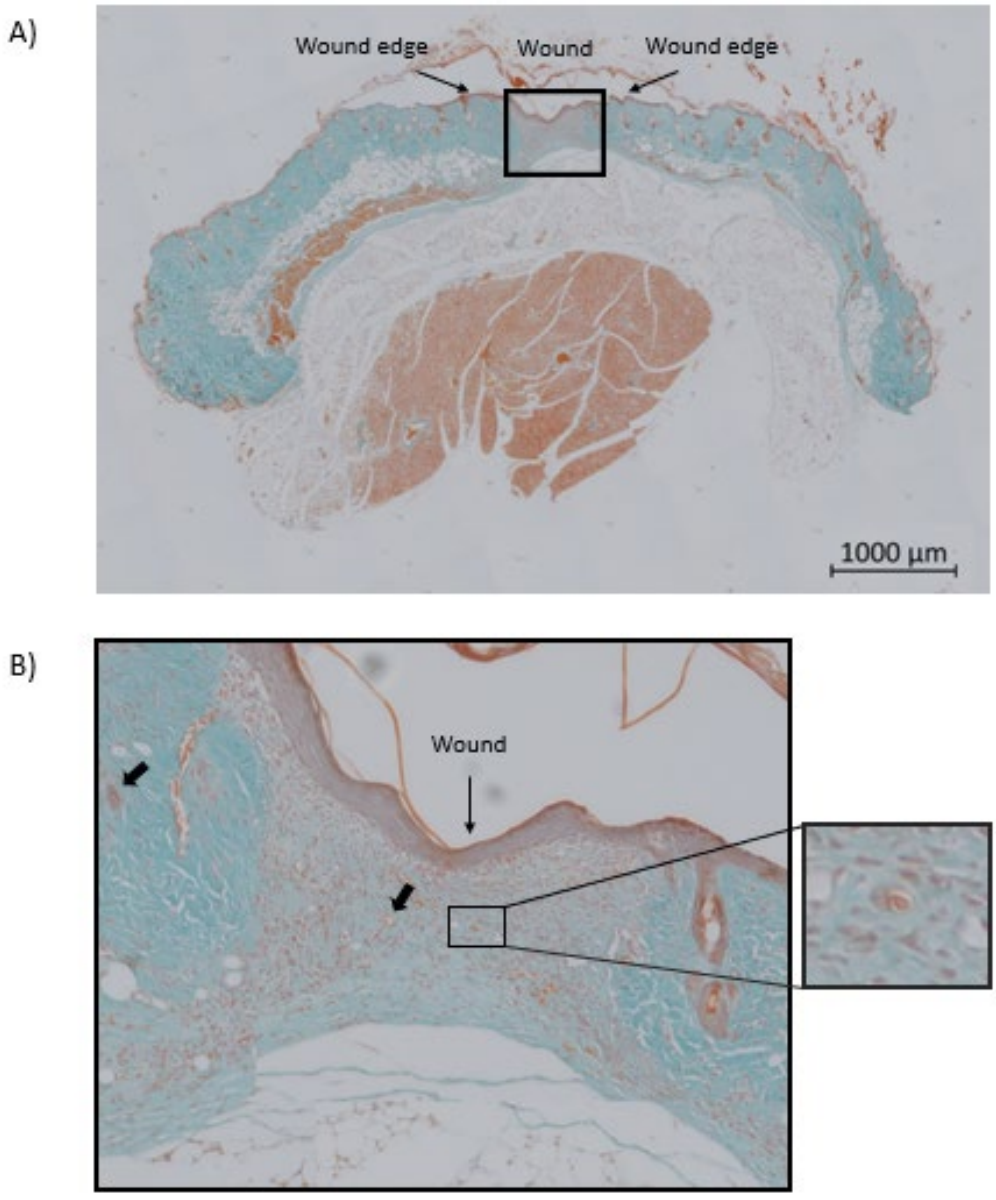

Figure 4.6. Representative images of histological analysis of Masson's trichrome stained tissue sections. A) Representative image of M&T staining indicating the wound edges and wounded area of an acute wound 7 days post wounding. **B)** Magnified image of wound area illustrating collagen deposition (blue) in the wounded area in an acute wound 7 days post wounding and capillaries (indicated by black arrows) within the wounded area and wound edges. The black outlined illustrates a magnified image of a blood capillary within the granulation tissue of the wound area.

4.9.5 Histology Scoring index

The overall histology scoring index was adapted from Galeano et al. (2001) and used as indication of wound healing dynamics (Table 4.1).

Table 4.1: Histological scoring index

Scoring	Feature
1 ±	Little epidermal and dermal organization (epithelial thickness < 30µm in wound area), few capillary vessels (<10), many infiltrated cells (<10%) and no granulation tissue formation.
2 ±	Moderate epidermal and dermal organization (epithelial thickness < 100µm in wound area), newly formed capillary vessels (>10%) in the entire wound area, granulation tissue (>100µm)
3 ±	Complete remodelling of the epidermis and dermis, well-formed capillary vessels.

Footnote: Scoring parameters table adapted from Galeano et al. (2001).

4.9.6 Substance P (Immunohistochemistry)

Tissue sections were stained using standard immunohistochemistry (IHC) techniques to assess the expression of substance P within the wounded area and wound edges. This procedure was done in association with the histology laboratory at the Department of Anatomy and Histology, FMHS, Stellenbosch University using the Leica Bond Max Auto Stainer.

Principle of the test: A primary anti-substance P antibody (ab10353, Abcam, United Kingdom) was used to bind to the substance P protein within the samples to form an antigen-antibody complex. A secondary antibody (conjugated with alkaline phosphatase) then binds to this complex and a substrate is added that reacts with the enzyme conjugated to the secondary antibody to produce a brown coloured product. Refer to Figure 4.7 A for a representative image of substance P IHC staining.

4.9.6.1 Image acquisition, data analysis and quantification:

Tile scan images (3x3) were taken at 10x magnification using the Zeiss Axio Vision microscope (Zeiss Axio Observer 7 Inverted microscope, Zeiss, Germany) of each wound edge and the wound area. Assessment of substance P expression was performed using Image J software (version 1.46, NIH.gov, USA). Images were opened in Image J. The *straight-line* tool was then used to measure the number of pixels that equates to 1 µm on the scale bar. This measured distance was then used to set the image scale. The image was converted to an 8-bit grey scale and a region of interest (ROI) was drawn using the *polygon selection tool* to trace around the wounded area and wound edges. The threshold

was then adjusted so that all the areas stained positive for substance P was selected as indicated in Figure 4.7 B. The percentage surface area stained positive within the wound and wound edges was then quantified.

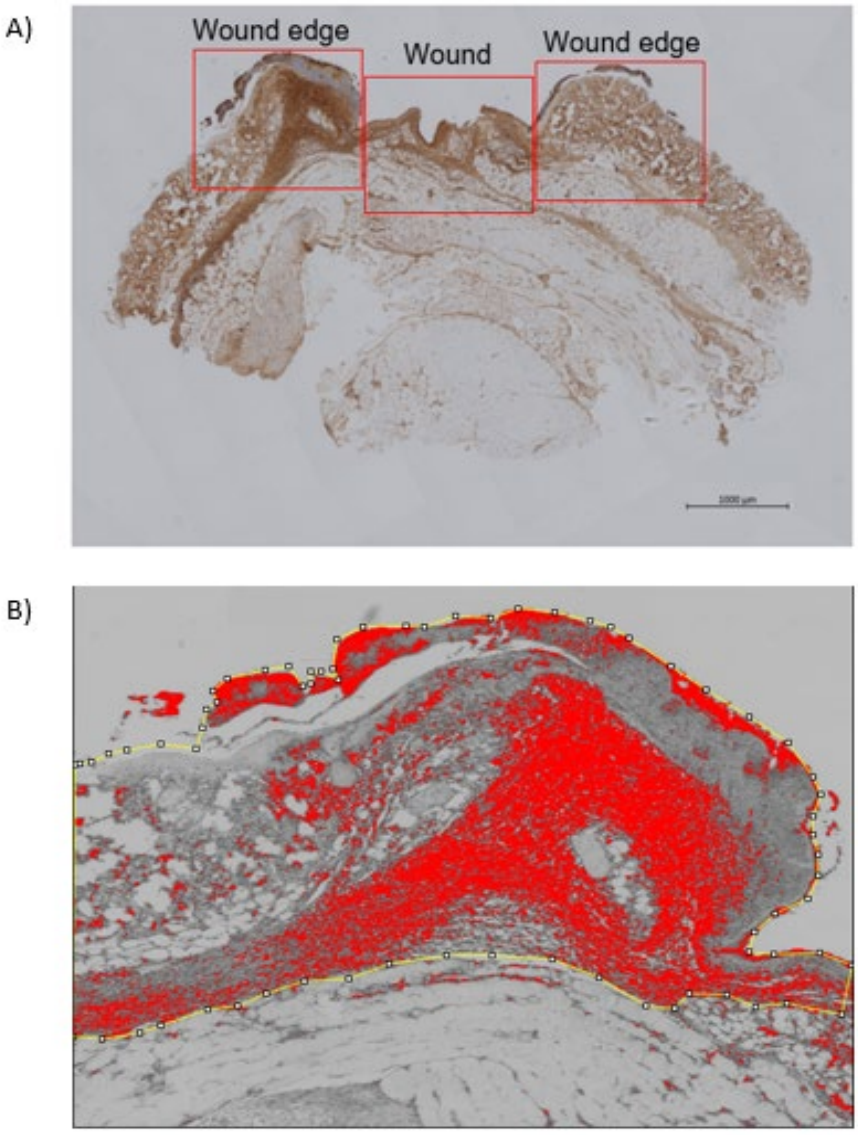

Figure 4.7. Immunohistochemistry of Substance P. A) Representative image indicating wound area and wound edges of a day 2 chronic wound. Area within the red outline box indicates positions that 3x3 tile scan images were taken at 10x magnification using the Zeiss Axio Vision microscope. **B)** Illustration of the region of interest (ROI) (yellow outline) identified as the left wound edge. The threshold was set to identify the positively stained areas (red highlight) of substance P. Image analysis was performed using Image J software.

4.10 Proteomics

The harvested wound tissue that was snap frozen in liquid N_2 underwent a series of extractions and protein solubilisation steps to obtain a sufficient amount and quality of protein for proteomic analysis. Given the nature of full thickness skin tissue, three tissue

extraction processes were required. Refer to Figure 4.8 below for an overview of the tissue processing workflow.

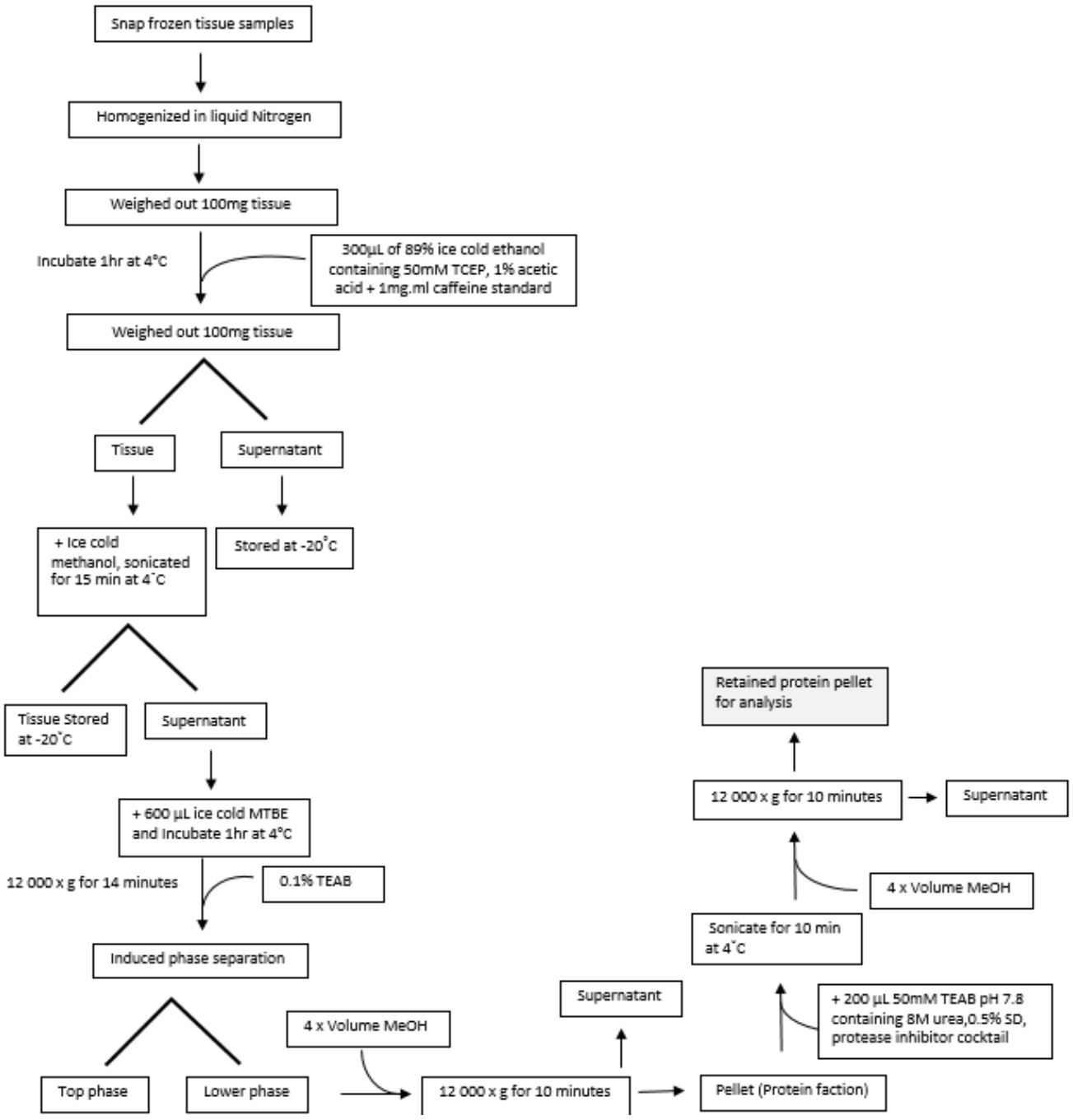

Figure 4.8. Flow chart of Tissue extraction for proteomic analysis. Tissue samples were homogenized in liquid nitrogen and 100 mg weighed out. Samples were then incubated for 1 h at 4°C in 89 % ethanol containing 50 mM Tris(2-carboxyethyl) phosphine (TCEP), 1% acetic acid and 1 mg/mL caffeine standard. The supernatant was removed, and the tissue samples were sonicated for 15 min with methanol at 4°C. The supernatant was removed and incubated with 600 µL of methyl tert-butylether (MTBE) for 1 h at 4°C. Phase separation was induced by adding 100 mM triethylammonium bicarbonate (TEAB) to each sample and centrifuged for 14 min at 12 000 x g. Four volumes of methanol were added to the lower phase and centrifuged at 12 000 x g for 10 min. The supernatant was removed, and the pellet was sonicated for 10 min at 4°C with 200 µL of 50 mM TEAB pH 7.8 containing 8 M urea, 0.5% SDS and a protease inhibitor cocktail. Four volumes of methanol were then added, and samples were centrifuged at 12 000 x g for 10 min. The supernatant was removed, and protein pellet was retained for proteomic analysis.

4.10.1 Tissue extraction

Frozen tissue samples were homogenized to a fine powder in liquid nitrogen using a mortar and pestle at 4°C and 100 mg of each sample was weighed out into pre-weighed labelled glass vials. 300 mL of 89% ice cold ethanol containing 50 mM tris(2-carboxyethyl) phosphine (TCEP; Fluka, South Africa), 1% acetic acid (Sigma Aldrich, South Africa) with 1 mg/mL caffeine standard (Thermo Scientific, Pierce, South Africa) was then added to each sample. This was then followed by an incubation step at 4°C for 1 h. The supernatant was then removed and aliquoted into labelled pre-weighed 2 mL glass vials and stored at -20°C.

Ice cold methanol (200 mL) was added to each tissue sample and sonicated for 15 min at 4°C. The supernatant was removed using a flattened pipette tip and transferred into pre weighed glass vials and stored in -20°C. The next day the supernatant samples were thawed and 600 mL ice cold MTBE (Methyl tert-butyl ether, Sigma Aldrich, South Africa) was added and incubated for 1 h at 4°C.

Phase separation was then induced by adding 154 mL of 100 mM% triethylammonium bicarbonate (TEAB, Sigma Aldrich, South Africa) with Halt protease inhibitor cocktail (Thermo Scientific, Pierce, South Africa). Samples were then centrifuged to separate phases 12 000g x 14 min. Phases were not separating therefore additional 50 µl (x2) of diethylether was added to each sample and centrifuged for 1 min at 12 000 x g to induce phase separation. Phase separation was not observed after this step therefore samples were then stored at -20°C overnight to induce separation. The next day separation of phases was observed in all samples. The upper phase was removed and placed in pre-weighed 2 mL glass vials and stored at -20°C.

The lower phase was removed and transferred to 2 mL Eppendorf microcentrifuge tubes. Four volumes of ice-cold methanol was added to the lower phase and incubated for 2 h at -20°C to allow for precipitation of proteins out of solution. The Lower phase was then centrifuged at 12 000 x g for 10 min. Supernatant (metabolite fraction) was removed and placed in pre-weighed 2 mL glass vials and stored at -20 °C.

To the extracted pellet, 200 mL 50 mM TEAB pH 7.8 containing 8 M urea (Sigma Aldrich, South Africa) and 0.5% SDS (Sigma Aldrich, South Africa) and protease inhibitor cocktail (Thermo Scientific, Pierce, South Africa) was then added and sonicated for 10 min at 4˚C. This was followed by a centrifugation step to bring solution down. Four volumes of ice-cold methanol was added to each samples and centrifuged at 12 000 x g for 10 min. The

supernatant was removed and discarded, and the protein pellet was retained for proteomic analysis.

4.10.2 Protein solubilisation

To the protein pellets 50 mL 50 mM TEAB pH 7.8 containing 8 M urea and 0.5% SDS were added and sonicated whilst intermittently vortexing until the pellet was dissolved. Each sample was then diluted 1:9 in deionized water. The remainder of the sample was then dried down in a Thermo Scientific™ SpeedVac™ Vacuum Concentrator for 1 h.

4.10.3 Concentration determination

A Bradford assay was performed to determine protein concentration within each sample. Bradford 1 x solution (10% Coommassie b.blue-G, 10% of 99% Methanol, 20% of 85% phosphoric acid and 70% distilled water) was made up and filtered. A BSA protein standard (Sigma Aldrich, South Africa) of 10 µL was aliquoted in the first row of the plate with protein concentrations ranging from 0 to 1 mg/mL and 10 µL of the 1:9 diluted samples were added to specific wells of the 96 well plate. Filtered Bradford reagent of 90 µL was added to each well and absorbance was read at 595 nm using a micro-plate reader (Multiskan GO 1.00.40, Thermo fisher scientific, USA).

4.10.4 Second Tissue Extraction

The skin structure did not open up properly therefore a higher detergent concentration was used in order to open up the structure.

First Extract: Five volumes (500 µL) of 2% Triton X100 (%v/v), 4 M guanidine hydrochloride in 25 mM 3-(N-morpholino) propanesulfonic acid pH 7.5 (MOPS, Sigma Aldrich, South Africa) containing 200 mM sodium chloride (Sigma Aldrich, South Africa), 5 mM TCEP and protease inhibitor cocktail was added to the remainder tissue extracts that were previously stored at -20°C. Proteins were extracted with intermittent sonication for 1 h at 4°C. The 500 µL of supernatant was removed and this step was repeated for the remaining tissue at 4°C overnight. The supernatant was removed, and the tissue was washed with five volumes of

deionized water in order to remove any guanine from the remaining tissue. The supernatants collected from this step were combined to form Extract 1.

Second Extract: The buffer used for the second extract was 3-[(3-**ch**olamidopropyl) dimethylammonio]-1-propanesulfonate 0.4% m/v (CHAPS; Sigma Aldrich, South Africa) in MOPS,4 M Urea (Sigma Aldrich, South Africa) containing 200 mM sodium chloride (Sigma Aldrich, South Africa), 5 mM TCEP and protease inhibitor cocktail were added to the remainder tissue extracts from extract 1. Proteins were extracted with intermittent sonication for 2 h at 4°C. Supernatant was collected and this step was repeated for the remainder tissue. The supernatants were collected and combined to form the second extract. (No wash needed because 3rd extract contains SDS which is compatible with reagents in the 2nd extract)

Third extract: Five volumes of 2% SDS in 100 mM sodium carbonate buffer pH 10 was added to remaining tissue from the second extract and incubated for 2 h at 4°C. The supernatant was collected. This step was repeated, and the supernatants were combined to form the third extract.

Clean up: The first extract received ten volumes liquid: liquid extraction with hexane followed by 2 x five volume liquid: liquid extraction with hexane. A chloroform methanol clean-up was then performed. Briefly, 4 volumes of methanol (Romil, United Kingdom) was added to 100 mL extract and vortexed vigorously before the addition of 100 mL chloroform (Merck, USA). The mixture was again vigorously vortexed before the addition of 300 mL deionized water. The sample was centrifuged at 12 000 x *g* to induce phase separation. The upper phase was aspirated without disturbing the protein wafer on the interphase. An additional 400 mL of methanol was added and the sample centrifuged to pellet the protein. This was done to prevent the Triton X100 from interfering with the Mass spectrometry analysis and trypsinisation. The second and third extracts received 2 x five volumes of hexane liquid: liquid clean up steps prior to chloroform methanol extraction.

All the extracts (i.e. first, second and third) were then combined and a Bradford assay was performed as described previously to determine protein concentration.

4.10.5 On-bead protein digestion

All reagents are analytical grade or equivalent. Samples were re-suspended in 50 mM triethyl ammonium bicarbonate (TEAB; Sigma Aldrich, South Africa) before reduction with 5

mM triscarboxyethyl phosphine (TCEP; Fluka, South Africa) in 50 mM TEAB for 1 h at 60°C. Cysteine residues were thiomethylated, with 20 mM *S*-Methyl methanethiosulfonate (Sigma Aldrich, South Africa) in 50 mM TEAB for 30 min at room temperature. After thiomethylation the samples were diluted two-fold with binding buffer (100 mM Sodium acetate, 30% acetonitrile, pH 4.5). The protein solution was added to MagResyn (Resyn Biosciences South Africa) HILIC magnetic particles prepared according to manufacturer's instructions and incubated overnight at 4°C. After binding, the supernatant was removed and the magnetic particles washed twice with washing buffer (95% acetonitrile, CAN, Romil, United Kingdom). After washing the magnetic particles were suspended in 50 mM TEAB containing trypsin (New England Biosystems, USA) to a final ratio of 1:10. After a 6 h incubation at 37°C the peptides were extracted once with 50 µL water and once with 50% acetonitrile (Romil, United Kingdom). The samples were dried down and re-suspended in 30 mL 2% acetonitrile: water; 0.1% Formic acid (FA; Sigma Aldrich, South Africa)

Residual digest reagents were removed using an in-house manufactured C_{18} stage tip (Empore Octadecyl C_{18} extraction discs, Supelco, Sigma Aldrich, South Africa). The samples were loaded onto the stage tip after activating the C_{18} membrane with 30 mL methanol (Romil, United Kingdom) and equilibration with 30 mL 2% acetonitrile: water; 0.1% FA. The bound sample was washed with 30 mL 2% acetonitrile: water; 0.1% FA before elution with 30 mL 50% acetonitrile: water 0.1% FA. The eluate was evaporated to dryness. The dried peptides were dissolved in 2% acetonitrile: water; 0.1% FA for LC-MS analysis.

4.10.6 Peptide quantification

Samples were first dried in a concentrator for 3 h and resuspended in 30 µL of distilled water. A Pierce™ Quantitative Colorimetric Peptide Assay (Thermo fisher scientific, South Africa) was then performed as per manufacturer's instructions. Standard solutions (20 µL each) were plated in the first row of the 96 well plate ranging from 0 to 50 mg/µL. The samples were then further diluted in a 1:1 ratio in 10 µL of distilled water and 20 µL of sample was added to specific wells in the 96 well plate. To each well 80 µL of working solution was added. The plate was then incubated at 37°C for 15 min then read at 480 nm using a micro-plate reader (Multiskan GO 1.00.40, Thermo fisher scientific, USA).

4.10.7 Adding TMT tags to samples

Tandem Mass Tag (TMT) tags (Thermo Scientific, Pierce, South Africa) were first brought to room temperature. Samples were dried in a concentrator for 3 h and resuspended in 10 µL 100 mM TEAB at pH 8.0. The TMT tags were resuspended in 100% acetonitrile and vortexed twice for 30 sec each. Tags were then centrifuged briefly to pool solution together. Half the volume of the tags were each added to 14 µg of their respective samples as seen on Table 4.2. Samples containing tags were then incubated at room temperature for 2 h. An aliquot of the samples was taken for Quality control analysis and the rest were stored at -80°C until further analysis. Refer to Figure 4.9 on how TMT tags bind to peptides and are able to distinguish between samples when they are detected simultaneously as a single and indistinguishable precursor ion peak.

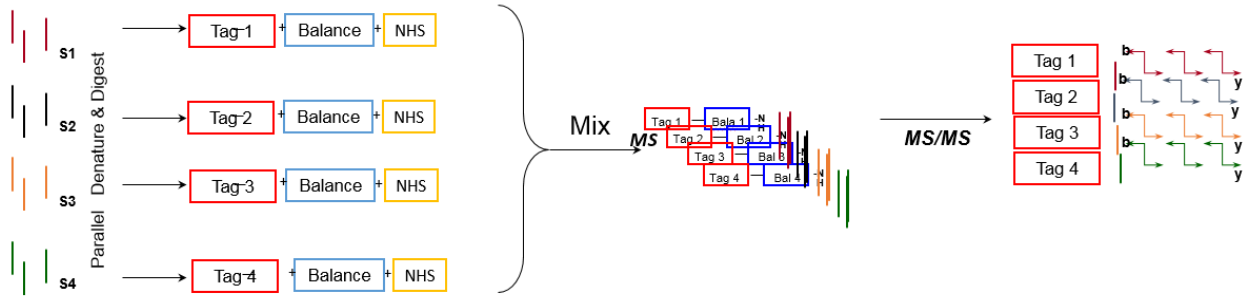

Figure 4.9. Theory of TMT tags. The tags consist of an MS/MS reporter group, a balancing arm and an amine reactive group (N- hydroxysuccinimide). The amine reactive group binds to the N- terminus of a peptide or to a lysine residue during labelling. Once labelled, all samples are mixed and analysed in a single liquid chromatography mass spectrometry (LC-MS) experiment. Because the isobaric tags possess the same chemical properties, all peptides from different TMT-labelled samples co-elute during LC separation. Once the peptides enter the mass spectrometer, they are detected simultaneously as a single and indistinguishable precursor ion peak.

Table 4.2. Identification of TMT tag added to specific samples.

Sample	ID label
3N7	126
3N5	127N
3N3	127C
3N4	128N
3N POOL	128C
CS3	129N
CS2	129C
CS1	130N
CS5	130C

4.10.8 First dimension High pH Reversed-Phase Peptide Fractionation

A high pH Reversed-Phase Peptide Fractionation Kit (Thermo Scientific, Pierce, South Africa) was performed as per manufactures instruction to fractionate the digested samples containing the TMT tags before LC/MS analysis. The purpose of this first dimension reversed phase fractionation is to simplify the mixture prior to LC-MS/MS and remove the unbound TMT tags from the sample.

Reversed-Phase Fractionation Spin Column containing 20 mg of resin in a 1:1 water/DMSO slurry was centrifuged at 5000 x *g* for 2 min to remove distilled water from column. The column was conditioned with 300 µL of 2% acetonitrile: water; 0.1% FA and centrifuged at 5000 x *g* for 2 min twice. The column was then treated with 300 µL of 0.1% Trifluoroacetic acid (TFA, Thermo Scientific, Pierce, South Africa) and centrifuged at 5000 x *g* for 2 min twice.

Digested samples were dried in a concentrator for 2 h leaving an oily residue. They were then combined, loaded on to Reversed-Phase Fractionation Spin Columns and centrifuged at 3000 x *g* for 2 min. The run through was collected and stored at -80°C. The column was then loaded with 300 µL of a gradient based step wise elution solutions with increasing acetonitrile (ACN): water; 0.1% TFA concentrations (5%, 10%, 12.5%, 15%, 17.5%, 20%, 22.5%, 25% and 50% ACN respectively) and centrifuged at 3000 x *g* for 2 min after each elution solution was added. The follow through fractions were collected after each eluting step into labelled 1.5 mL Eppendorf's. Fractions were then dried overnight in a concentrator for further analysis on the LC/MS.

4.10.9 Liquid chromatography

Quality control analysis: Dionex nano-RSLC

Liquid chromatography was performed on a Thermo Scientific Ultimate 3000 RSLC equipped with a 5 mm x 300 µm C_{18} trap column (Thermo Scientific, South Africa) and a nanoEase M/Z Peptide CSH 25cmx75µm 1.7 µm particle size C_{18} column (Waters, South Africa) analytical column. The solvent system employed was loading: 2% acetonitrile: water; 0.1% FA; Solvent A: 2% acetonitrile: water; 0.1% FA and Solvent B: 100% acetonitrile: water. The samples were loaded onto the trap column using loading solvent at a flow rate of 2 µL/min from a temperature controlled autosampler set at 7°C. Loading was performed for 5 min before the sample was eluted onto the analytical column. Flow rate was set to 300

nL/min and the gradient generated as follows: 5.0% -35%B over 80 min using Chromeleon non-linear gradient 6; 30% -50% B from 80 -100. Chromatography was performed at 45°C and the outflow delivered to the mass spectrometer through a stainless-steel nano-bore emitter.

4.10.10 Tandem Mass Tag analysis

Liquid chromatography was performed on a Thermo Scientific Ultimate 3000 RSLC equipped with a 5 mm x 300 µm C_{18} trap column (Thermo Scientific, South Africa) and a nanoEase M/Z Peptide CSH 25 cm x75 µm 1.7 µm particle size C_{18} column (Waters, South Africa) analytical column. The solvent system employed was loading: 2% acetonitrile: water; 0.1% FA; Solvent A: 2% acetonitrile: water; 0.1% FA and Solvent B: 100% acetonitrile: water. The samples were loaded onto the trap column using loading solvent at a flow rate of 2 µL/min from a temperature controlled autosampler set at 7°C. Loading was performed for 5 min before the sample was eluted onto the analytical column. Flow rate was set to 300 nL/min and the gradient generated as follows: 5.0% -35%B over 130 min; 30% -50% B from 130-150 min using Chromeleon non-linear gradient 6. Chromatography was performed at 45°C and the outflow delivered to the mass spectrometer through a stainless-steel nano-bore emitter.

4.10.11 Mass spectrometry

Quality control analysis: Mass spectrometry was performed using a Thermo Scientific Fusion mass spectrometer equipped with a Nanospray Flex ionization source. The sample was introduced through a stainless-steel emitter. Data was collected in positive mode with spray voltage set to 1.8 kV and ion transfer capillary set to 175°C. Spectra were internally calibrated using polysiloxane ions at m/z = 445.12003 and 371.10024. MS1 scans were performed using the orbitrap detector set at 120 000 resolution over the scan range 350-1500 with AGC target at 4 E5 and maximum injection time of 50 ms. Data was acquired in profile mode.

MS2 acquisitions were performed using monoisotopic precursor selection for ion with charges +2-+7 with error tolerance set to +/- 10 ppm. Precursor ions were excluded from fragmentation once for a period of 60 sec. Precursor ions were selected for fragmentation in HCD mode using the quadrupole mass analyser with HCD energy set to 30%. Fragment

ions were detected in the orbitrap mass analyzer set to 30 000 resolution. The AGC target was set to 5E4 and the maximum injection time to 80 ms. The data was acquired in centroid mode.

Tandem Mass Tag Analysis – first pass: Mass spectrometry was performed using a Thermo Scientific Fusion mass spectrometer equipped with a Nanospray Flex ionization source. The sample was introduced through a stainless-steel emitter. Data was collected in positive mode with spray voltage set to 1.8 kV and ion transfer capillary set to 175°C. Spectra were internally calibrated using polysiloxane ions at m/z = 445.12003 and 371.10024. MS1 scans were performed using the orbitrap detector set at 120 000 resolution over the scan range 350-1750 with AGC target at 4 E5 and maximum injection time of 50ms. Data was acquired in profile mode.

MS2 acquisitions were performed using monoisotopic precursor selection for ion with charges +2-+7 with error tolerance set to +/- 10 ppm. Precursor ions were excluded from fragmentation once for a period of 60 sec. Precursor ions were selected for fragmentation in HCD mode using the quadrupole mass analyser set at 0.7 m/z isolation width with HCD energy set to 38%. Fragment ions were detected in the orbitrap mass analyzer set to 50 000 resolution. The AGC target was set to 1E5 and the maximum injection time to 105 ms. The data was acquired in centroid mode.

Tandem Mass Tag Analysis – Second Pass: Mass spectrometry was performed using a Thermo Scientific Fusion mass spectrometer equipped with a Nanospray Flex ionization source. The sample was introduced through a stainless-steel emitter. Data was collected in positive mode with spray voltage set to 1.8 kV and ion transfer capillary set to 175°C. Spectra were internally calibrated using polysiloxane ions at m/z = 445.12003 and 371.10024. MS1 scans were performed using the orbitrap detector set at 120 000 resolution over the scan range 350-1750 with AGC target at 4 E5 and maximum injection time of 50 ms. Data was acquired in profile mode.

The targeted mass exclusion filter was populated using unambiguously assigned precursor m/z from the analysis of the first pass with a retention window of 1 min. MS^2 acquisitions were performed on ions not excluded using monoisotopic precursor selection for ion with charges +2-+7 with error tolerance set to +/- 10 ppm. Precursor ions were excluded from fragmentation once for a period of 60 sec. Precursor ions were selected for fragmentation in HCD mode using the quadrupole mass analyser set at 0.7 m/z isolation width with HCD energy set to 38% ±5%. Fragment ions were detected in the orbitrap mass analyzer set to

50 000 resolution. The AGC target was set to 1E5 and the maximum injection time to 125 ms. The data was acquired in centroid mode.

4.10.12 Data Analysis

The raw files generated by the mass spectrometer were imported into Proteome Discoverer v1.4 (Thermo Scientific, South Africa) and processed using the Sequest and MSAmanda algorithms. Database interrogation was performed against a concatenated database created using uniprot *Mus musculus* database (reviewed entries only; 17461 entries) concatenated with the cRAP contaminant database (https://www.thegpm.org/crap/). Semi-tryptic cleavage with 2 missed cleavages was allowed. Precursor mass tolerance was set to 20 ppm and fragment mass tolerance set to 0.05 Da. Demamidation (NQ), oxidation (M) were allowed as dynamic modifications and thiomethyl of C, TMT-6 of K and n as static modification. Peptide validation was performed using the Target-Decoy PSM validator node. The results files were imported into Scaffold 1.4.4 and identified peptides validated with the Peptide and Protein Prophet algorithms included in Scaffold. Reporter ion extraction was also performed by Scaffold.

A cut off of 1.5 fold difference between the acute and chronic groups was considered a good way to identify proteins of interest to investigate further. The identified proteins were then inserted into STRING (Szklarczyk et al., 2019) (freely available biological data base cite: https://string-db.org/) to identify their functional protein association networks.

Chapter 5 : Results

5.1 Phase I: Determination of optimum NEP concentration for chronic wound induction.

5.1.1 Animal welfare during the early stages (2 days) post wounding

For day 0 sample collection, full-thickness excisional wounds were made on a total of 17 obese pre-diabetic (B6.Cg-Lepob/J, ob/ob) mice (>40 g, 10-14 weeks old) [treatment groups: Saline (n=4), Low NEP (n=4), NEP medium (n=4) and NEP high (n=5)]. During the optimization of the surgical procedures, an initial survival rate of 83% was observed (3 died) and samples from these animals were excluded and not counted in the n=28. NEP treatment had no effect on the survival rate of the animals, instead prolonged exposure to anaesthesia (> 20 min) resulted in respiratory problems and heart failure in the ob/ob mice. To avoid this adverse effect, animals were shaved a day prior to wounding in order to limit the required period under anaesthesia. Following this adjustment, an additional 14 obese-prediabetic mice were wounded [treatment groups: Saline (n=3), low NEP (n=3), medium NEP (n=3) or high NEP (n=5)] and tissue harvested on day 2 post wounding.

For each animal, a wellness score was calculated based on appearance and behaviour during the initial 2 days post wounding and treatment (Refer to *Appendix B* for the animal welfare monitoring sheet template and scoring parameters). No significant difference was observed in appearance and behaviour of the animals within the different treatment groups with scores ranging between 1 and 2 (Fig. 5.1 A-B). During this initial phase following wounding, animals were slightly less attentive and interactive than before wounding however, no significant differences were observed between day 0 to 2. Pain management in the form of locally applied lignocaine and oral acetaminophen did however ensure that animals were able to feed normally. No difference was observed in appearance and behaviour comparing the NEP groups to the control saline group or between the different treatment groups. There were no significant differences in body weight (g) between day 0 (Saline 49.22 ± 1.30 g; low NEP 46.29 ± 2.31 g, medium NEP 44.68 ± 0.95 g, high NEP 44.98 ± 1.46 g) (mean ± SE g) and day 2 (Saline 45.93 ± 0.26 g; low NEP 40.63 ± 0.66 g, medium NEP41.35 ± 2.21 g, high NEP 42.53 ± 1.79 g) within the treatment groups (Fig. 5.1 C). No significant difference was observed between the treatment groups on both day 0 and 2. Significance may differ between days 0 and 2 if the number of animals per group was increased.

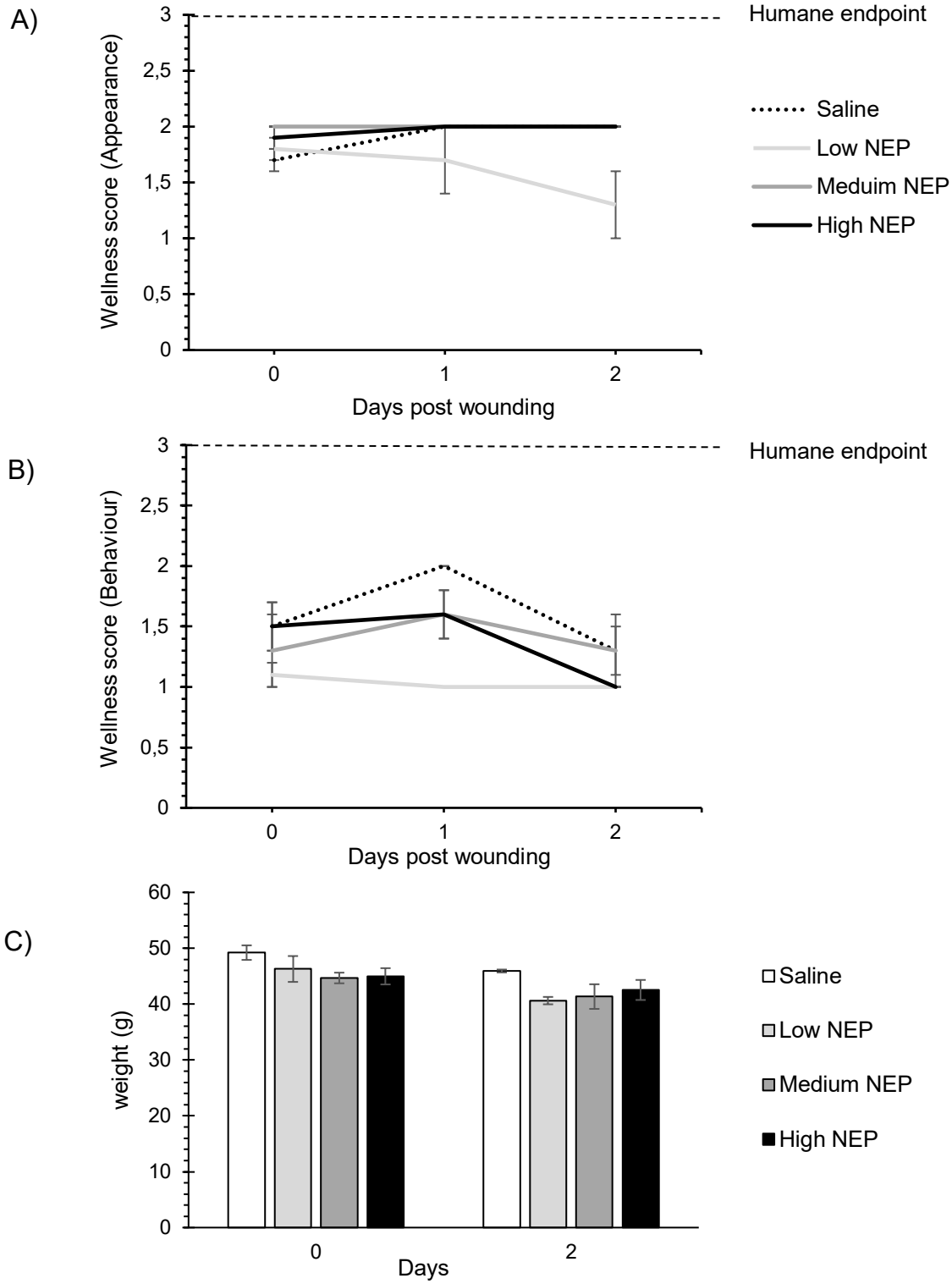

Figure 5.1. Animal wellness during the initial 2 days post wounding. Animal (B6.Cg-Lep^{ob}/J, ob/ob) wellness was measured over a period of 2 days post wounding by assessing A) Appearance, B) Behaviour and C) body weight. For the treatment groups either Saline (n=3), low NEP concentration (0.33 mg/µL, n=3), medium NEP concentration (0.68 mg/µL, n=3) or high NEP concentration (1.02 mg/µL, n=5) were injected around the wound edges immediately after injury. **A)** Animal wellness: Appearance. The Appearance score was assigned as follows: 1 – Well groomed, no discharges/ lesions and normal breathing/ posture; 2 – rough coat, slight discharges/lesions and abnormal breathing and 3 – very rough coat, noticeable discharges/ lesions and definite difficulty breathing. **B)** Animal wellness: Behaviour. The behaviour score was assigned as follows: 1 – attentive, inquisitive, interactive and normal walk/pace; 2 – not very interactive, less attentive, less active and abnormal walk/pace and 3 – not active, unresponsive. **C)** Animal weight (g) was measured on day 0 pre-wounding and on day 2 post wounding. **Statistical analysis:** Factorial ANOVA with Tukey's post hoc test, *p<0.05 was considered significant.

5.1.2 Wound edge NEP enzymatic activity at 2 days- post wounding.

Firstly, there were no significant differences in NEP activity in saline control (892 ± 153 pmol) (mean ± SE) versus low NEP (665 ± 99 pmol), medium NEP (750 ± 61 pmol) and high NEP (909 ± 104 pmol) treatments on Day 0 (Figure 5.2). A similar result was obtained on Day 2, with no significant differences between saline (286 ± 52 pmol), low NEP (389 ± 33 pmol), medium NEP (282 ± 58 pmol) and high NEP (301 ± 29 pmol) treatment groups (Figure 5.2). A significant effect of time ($p<0.001$) was evident in all four treatment groups with NEP activity being higher on day 0 compared to day 2, Saline: x3 fold higher, low NEP: x1.7 fold higher, medium NEP: x2.7 fold higher and high NEP: x3 fold higher. No difference could however be detected in NEP activity between treatment groups at the same time point (Fig. 5.2).

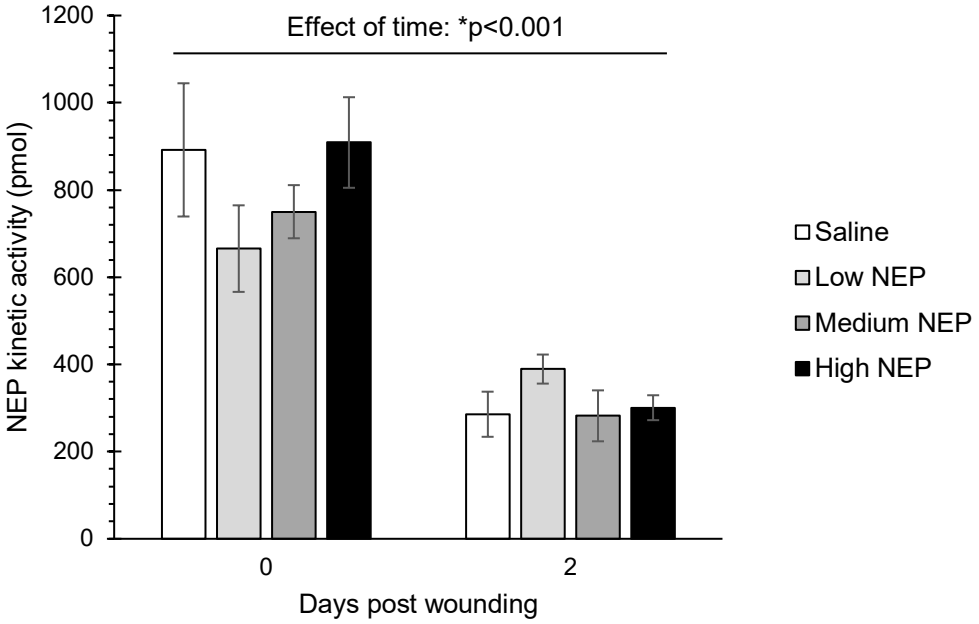

Figure 5.2. NEP enzymatic activity. NEP enzyme activity was measured in kinetic mode over a period of 120 min in 6 µg of protein extracted from wound tissue (n=3 biological repeats per group). **Statistical analysis:** Repeated measures ANOVA with Tukey's post hoc test. *p<0.001 indicate significant effect of time.

5.1.3 The expression of substance P within the wounded area and wound edges during the early stages (2 days) post wounding within each treatment group.

The expression of substance P was quantified as the percentage surface area stained positive within either the wounded area or the wound edges for each treatment group (Fig. 5.3-5.4). Within the wounded area, a significant effect of time ($p<0.01$) was evident with an increase from day 0 to day 2 in substance P staining in all treatment groups, Saline: x6 fold increase, low NEP: x6 fold increase, medium NEP: x5 fold increase and high NEP: x5 fold

increase (Fig. 5.3 A). There were no significant differences in substance P expression in the wound area between treatment groups on day 0, saline (1.6 ± 0.45%) (mean ± SE %), low NEP (2.6 ± 0.5%), medium NEP (1.6 ± 0.26%) and high NEP (1.5 ± 0.38%). On day 2, a greater percentage (x2 fold higher) ($p<0.05$) of the wound area stained positive for substance P in the animals treated with a low concentration of NEP (15 ± 3.76%) compared to the high concentration (7.1 ± 1.44%) (Fig. 5.3 A). Medium concentration (7.1 ± 2.29%) did not differ significantly between saline (9.3 ± 2.08%), low and high NEP treatments within the wound area on day 2. In the wound edges, no difference could be detected in substance P staining between treatment groups at the same time point (Fig. 5.3 B). Representative IHC images are shown in Figure 5.4.

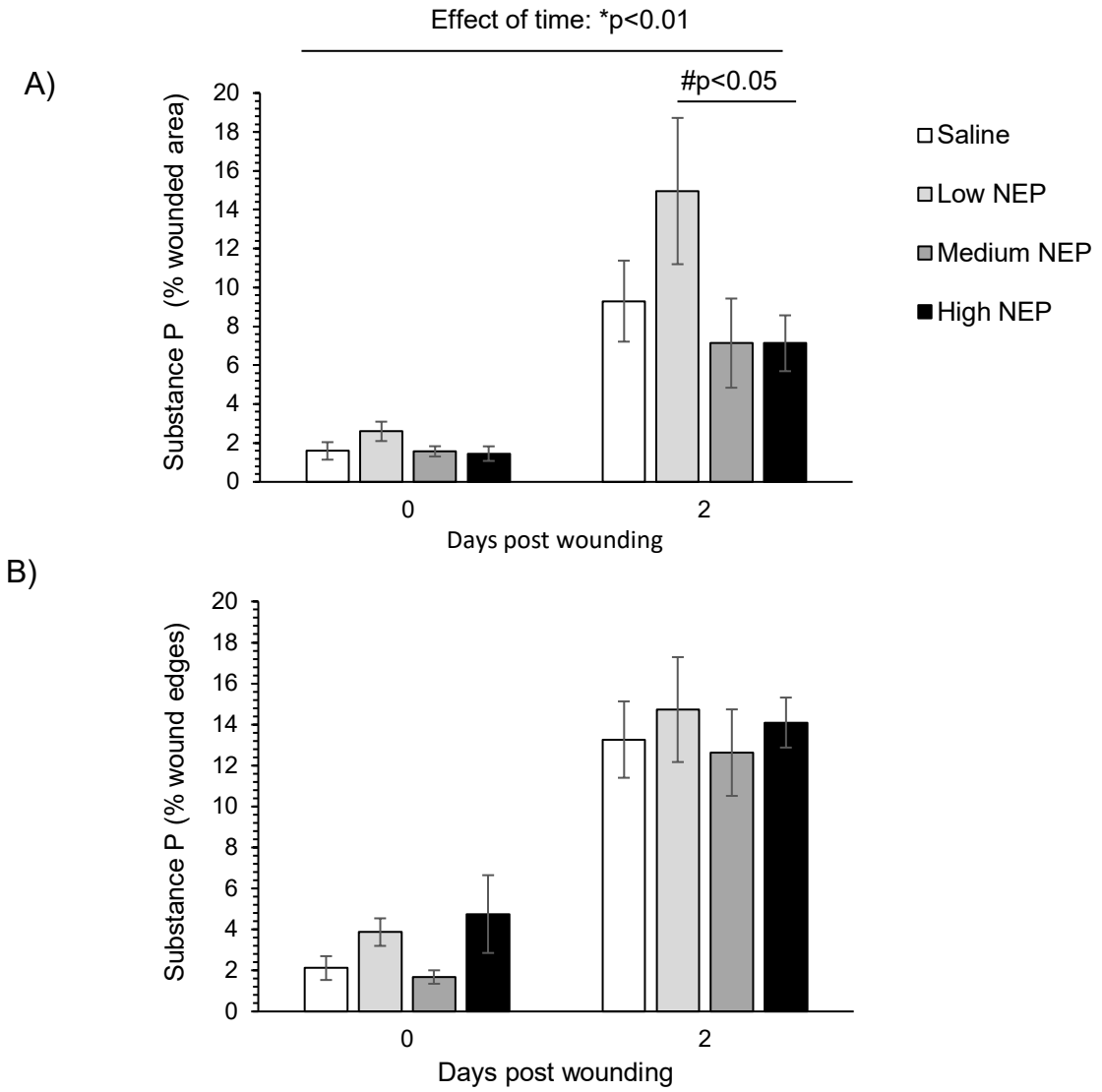

Figure 5.3. Substance P expression in wound area and wound edge (% surface area). Positive IHC staining for Substance P was assessed in **A)** Wound area and **B)** Wound edges on days 0 and 2 post wounding. For the treatment groups either Saline (n=3), low NEP concentration (0.33 mg/µL, n=3), medium NEP concentration (0.68 mg/µL, n=3) or high NEP concentration (1.02 mg/µL, n=5) were injected around the wound edges immediately following injury. **Statistical analysis:** Factorial ANOVA with Tukey's post hoc test. *p<0.01 indicate significant effect of time #p<0.05 indicates significant treatment effect at the same time point.

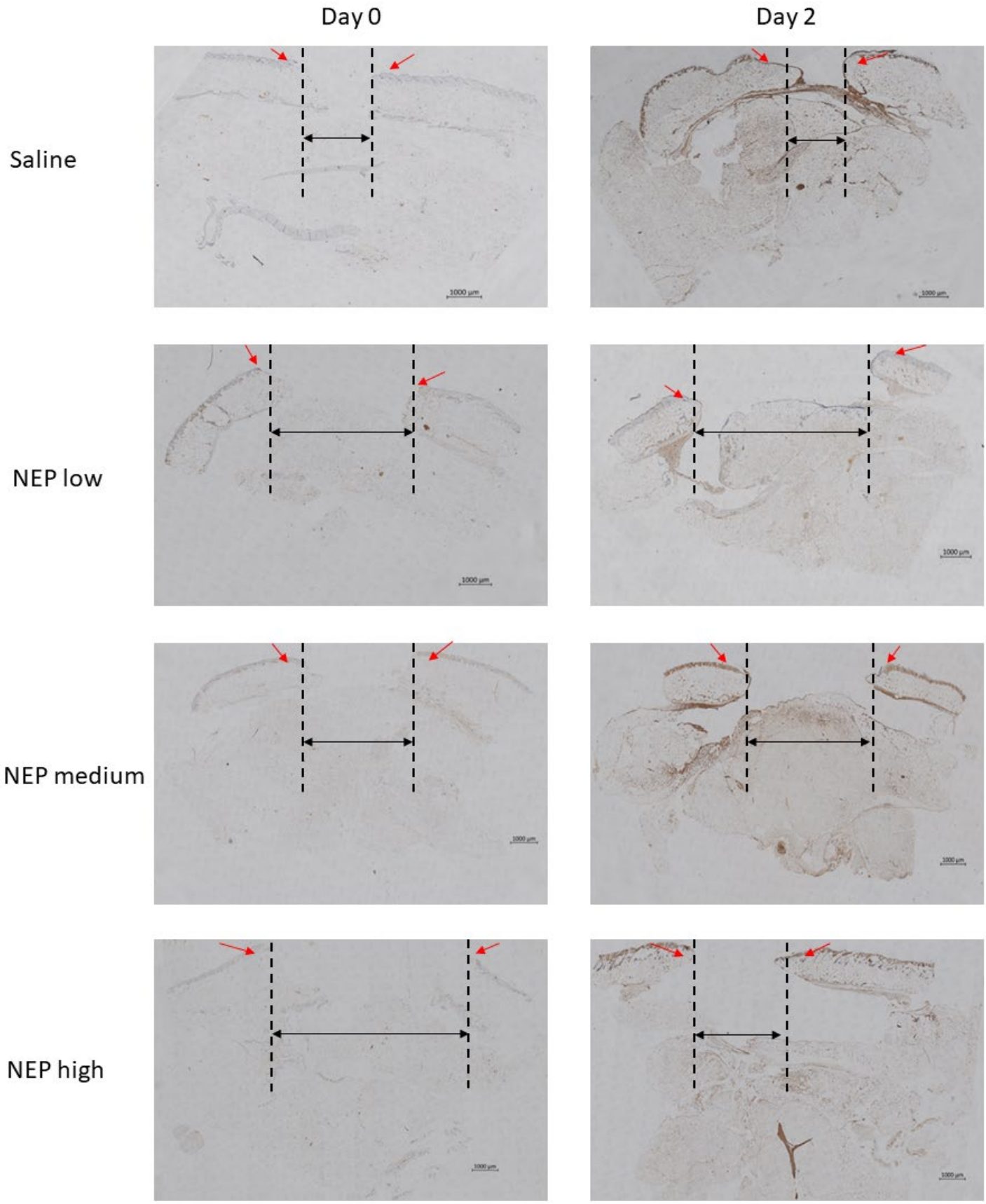

Figure 5.4. Representative IHC images of Substance P staining. Histological cross sections were stained with an anti-Substance P antibody (Immunohistochemistry) and an eosin stain. Images (tile scan) were acquired at 10x magnification indicating wound area (black dotted line) and wound edges (red arrows). For the treatment groups either Saline (n=3), NEP low (n=3), NEP medium (n=3) or NEP high (n=5). were injected around the wound edges immediately following injury. Scale bar= 1000µm.

5.1.4 The high dose of NEP (1.02 mg/μL) injected around the wound edges on day 0 increased MMP-9 expression two days post wounding.

Tissue MMP-9 expression on day 0 and 2 post wounding was determined using an ELISA assay in all treatment groups. Sample harvested immediately post injury (day 0) revealed no difference in MMP-9 expression between the treatment groups, saline (0.298 ± 0.1 OD) (mean ± SE OD), low NEP (0.302 ± 0.03 OD), medium NEP (0.209 ± 0.15 OD) and high NEP (0.453 ± 0.12 OD) (Fig. 5.5). A significant increase (x2.3fold, $p<0.05$) in tissue MMP-9 expression was however evident on day 2 post wounding in the animals treated with a high concentration of NEP (0.479 ± 0.04 OD) compared to saline (0.211 ±0.01 OD) at the same time point. No significant differences were seen on day 2 between saline control, low (0.143 ± 0.01 OD) and medium (0.093 ± 0.23 OD) NEP treatments (Fig.5.5). There were no differences observed between day 0 and day 2 for all the treatment groups.

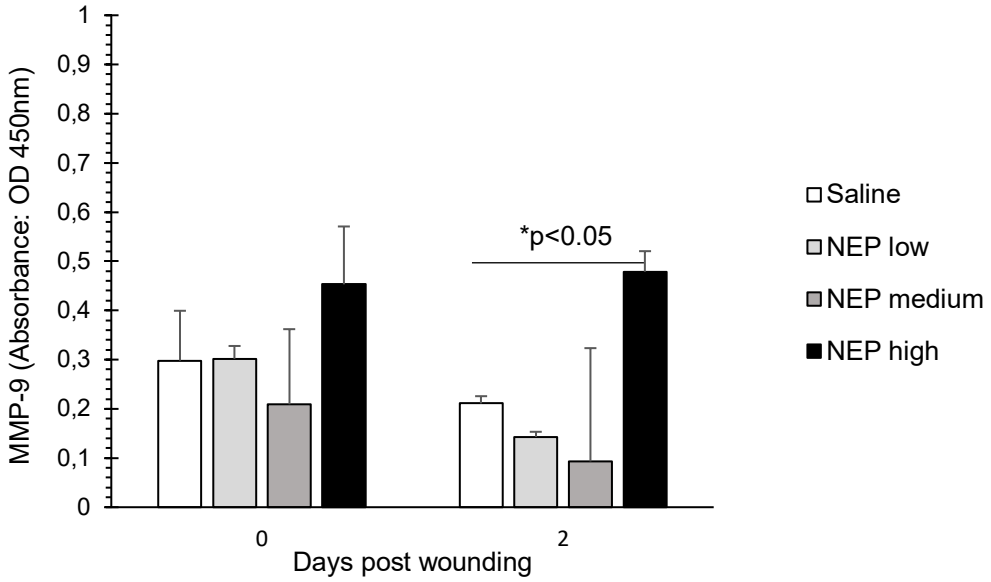

Figure 5.5. Tissue MMP-9 expression during the first two days post wounding. Wound tissue was collected (n=3 mice per treatment group, x2 wounds per animal) and total protein extracted (0.25mg/μL) from these samples to determine MMP-9 expression levels. Treatment groups: Saline (vehicle control), low NEP concentration (0.33 mg/μL), medium NEP concentration (0.68 mg/μL) or high NEP concentration (1.02 mg/μL). **Statistical analysis:** Factorial ANOVA with Tukey's post hoc test. *$p<0.05$ indicates significant differences between groups at the same time point. NOTE: Known standards were not included onto the assay, therefore quantification in terms of pg/mL were unfortunately not possible. Values are thus presented as absorbance read (OD450nm).

5.1.5 Wound fluid: The high dose of NEP (1.02 mg/μL) injected around the wound edges on day 0 decreased cytokine levels 2 days post wounding

Wound fluid was collected on day 2 post wounding for all treatment groups and the cytokine profile of 10 pro-inflammatory cytokines; 7 chemokines and 5 anti-inflammatory cytokines within the wound fluid was assessed using a multi-plex bead array assay (Table 5.1). Due

to the small volume of wound fluid collected from each animal, all biological repeats (n=3) for the same treatment group were pooled together prior to analysis. Compared to saline, treatment with a high concentration of NEP induced an overall decrease (> 2-fold) in the levels of pro-inflammatory cytokines (IL-1β, IL-6, IL-9, IL-12p40, IL-12p70, IL-17, IFNγ), chemokines (Eotaxin, G-CSF, GM-CSF, KC, MIP-1α, MIP-1β) and anti-inflammatory cytokines (IL-2, IL-3, IL-4, IL-5, IL-10, IL-13). Refer to table 5.1.

Table 5.1: Cytokine Profile of day 2 wound fluid comparing pooled samples from saline versus pooled samples of each individual NEP group.

	ob/ob									
	Saline		NEP low			NEP medium			NEP high	
	pg/mL	(set=1)	pg/mL	fold change		pg/mL	fold change		pg/mL	fold change
Proinflammatory										
IL-1α	266	(1,0)	280	(1,1)	-	587	(2,2)	↑	219	(0,8) -
IL-1β	54	(1,0)	37	(0,7)	-	88	(1,6)	-	19	(0,4) ↓
IL-6	2672	(1,0)	2702	(1,0)	-	3569	(1,3)	-	873	(0,3) ↓
IL-9	11	(1,0)	4	(0,4)	↓	7	(0,6)	-	6	(0,5) ↓
IL-12(p40)	84	(1,0)	100	(1,2)	-	171	(2,0)	↑	45	(0,5) ↓
IL-12(p70)	227	(1,0)	116	(0,5)	↓	186	(0,8)	-	97	(0,4) ↓
IL-17	8	(1,0)	2	(0,3)	↓	7	(0,8)	-	2	(0,3) ↓
IFN-γ	13	(1,0)	5	(0,4)	↓	8	(0,6)	-	6	(0,5) ↓
RANTES	72	(1,0)	128	(1,8)	-	96	(1,3)	-	73	(1,0) -
TNF-a	106	(1,0)	59	(0,6)	-	241	(2,3)	↑	56	(0,5) ↓
Chemokines										
Eotaxin	630	(1,0)	604	(1,0)	-	487	(0,8)	-	226	(0,4) ↓
G-CSF	10425	(1,0)	7357	(0,7)	-	17277	(1,7)	-	5200	(0,5) ↓
GM-CSF	45	(1,0)	22	(0,5)	↓	35	(0,8)	-	16	(0,3) ↓
KC	5031	(1,0)	3402	(0,7)	-	7085	(1,4)	-	1258	(0,3) ↓
MCP-1	10444	(1,0)	6812	(0,7)	-	13694	(1,3)	-	5858	(0,6) -
MIP-1α	1115	(1,0)	714	(0,6)	-	5308	(4,8)	↑	436	(0,4) ↓
MIP-1β	1336	(1,0)	901	(0,7)	-	2005	(1,5)	-	555	(0,4) ↓
Anti-inflammatory										
IL-2	5	1,0	2	(0,4)	↓	4	(0,7)	-	3	(0,6) -
IL-3	7	1,0	4	(0,5)	↓	4	(0,6)	-	3	(0,5) ↓
IL-4	16	1,0	1.09	(0,07)	↓	9	(0,5)	↓	0.27	(0,02) ↓
IL-5	8	1,0	3	(0,3)	↓	4	(0,5)	↓	3	(0,4) ↓
IL-10	45	1,0	21	(0,5)	↓	47	(1,1)	-	22	(0,5) ↓
IL-13	116	1,0	73	(0,6)	↓	89	(0,8)	-	61	(0,5) ↓

Footnote: Cytokine profile was generated by analysing wound fluid collected on day 2 post wounding. Wound fluid was pooled for each treatment group and analysed using Bioplex 23 cytokine assay kit. Cytokine results are expressed in pg/mL and changes of more than 2 fold were indicated by ↑ (increase) and ↓ (decrease). **Abbreviations:** IL, interleukin; IFN- γ, interferon gamma; TNF-α, tumor necrosis factor alpha; GCSF, granulocyte colony-stimulating factor; GMCSF, granulocyte macrophage colony-stimulating factor; KC, keratinocyte chemoattractant; MCP, macrophage chemoattractant protein; MIP, macrophage inflammatory protein.

Taken together, the data from phase I suggests that the high concentration of NEP (1.02 mg/µL) is needed to mimic some of the characteristics of a chronic wound during the early stages post wounding, namely overexpression of MMP-9 and delayed onset of inflammation.

5.2 Phase II: Comparison of the wound healing dynamics between the Acute and newly developed Chronic wound models over a period of 7 days.

The wound healing dynamics were compared in Acute (wild-type C57BL/6J mice: saline treatment) and Chronic (obese prediabetic B6.Cg-Lep^{ob}/J, ob/ob mice: optimum NEP treatment) wounds over 7 days.

5.2.1 Animal welfare over a period of 7 days post wounding

A significant difference was evident in the weight of the wild-type (n=5) (28.17 ± 0.36 g) (mean ± SE g) and ob/ob (n= 5) (44.98 ± 1.46 g) animals on day 0 pre-wounding (Fig. 5.6 A). Both the wild-type control and ob/ob animals lost approximately 3 g of their body weight during the initial 3 days post wounding. This accounted for 4-6% of total body weight in the ob/ob (chronic wound) and 12% in the wild-type (acute wound) groups. The acutely wounded animals (wild-type) were unable to recover their weight 7 days post wounding (25.19 ± 0.99 g) ($p<0.05$) compared to day 0 (28.17 ± 0.36 g). Whereas, the chronically wounded animals (ob/ob) were able to regain the lost body weight with no difference detected between day 0 (44.96 ± 1.46 g) and day 7 (45.62 ± 0.99 g) (Fig. 5.6 A). Both groups had a 100% survival rate over the 7 days post wounding (Fig. 5.6 B1-2).

The wounding procedure affected the appearance of both groups similarly with a score of 2 (rough coat, slight discharges/lesions) throughout the 7 days (Fig. 5.6 C1). A similar change in behaviour was also evident in both groups with a peak score of 1.5 (less attentive and interactive) within the first 24h post wounding and then returning to normal from day 2 onwards (Fig. 5.6 C2).

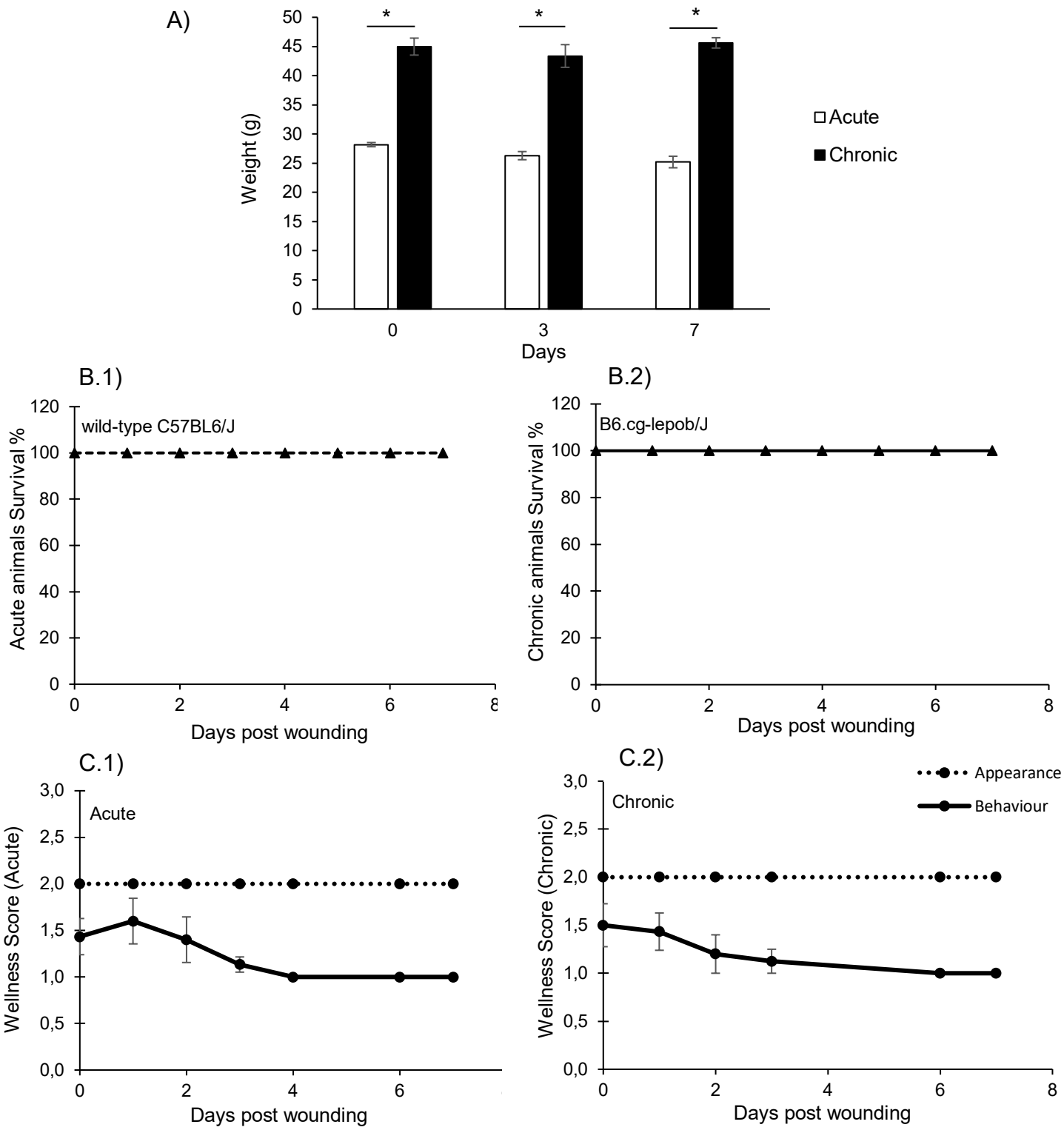

Figure 5.6. Comparison of animal wellnes in mice with acute (wild-type C57BL6/J) (n=5) **and chronic wounds** (B6.cg-lepob/J, ob/ob) (n=5) **over a period of 7 days. A)** Animal weight (g) of control (n=5) and obese (n=5) obtained on day 0 pre-wounding and day 2 and 7 post wounding and treatment**. B)** Kaplan-meier survival curve (%) of animals with B.1) Acute and B.2) Chronic wounds over 7 days post wounding. **C)** Wellness score in C.1) Acute and C.2) Chronic wounded animals were calculated by measuring appearance and behaviour. The dotted line indicates the appearance score which was assigned as follows: 1 – Well groomed, no discharges/ lesions and normal breathing/ posture; 2 – rough coat, slight discharges/lesions and abnormal breathing and 3 – very rough coat, noticeable discharges/ lesions and definite difficulty breathing. The solid line indicates the behaviour score which was assigned as follows: 1 – attentive, inquisitive, interactive and normal walk/pace; 2 – not very interactive, less attentive, less active and abnormal walk/pace and 3 – not active, unresponsive. **Statistical analysis:** Paired two-tailed T test. *p<0.05 indicates significant differences between groups at the same time point.

5.2.2 *Macroscopic wound closure is impaired in the new chronic wound model compared to acutely wounded animals*

The wounding procedure was performed consistently in both the acute and chronically wounded animals with no difference detected in macroscopic wound size between groups on day 0 immediately post wounding (Fig. 5.7 A). On day 7 post wounding, healing was evident in the acute group with wound closure and re-epithelialization visible, whereas no macroscopic signs of healing was evident within the chronic group (Fig. 5.7 B). Quantification of the percentage wound closure over the period of 7 days indicated a significant group effect ($p<0.05$) with 73.54 ± 3.08% (mean ± SE) wound closure in the acute group and only 43.51 ± 6.91% in the chronic group (Fig. 5.7 C).

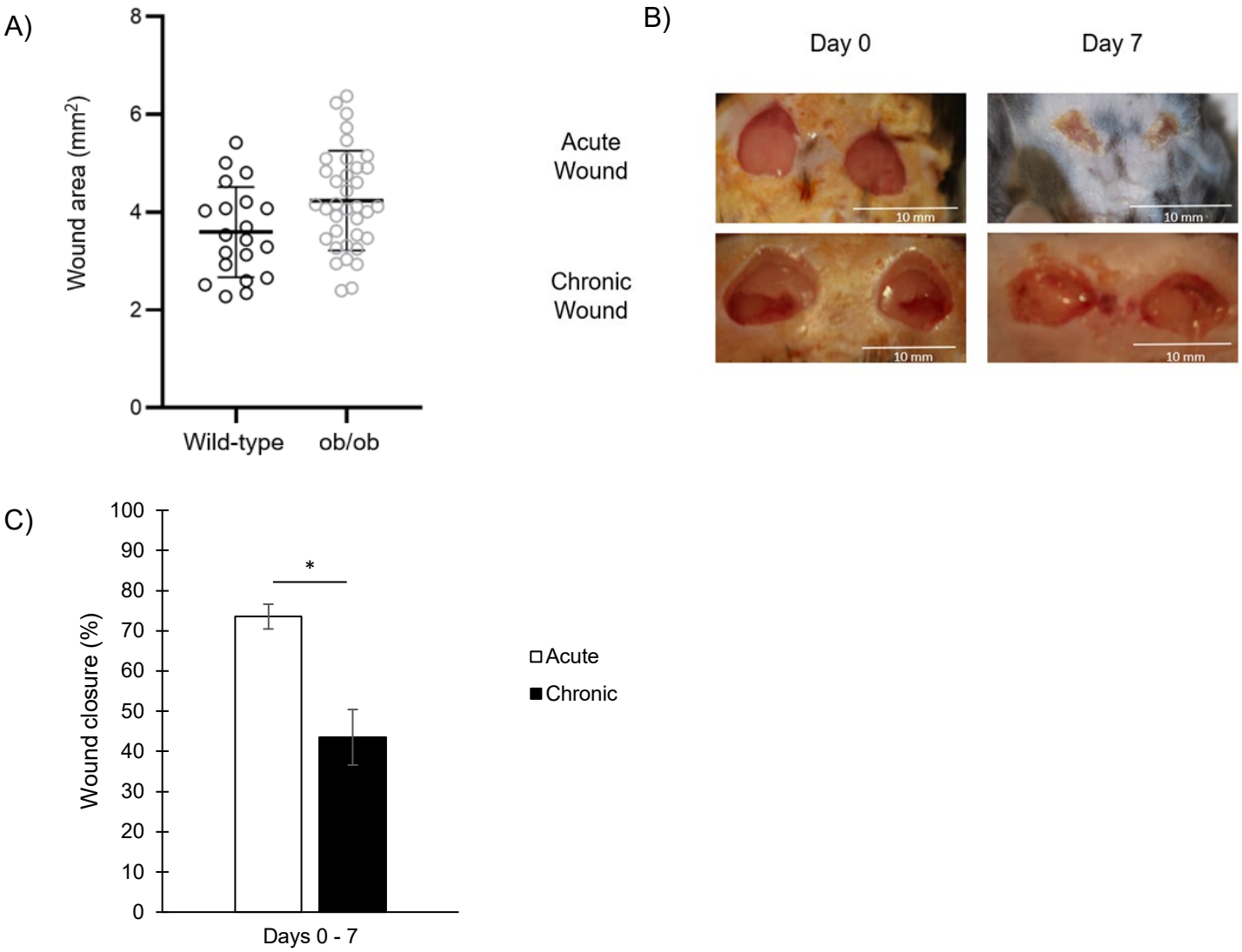

Figure 5.7. Macroscopic wound closure in acute versus chronic wounds. A) Wound area (mm^2) on day 0 immediately post wounding. **B)** Representative images of acute and chronic wounds on day 0 and day 7 post wounding of wild-type C57BL6/J mice treated with saline (Acute wound) and B6.cg-lepob/J (ob/ob), treated with NEP high (chronic wound). **C)** Percentage wound closure between day 0 and day 7 for both acute and chronic wounds were calculated using Image J software. **Statistical analysis:** Paired two-tailed T test. *$p<0.05$ indicates significant differences between groups at the same time point.

5.2.3 Histological scoring index: microscopic wound healing

5.2.3.1 Re-epithelialization is not evident in the chronic wounds

In the wound edges, the epithelial layer was thicker in the ob/ob animals (chronic wounds) (92 ± 7 µm) (mean ± SE µm) than in the wild type animals (acute wounds) (65 ± 7 µm) (Fig. 5.8-5.9). No signs of re-epithelization were however evident in the wound area of the chronic wounds (ob/ob animals) on day 7 post wounding, whereas newly formed epithelial were clearly visible in the acute wounds (wild type animals) at the same time point (Fig. 5.8-5.9). The newly formed epithelial layer in the wounded area of the acute wounds were furthermore thicker (89 ± 14 µm) than in the acute wound edges (65 ± 7 µm). Representative images illustrating re-epithelialization are shown in Figure 5.9.

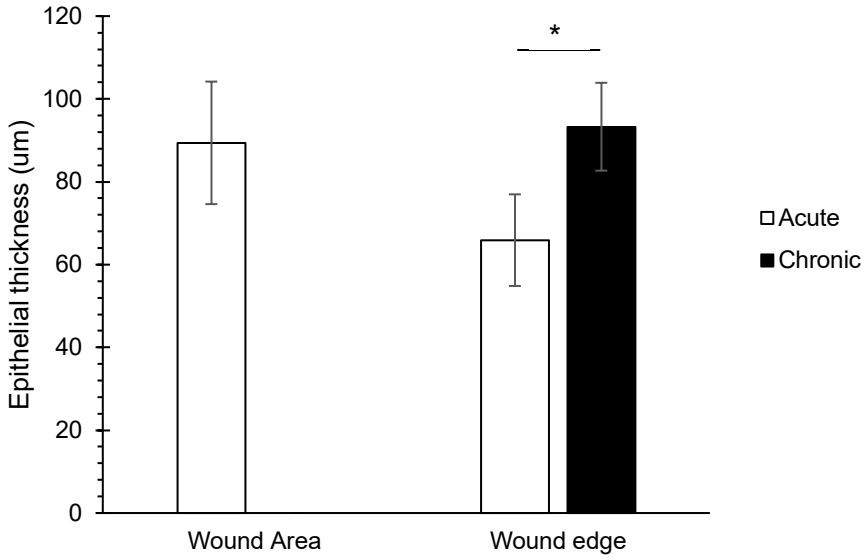

Figure 5.8. Epithelial thickness (µm). Epithelial thickness (µm) on day 7 post wounding of wild-type C57BL6/J mice treated with saline (Acute wound) and B6.cg-lepob/J (ob/ob), treated with high NEP (chronic wound) calculated using Image J software **Statistical analysis:** Paired two-tailed T test. *p<0.05 indicates significant differences between groups at the same time point. Statistical analysis for epithelial thickness in the wound area was not done because all values for chronic were 0.

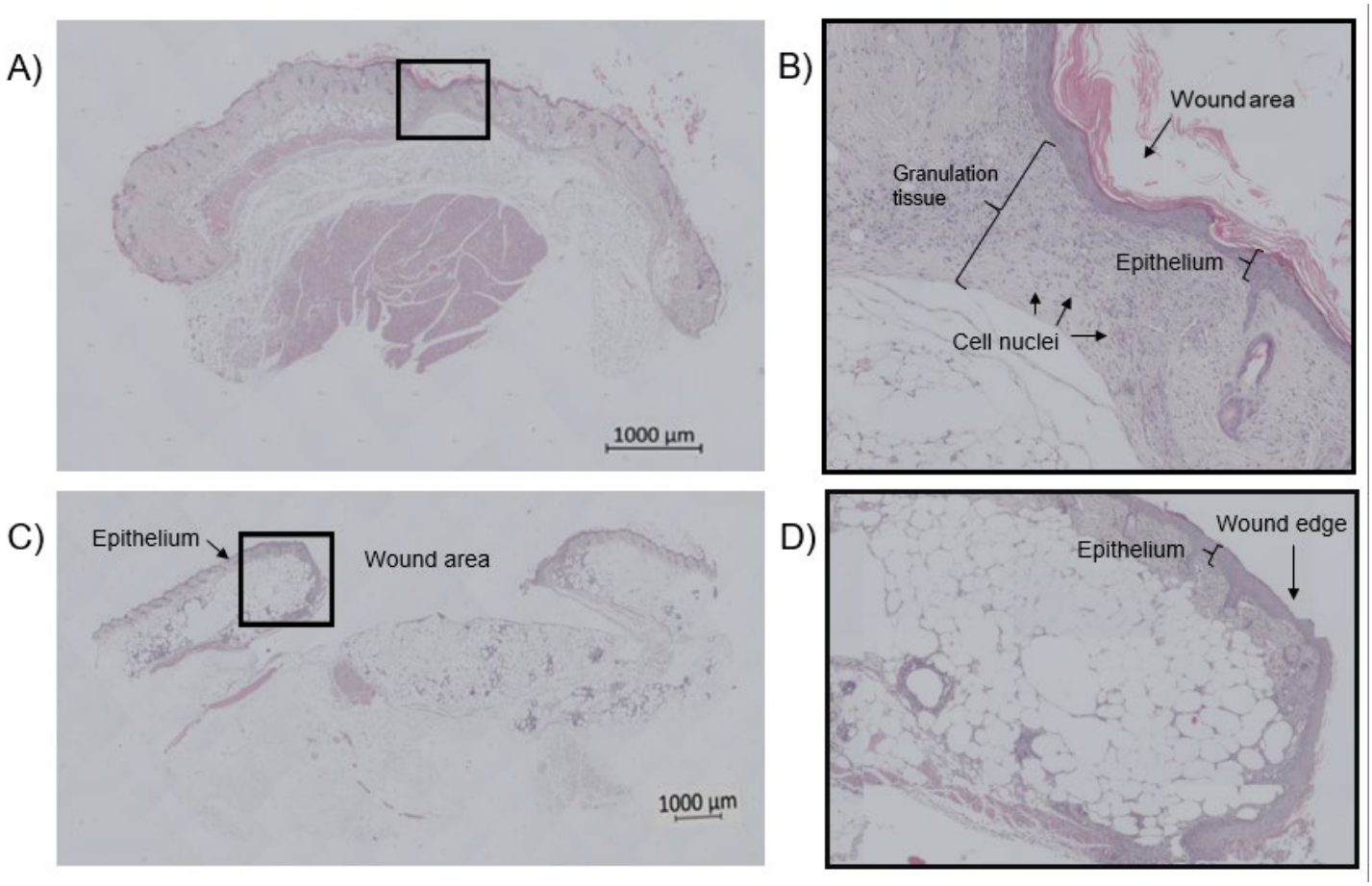

Figure 5.9. H&E stains of acute versus chronic day 7 wounds. Histological cross section of day 7 post wounding of **A)** type C57BL6/J mice treated with saline (Acute wound) and **B)** magnification of wound area (Black outlined box) showing granulation tissue formation epithelial thickness and cell nuclei within granulation tissue. **C)** B6.cg-lep ob/J (ob/ob), treated with high NEP (chronic wound) and **D)** magnification of wound edge (Black outlined box in image B) of chronic wound indicating wound edge and epithelium. Images (tile scan) were acquired at 10x magnification.

5.2.3.2 The formation of granulation tissue is not evident in the chronic wounds

No signs of granulation tissue was evident in the wound area of the chronic wounds (ob/ob animals) on day 7 post wounding, whereas newly formed granulation tissue was clearly noticeable in the acute wounds (wild type animals) (923.99 ± 131.71 µm) at the same time point (Fig. 5.9-5.10). Representative images showing granulation tissue formation are shown in Figure 5.9.

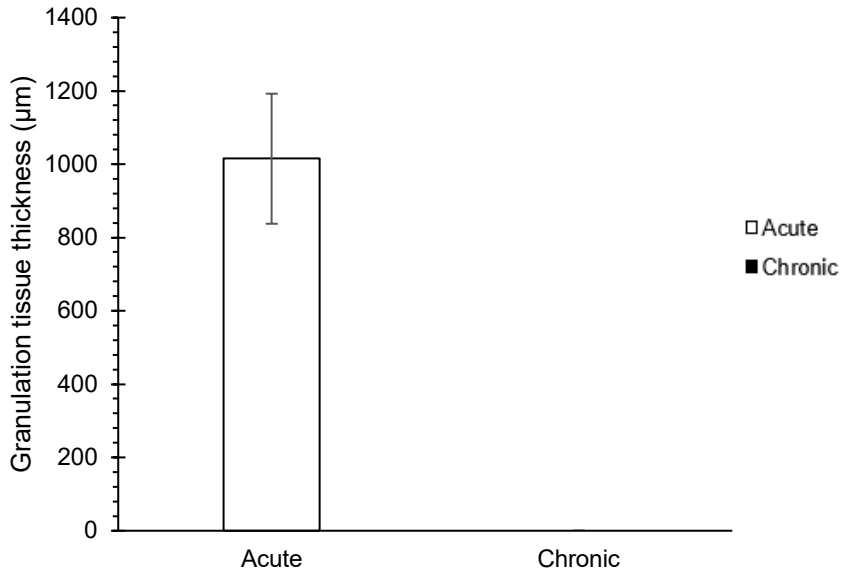

Figure 5.10. Granulation tissue (µm). Granulation tissue thickness (µm) on day 7 post wounding of wild-type C57BL6/J mice treated with saline (Acute wound) and B6.cg-lepob/J (ob/ob), treated with high NEP (chronic wound) calculated using Image J software. **Statistical analysis:** was not done because all values for chronic were 0.

5.2.3.3 Cellularity within granulation tissue

Cellularity within the granulation tissue was measured on day 7 post wounding by assessing the nuclear content (% of granulation tissue) within the acute vs chronic wounded areas. The chronic wounds had no evidence of granulation tissue formation and cellularity and could therefore not be assessed, whereas as 11.39 ±1.07% of the granulation tissue within acute wounds showed presence of nuclei at the same time point (Fig 5.11). Representative images indicating cellularity within the granulation tissue are shown in Figure 5.9.

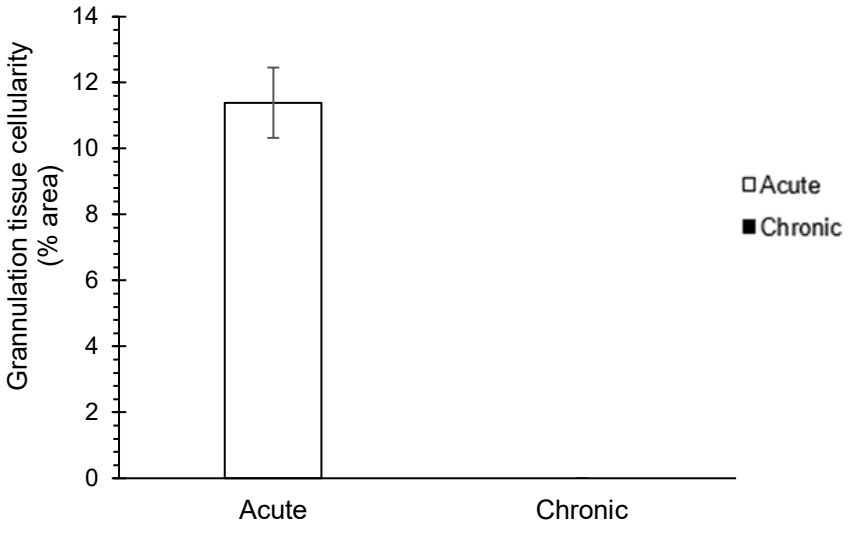

Figure 5.11. Cellularity in granulation tissue. Cellularity (percentage area) within granulation tissue on day 7 post wounding of wild-type C57BL6/J mice treated with saline (Acute wound) and B6.cg-lepob/J (ob/ob), treated with high NEP (chronic wound) calculated using Image J software. **Statistical analysis:** was not done because all values for chronic were 0.

5.2.3.4 Blood vessels within granulation tissue of acute day 7 wounds

Angiogenesis was measured by quantifying the number of blood vessels within the granulation tissue 7 days post wounding in acute and chronic wounds. The chronic wounds had no granulation tissue formation within the wound area hence no blood vessels whereas acute wounds had 43 ±13.42 blood vessels at the same time point within the wound area (Fig 5.12). Representative images showing angiogenesis within granulation tissue are shown in Figure 5.13.

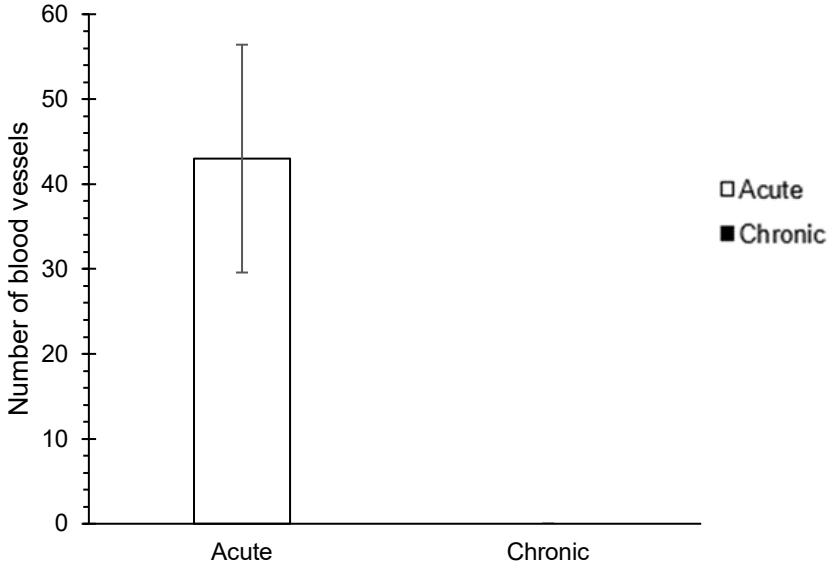

Figure 5.12. Number of Blood vessels in granulation tissue. Number of blood vessels within granulation tissue on day 7 post wounding of wild-type C57BL6/J mice treated with saline (Acute wound) and B6.cg-lepob/J (ob/ob), treated with high NEP (chronic wound) calculated using Image J software. **Statistical analysis:** was not done because all values for chronic were 0.

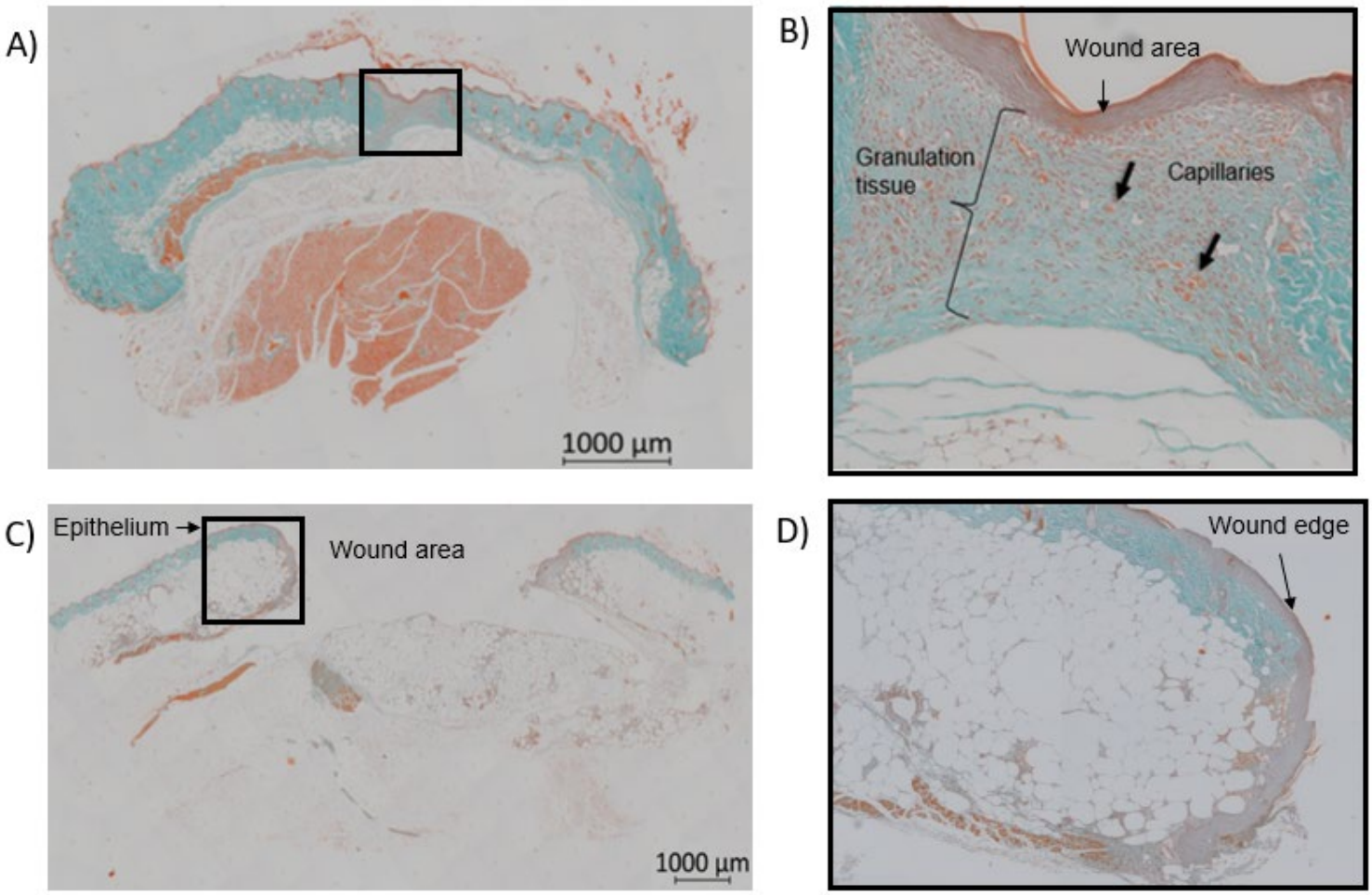

Figure 5.13. Acute versus chronic day 7 wound Masson trichrome stains. Histological cross section on day 7 post wounding of **A)** type C57BL6/J mice treated with saline (Acute wound) and **B)** magnification of wound area (Black outlined box) indicating granulation tissue and epithelium. **C)** B6.cg-lep ob/J (ob/ob), treated with high NEP (chronic wound) and **D)** magnification of wound edge (Black outlined box in image B) of chronic wound indicating wound edge. Images (tile scan) were acquired at 10x magnification.

5.2.3.5 Histological scoring parameters

The overall histology index was used to give an indication of healing dynamics within the acute and chronic wounds on day 7 post wounding. Acute wounds (1.92 ± 0.64) had a 1.9 fold higher histology score compared to the chronic wounds (1 ± 0) at the same time point (Fig. 5.14).

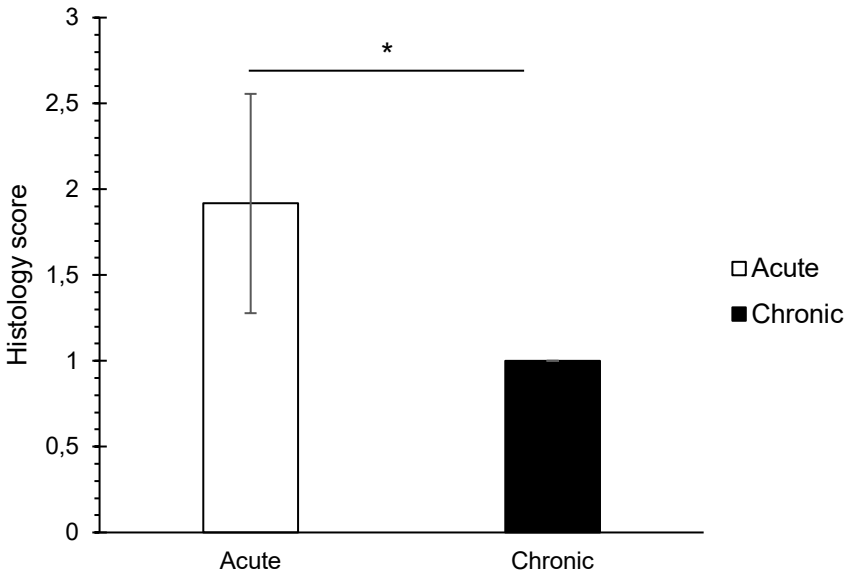

Figure 5.14: Histology index of acute and chronic day 7 wounds. Histology score was assigned to acute and chronic day 7 wounds based on epithelial thickness, granulation tissue formation, cellularity and angiogenesis. Histological scoring was assigned as follows: ± 1 for little epidermal and dermal organization (epithelial thickness < 30µm in wound area), few capillary vessels (<10), many infiltrated cells (<10%) and no granulation tissue formation, ±2 for moderate epidermal and dermal organization (epithelial thickness < 100µm in wound area), newly formed capillary vessels (>10%) in the entire wound area, granulation tissue (>100µm) and ±3 for complete remodelling of the epidermis and dermis, well-formed capillary vessels. **Statistics:** All scores for chronic were 1. Paired two-tailed T test. *p<0.05 indicates significant differences between groups at the same time point.

5.2.4 MMP-9 expression is higher in Chronic wounds compared to acute wounds

Matrix metalloprotease-9 expression within the wounded area was determined during the first seven days post wounding (i.e. on day 0, 2 and 7) within acute and chronic wounds. The chronic wound group showed no significant change between day 0 (4.79 ±2.8) (mean fold change ± standard error of the mean), day 2 (5.06±4.22), and day 7 (2.82 ±0.87) (Fig. 5.15). In the acute wound group, there was no significant differences between day 0 (1 ± 0.3), day 2 (0.65 ± 0.05) and day 7 (1.04 ± 0.29) (Fig. 5.15). Although there was no significant difference within the groups there were significant differences in MMP-9 expression between the acute and chronic wound groups on all 3 days (day 0, 2 and 7 post wounding). The chronic wound consistently produced significantly more MMP-9 compared to the acute wounds (4.8 fold difference on day 0; 7.8 fold on day 2 and 2.7 fold on day 7).

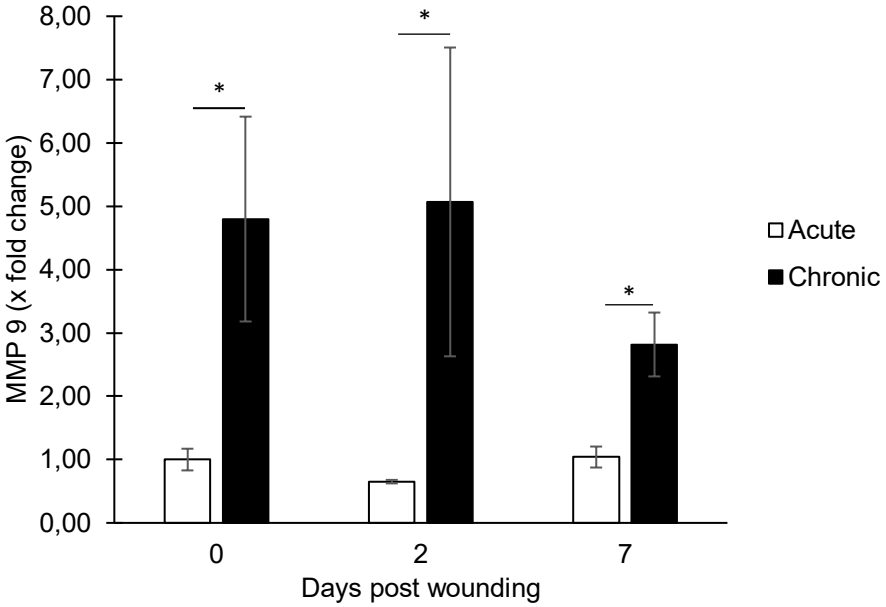

Figure 5.15. MMP-9 expression in acute versus chronic wounds over 7 days, post wounding. Wound tissue was collected from wild-type C57BL6/J mice treated with saline (Acute wound) and B6.cg-lepob/J (ob/ob), treated with high NEP concentration (chronic wound) (n=3). Total protein extracted (0.25mg/µL) from these samples to determine MMP-9 expression levels. MMP-9 measurement is expressed in x fold change to Acute day 0 wound reference sample (Absorbance at 450nm). **Statistical analysis:** Repeated measures ANOVA with Dunnet's multiple comparison test. *p<0.05 indicates significant differences between groups at the same time point. Values are presented as absorbance read (ELISA assay) (mean±SE).

5.2.5 The protein profile varies between acute and chronic wounds in the early stages of healing

Initially 663 proteins were detected in the acute and chronic day 2 wounds. Figure 5.16 shows the raw data of the overall protein profile of all samples (acute and chronic). From these 663 proteins, 80 showed to have more than 1.5 fold change and 17 proteins from the 80 were observed to be significantly different between the acute and chronic wound groups at the same time point. Figure 5.17 shows the 17 proteins observed to be significantly different between the acute and chronic groups.

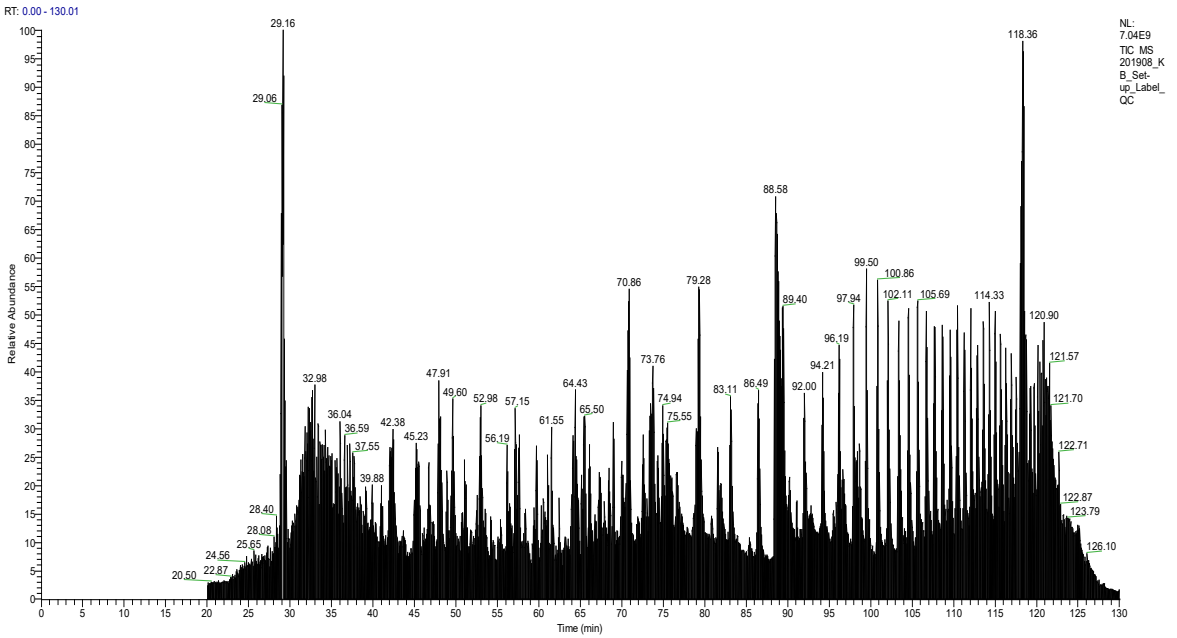

Figure 5.16. Raw mass spectrometry data of the 663 identified proteins. Protein profile of tagged proteins detect in both wild-type C57BL6/J mice treated with saline (Acute wound) and B6.cg-lepob/J (ob/ob), treated with high NEP (chronic wound). Relative absorbance was measured over 2 h using the mass spectrometer.

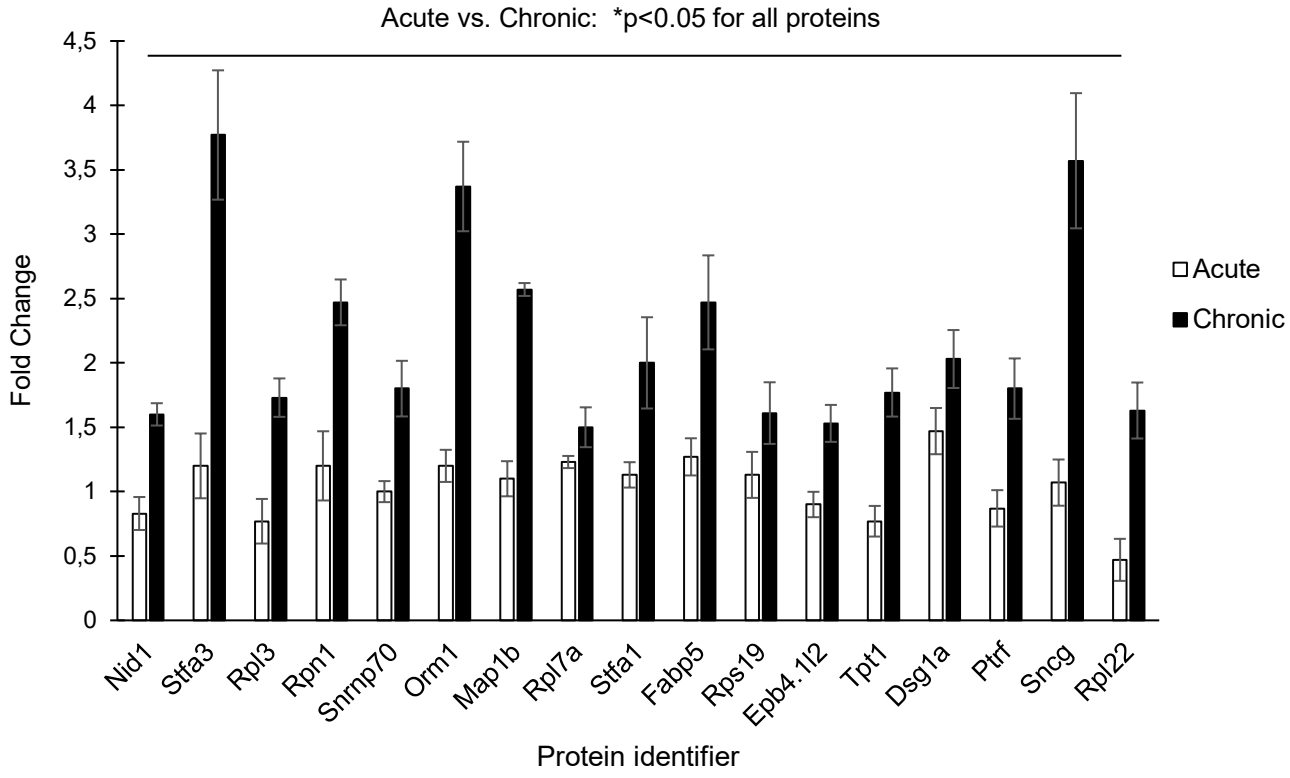

Figure 5.17. Protein observed to be significant between acute and chronic wounds. Proteomic analysis of type C57BL6/J mice treated with saline (Acute wound) and B6.cg-lep ob/J (ob/ob), treated with high NEP (chronic wound) observed significant differences in the expression of 17 proteins between the 2 groups. **Statistics:** Paired two-tailed T test. *p<0.05 indicates significant differences between groups at the same time point.

Chapter 6 : Discussion

During normal wound healing there are four distinct overlapping phases (haemostasis, inflammation, proliferation and remodelling), however in non-healing diabetic wounds the progression from inflammation to proliferation and remodelling does not occur (Landén et al., 2016, Zhao et al., 2016). The inability of these wounds to advance through the wound healing sequence is not yet fully understood. One of the leading causes of death in diabetic patients are complications arising from these nonhealing foot ulcerations. The complex nature of these non-healing diabetic wounds has led to the failure of many therapeutic strategies in clinical settings, despite that they were successful in substandard animal models. Therefore, a need for an animal model that is able to reflect the features and complications of a human chronic wound environment will greatly inform us on complications that occur during the early stages of healing which could inform us on potential therapies for treatment of impaired healing in future. This study successfully demonstrated the development a non-healing diabetic wound in ob/ob mice that more closely mimics what is seen in patients' wounds. In particular, this study showed administration of a high NEP concentration (1.02 mg/µL) to the margins of full-thickness excisional wounds on the dorsal surface of B6.Cg-Lepob/J (ob/ob) resulted in a) a lower initial inflammatory cytokine response in day 2 wound fluid, b) altered MMP-9, that remained elevated 2 and 7 days after wounding, compared to saline control, c) delayed wound closure and d) change in the levels of 17 proteins identified using mass spectrometry which are related to inflammation, proliferation, protease activity, remodelling, ribosomal function, cytoskeleton, neurofilament network, cell cycle processes and cell adhesion.

The neuropeptide substance P plays an important role in the progression of the wound healing process specifically in a) the release of pro-inflammatory cytokines, b) as a chemoattractant for neutrophils, lymphocytes, monocytes and fibroblasts, c) the promotion of vasodilation and cell adhesion between leukocytes and endothelial cells and d) the initiation of DNA synthesis and proliferation of keratinocytes, fibroblasts and endothelial cells (Pradhan et al., 2011, Pradhan et al., 2009, Delgado et al., 2003, Antezana et al., 2002). Substance P expression is however regulated through enzymatic degradation by NEP. The insufficient production of this neuropeptide and the over expression of NEP has been shown to be one of the contributing factors in the delayed healing process in non-healing diabetic foot ulcers (Antezana et al., 2002, Spenny et al., 2002, Leal et al., 2015).

Studies have demonstrated NEP enzyme activity of 20.6 ±4.5 pmol/hour/µg in diabetic unwounded mouse skin, an activity of 47.5 pmol/hour/µg in the margins of diabetic foot

ulcers in patients which is significantly higher than the 3.65 pmol/hr/µg activity in nondiabetic patients (Spenny et al., 2002, Antezana et al., 2002). We hypothesized that administration of NEP to the margins of full-thickness excisional wounds, induced in pre-diabetic mice B6.Cg-Lep^{ob}/J (ob/ob) would impair healing to an extent that a chronic wound develops which resembles the phenotype of diabetic ulcers in the clinical setting. In this study a dose response of three concentrations of NEP were used. The first low NEP concentration (0.33 mg/µL -50 pmol/hour/ug) was based on the NEP activity in ulcer margins of diabetic patients mentioned previously, however these mice have a higher metabolic turnover compared to humans (Kleiber, 1975) and hence higher concentrations were used as dose treatments – medium NEP (0.68 mg/µL-100 pmol/hour/ug) and high NEP (1.02 mg/µL-150 pmol/hour/ug). This study demonstrated a diabetic wound model in pre-diabetic mice B6.Cg-Lep^{ob}/J (ob/ob) that resembles the patient diabetic ulcer using the high NEP treatment. Although there were no significant differences in NEP activity (day 2) between the treatment groups, the high NEP treatment produced consistently high MMP-9 expression (day 2 and day 7 post wounding), significantly lower substance P within wound area compared to NEP low treatment, a low chronic pro-inflammatory profile within wound fluid (day 2), delayed wound closure (day 7) with no formation of granulation tissue, re-epithelization and angiogenesis within the wound area of the chronic wound (day 7) and significant differences in the expression of proteins between chronic and acute day 2 wounds that have not been previously described to be directly implicated in wound healing but have downstream interactions that could possibly play a role in healing.

During the optimization of the wounding procedure in phase I, an 83% survival rate was observed in the B6.Cg-Lep^{ob}/J (ob/ob). This is thought to be because of the adverse effects that the anaesthesia had on the mice upon prolonged exposure resulting in respiratory and heart failure (Gargiulo et al., 2012). In order to overcome this, exposure was decreased to ≤ 10 minutes and the mice were shaved the day before wounding and not on the day of.

A significant effect of time was observed in NEP activity of all four treatment groups (Saline, low NEP, medium NEP and high NEP) with a higher activity on day 0 compared to day 2. The presence of NEP within the wound bed was first detected 6 hours post wounding (Olerud et al., 1999), which could mean that peak increase in NEP might have been missed between the day 0 and day 2 time points. This diminished NEP activity could possibly be due to interactions with its substrate, substance P, resulting in decreased activity over time. The immunohistochemistry results of substance P staining showed greater expression on day 2 compared to the day 0 time point for all four treatment groups within the wound area

thereby further reaffirming substance P's role in wounding healing. The decrease in NEP activity at the day 2 time point could be the reason for the increase in substance P expression at the same time point for all four treatment groups. In order to overcome the limitation of decreased NEP activity over time, an investigation into increasing the number and frequency of NEP treatments should be conducted.

During normal wound healing, MMP-9 degrades matrix proteins and growth factors, and as the wound progresses through the healing cascade its expression decreases. Previous studies have shown in chronic wounds MMP-9 has increased activity hindering the re-epithelialization process and keratinocyte migration and attachment (Liu et al., 2009, Lobmann et al., 2002, Reiss et al., 2010). The high NEP treatment produced significantly greater MMP-9 compared to saline treatment group on day 2, which is consistent with increased MMP-9 expression in chronic wounds.

The high concentration of NEP induced an overall decrease in levels of pro-inflammatory cytokine, chemokine and anti-inflammatory cytokine profile within the day 2 wound fluid compared to the saline treatment which indicates an initial delay in the inflammatory response. This delayed inflammatory response indicates that these wounds have been delayed in the onset of healing.

The second phase of this study investigated and compared the wound healing dynamics and differences in the protein profile of the high NEP dosage in the creation of a chronic non-healing wound (in B6.Cg-Lep^{ob}/J ob/ob mice) to an acute wound (in wild-type C57BL6/J mice) during the early stages of wound healing. Mice in the chronic wound (B6.Cg-Lep^{ob}/J ob/ob) group had a significantly higher weight compared to the acute wounded group (wild-type C57BL6/J) .

Impaired wound healing in T2DM due to the hyperglycaemic environment results in decreased cellular proliferation, collagen synthesis and angiogenesis leading to delayed healing (Okonkwo and DiPietro, 2017). The chronic wounded group had significantly decreased percentage wound closure compared to the acute wounded group on day 7. The acute wounds on day 7 had almost completely re-epithelialized were as the chronic wounds displayed open wounds indicating delayed healing. These results were further reaffirmed by comparing the histological parameters of the acute and chronic wounds. The acute wounds had thicker epithelium, greater granulation tissue formation within the wound area compared to the chronic wound and a higher percentage cellularity (infiltrating cell) and number of blood vessels (angiogenesis) within the granulation tissue indicating that healing is in fact taking place within the control group. The chronic wound had no granulation tissue or

epithelium formation within the wound area and therefore no infiltrating cells and angiogenesis occurring. This lack of granulation tissue formation is consistent with what is observed in chronic wounds in diabetic patients (Berlanga-Acosta et al., 2013). The MMP-9 expression in the chronic wounds at all 3 time points (day 0, 2 and 7) was found to be significantly greater than the acute wound. These observations taken together indicate that wounding healing in the chronic group has been successfully delayed by the administration of the high NEP treatment thereby resembling phenotypes observed in patient diabetic ulcerations.

Out of the 663 proteins detected in the proteomic analysis of acute and chronic day 2 wounds, there were 80 proteins of interest (Table 6.1). Of the 80 proteins only 17 proteins were deemed significantly different between the acute and chronic wound groups. From these 17 proteins Nidogen-1 and Alpha-1-acid glycoprotein 1 were shown to be the only known proteins to be directly involved in the wound healing process, specifically in the inflammation (Alpha-1-acid glycoprotein 1), proliferation and remodeling (Nidogen-1) stages.

Alpha-1-acid glycoprotein 1 is an acute phase protein whose concentration increases in response to injury and inflammation and is known to modulate inflammation during the healing process (Fournier et al., 2000, van Dijk et al., 1991). Nidogen-1 is essential for the epidermal basement membrane formation and interacts with laminin and collagen IV to achieve this (Baranowsky et al., 2010). Nidogen-1 has also been shown to have interactions with MMPs (specifically MMP-3 and MMP-7). The remaining proteins have not been previously described directly in relation to wound healing: a) Stafin-1 and Stafin-3 have interactions with each other and function as intracellular thiol proteinase inhibitors (Bilodeau et al., 2009), b) Rpl3, Rpn1, Snrnp70, Rpl7a, Rps19, and Rpl22 are ribosomal proteins and interact with various other ribosomal subunits/proteins (Table 6.1), c) Microtubule-associated protein 1B is a component of the neural cytoskeleton (Lu et al., 2004), d) Fatty acid-binding protein facilitates transport of fatty acid within the cytosol and between the cytosol and nucleus (Kaczocha et al., 2012), e) Band 4.1-like protein 2 could possibly be involved in anaphase of the cell cycle, f) Translationally controlled tumor protein could possibly be involved in cell growth, acute allergic response, and apoptosis (Fiucci et al., 2003), g) Desmoglein-1-alpha forms a part of desmosomes located in the upper epidermis and mediates cell to cell adhesions (Kljuic and Christiano, 2003), h) Caveolae-associated protein 1 is involved in the organisation and formation of caveolae (Couet et al., 1997) and

i) Gamma-synuclein plays a role in neurofilament network integrity (Buchman et al., 1998) and could regulate the keratin network in skin by similarity.

Although these proteins have no known function in wound healing some show shared common interactions and sometimes interact with each other. We were unable to find literature that define the role of ribosomal proteins that were significantly different between the groups in wound healing, this hence warrants further investigation. Stefin-1 and Stefin-3 interact with each other and could potentially play a regulator role in antigen presentation (Bilodeau et al., 2009). They also interact commonly with Csta1, Gm5416, BC117090, BC100530 which are Cystatin type proteins that possibly function as endopeptidase inhibitors. Microtubule-associated protein 1B interacts with Gsk3b (Glycogen synthase kinase-3 beta – negative regulator of glucose homeostasis) (Tanabe et al., 2008) and Pafah1b1 (Platelet-activating factor acetylhydrolase IB subunit alpha) could possibly play a role in migration of fibroblasts during wound healing. Band 4.1-like protein 2 interacts with Epb4.13 (Band 4.1-like protein 3 – promotes apoptosis and inhibits cell proliferation). Caveolae-associated protein 1 interacts with Cav-1 (Caveolin-1 – T-cell activation and proliferation) (Ohnuma et al., 2007). Gamma-synuclein interacts with Mmrn2 (Multimerin-2-negative regulator of angiogenesis and inhibitor of epithelial cell mobility) (Lorenzon et al., 2012). These proteins although not directly implicated in wound healing, have interactions with proteins that do and are overexpressed in the chronic compared to the acute wounds.

There are two possible explanations for the overexpression of these proteins in chronic wounds – 1) a positive feedback loop or 2) delayed onset healing. The positive feedback loop refers to a lack of the usual negative feedback control resulting in accumulation of proteins in the chronic wounds. In the acute wounded groups the significantly higher proteins should have already been downregulated but in the chronic wounded group they remained high with delayed onset healing.

This information suggests that there are dysregulations in overexpression and further research to investigate more details of the dysregulation and where exactly it originates needs to be conducted. The question can be asked: Is it because of a positive feedback loop or a delay in the onset of healing? A greater number of time points with higher animal numbers are needed to definitively answer this question.

Table 6.1: Protein expression in acute versus chronic wounds.

Accession Number	Identifier	Known function in wound healing	Novel Identified	Interactions	Acute	Chronic
DDX5_MOUSE	Probable ATP-dependent RNA helicase DDX5 (Ddx5)	-		Dhx5, Cdc5l, Hnrnph1. Dhx9, Hnrnpk, Drosha, Hnrnpa2b1, Hnrnph2, Srsf6 and Hnrnpa1.	0,70	2,00
NID1_MOUSE	Nidogen-1 (Nid1)	Proliferation and remodelling (Baranowsky et al., 2010).	-	Lamc1, Lamb1, lama2, Lama1, Lama4, Lama5, MMP3, MMP7, Lamb2 and Lamc 3.	0,83	1,60*
NUDC_MOUSE	Nuclear migration protein (NudC)	-	Roles in neurogenesis and neuronal migration (Keays, 2007, Sasaki et al., 2005).	Pafah1b1, Dync1h1, Plk1, Ndel1, Nde1, Dync1i1, Clip1, Zw10, Dynll2 and Nuf2.	1,07	1,77
CYT3_MOUSE	Stefin-3 (Stfa3)	-	Intracellular thiol proteinase inhibitor(Bilodeau et al., 2009).	mCG_130165, Stfa2l1, BC100530, Stfa1, BC117090, Gm5416, Gm5483, Rptn, Sprr3 and Csta1.	1,20	3,77*
RL3_MOUSE	60S ribosomal protein L3 (Rpl3)	-	L3 protein is a component of the large subunit of cytoplasmic ribosomes.	Rpl8, Rps8, Rps3, Rps5, Rps19, Rpl10a, Rps11, Rpl23, Rps6 and Rps14.	0,77	1,73*
sp|P37889|	Fibulin-2 (Fbln2)	Proliferation and remodelling (Longmate et al., 2014, Lee et al., 2004).	-	Mfap5, Mfap2, Vtn, Mfap4, Mfap3, Eln, Fn1, Col6a1, Fstl1 and Loxl1.	1,57	2,63
PIN1_MOUSE	Peptidyl-prolyl cis-trans isomerase NIMA-interacting 1 (Pin1)	Angiogenesis and proliferation (Atabay et al., 2015, Su et al., 2018).	-	Trp53, Hipk2, Irf3, Pip4k2a, Pip4k2b, Pip4k2c, Trp53inp1, Fkbp1a and Fkbp1b.	1,17	1,77
sp|Q9DB34|	Charged multivesicular body protein 2a (Chmp2a)	Remodelling (Olmos and Carlton, 2016).	Formation and sorting of endosomal cargo proteins into multivesicular bodies through endosomal sorting required for transport complex III (ESCRT-III).	Vps4b, Chmp4b, Chmp5, Chmp4c, Vps4a, Vta1, Chmp6, Chmp7, Vps36 and Chmp3.	0,87	2,07
CALU_MOUSE	Calumenin (Calu)		Calcium-binding protein localized in the endoplasmic reticulum (Yabe et al., 1997).	P4hb, Hsp90b1, Pcsk9, Pdia6, Alb, Nucb1, Fga, Fn1, Il6, Fstl1.	1,00	2,47
STRN_MOUSE	Striatin (Strn)		Protein regulator of vesicular trafficking in neurons that also binds caveolin-1 and Ca^{2+}-calmodulin(Garza et al., 2015).	Mob4, Strip1, Strip2, Mst4, Cttnbp2nl, Stk24, Ppp2r1a, Stk25, Slmap and Cttnbp2.	1,50	1,93
sp|Q8R326|	Paraspeckle component 1 (Pspc1)		Control of gene expression during many cellular processes including differentiation, viral infection, and stress responses (Fox and Lamond, 2010).	Sfpq, Nono, Rbm14, Tatdn1, Cdc5l, Ppp5c, Srsf1, Fus, Cpsf6 and Ciz1.	1,47	2,03
RPN1_MOUSE	Dolichyl-diphosphooligosaccharide--protein glycosyltransferase subunit 1 (Rpn1)		Recognition of several ligands of the proteasome(Elsasser et al., 2002).	Rpn2, Ddost, Stt3a, Stt3b, Dad1, Ostc, Sec61a1, Tusc3, Ost4 and Sec61g.	1,20	2,47*

Accession Number	Identifier	Known function in wound healing	Novel Identified	Interactions	Acute	Chronic
sp|Q91VJ2|	Caveolae-associated protein 3 (rkcdbp)		Caveolin-3 knockout mice showed increased adiposity and insulin resistance and instability of the insulin receptor in skeletal muscle (Capozza et al., 2005).	Cav1, Sprtn, Nenf, Mthfd1, Ssr4, Cav3, Cdh2, E4f1, Pcx and Cav2.	1,60	1,67
RU17_MOUSE	U1 small nuclear ribonucleoprotein 70 kDa (Snrnp70)		mRNA splicing factor and component of the spliceosomal U1 snRNP (Carlson et al., 2015).	Snrpc, Snrpd3, Snrpd1, Snrpd2, Snrpd, Snrpe, Snrpf, Gm8186, Srsf1 and Snrpa.	1,00	1,80*
sp|P14873|	Microtubule-associated protein 1B (Map1b)		Major component of the neuronal cytoskeleton(Bloom et al., 1985, Lu et al., 2004).	Gan, Fmr1,Dig4, Gsk3b, Pafah1b1, Map1lc3a, Dag2, Cyfip1, Mapre3 and Map2.	1,10	2,57*
sp|Q60590|	Alpha-1-acid glycoprotein 1 (Orm1)	Inflammation (Van Dijk et al., 2013, Fournier et al., 2000).		Ahsg, Hp, Ttr, Alb, Orm2, Fgb, Fga, C3, A2m and Fgg.	1,20	3,37*
SSBP_MOUSE	Single-stranded DNA-binding protein, mitochondrial (sbp1)		DNA replication, recombination and repair by binding to single-stranded DNA (Ruhanen et al., 2010).	Peo1, Polg, Tfam, Polrmt, Mrps6, Nip7, Polg2, Ccdc58, Nhp2 and Dut.	1,00	1,80
RL7A_MOUSE	Ribosomal protein L7A (Rpl7a)		Encodes 60S ribosomal protein L7a.	Rpl8, Rpl19, Rpl7, Rpl26, Rpl37a, Rpl32, Rpl18, Rpl15, Rpl30 and Rpl23.	1,23	1,50*
sp|Q80WJ7|	Protein LYRIC (Mtdh)		Activates the nuclear factor kappa-B (NF- kappa-B) transcription factor (Noch and Khalili, 2013).	Snd1, Lpar6, Sgol1, Rasal2, Emp2, Zcrb1, Cyp24a1, Slc1a2, Tspyl5 and Mmp9.	1,70	1,6
PPIB_MOUSE	Peptidyl-prolyl cis-trans isomerase B (Ppib)		Catalyses the cis-trans isomerization of proline imidic peptide bonds in oligopeptides (Lang et al., 1987).	Crtap, Lepre1, P4hb, Leprel1, Serpinh1, Pdia4, Leprel2, Col1a1, Col1a2 and Hspa5.	0,80	2,63
RS11_MOUSE	Ribosomal protein S11 (Rps11)		Encodes 40S ribosomal protein S11.	Rpl8, Rps14, Rps5, Rps15a, Rpl10a, Rps3a1 , Rps13, Rpl23, Rpl35a and Rps25.	1,30	1,97
LBR_MOUSE	Lamin-B receptor (Lbr)		Integral membrane protein of the interphase nuclear envelope (Olins et al., 2010).	Lmnb1, Lemd3, Cbx5, Emd, Cyp51, Sqle, Ahctf1, Sun2, Banf1 and Hsd17b7.	1,33	2,10
CYT1_MOUSE	Stefin-1 (Stfa1)		Intracellular thiol proteinase inhibitor.	BC100530, Staf2l1, Gm5483, Staf3, Gm5416, Bc117090, mCG_130165, Gm4758, Csta1 and Gm5689.	1,13	2,00*
sp|Q05816|	Fatty acid-binding protein, epidermal (Fabp5)		Apart of the fatty acid binding family and has a high specificity for fatty acids.	Ppard, Rxra, Grn, Acly, Retn, Trtr, Abca13, Pygb, Nckap1l and Fuca1.	1,27	2,47*

Accession Number	Identifier	Known function in wound healing	Novel Identified	Interactions	Acute	Chronic
RS19_MOUSE	40S ribosomal protein S19 (Rps19)		Needed for pre-rRNA processing and maturation of 40S ribosomal subunits.	Rpl8, Rpl10a, Rps11, Rps25, Rps24, Rpl3, Rpl23, Rps15a, Rpl5 and Rps14.	1,13	1,61*
sp|Q8CGN5|	Perilipin-1 (Plin1)		Controls adipocyte lipid metabolism.	Abhd5, Cav1, Cidec, Prkacb, Prkaca, Pnpla2, Lipe, Prkg1, Prkg2 and Adipoq.	1,30	2,43
HPT_MOUSE	Haptoglobin (Hp)	Haemostasis and Inflammation (Venteclef et al., 2011, MacKellar and Vigerust, 2016).	Acts as an antioxidant, has antibacterial activity and plays a role in modulating many aspects of the acute phase response (Wassell, 2000).	Cd163, Apoa1, Hba-a1, Orm1, Hbb-bs, Orm2, Ltf, Lrg1, Cyfip1 and Fth1.	1,07	2,20
VIME_MOUSE	Vimentin (Vim)	Proliferation, differentiation and re-epithelization (Cheng et al., 2016, Walker et al., 2018, LeBert et al., 2018, Cheng and Eriksson, 2017).		Des, Tpm4, Casp3, Neb, Tpm2, Tpm1, Casp8, Tnnt3, Casp7 and Casp6.	0,87	1,97
sp|O70318|	Band 4.1-like protein 2 (Epb4.1l2)		Involved in anaphase of cell cycle.	Epb4.1l3, Cask, Nrxn3, Nrxn2, Nrxn1, Epb4.1l1, Epb4.1l5, Epb4.1, Nlgn2 and Nlgn1	0,90	1,53*
ZO1_MOUSE	Tight junction protein ZO-1 (Tjp1)	Angiogenesis (Shi et al., 2018).		Gja1, Ocln, Src, Mllt4, Casp3, Cldn2, Cldn5, Wwtr1, Vcl and Ctnna1.	1,10	1,73
K2C1_MOUSE	Keratin, type II cytoskeletal 1 (Krt1)	Inflammation and re-epithelialization (Roth et al., 2012, Tao et al., 2007, Nuutila et al., 2012, Kobielak and Boddupally, 2014).		Lor, Krt5, Krt19, Krt77, Krt2, Krt10, Tgm1, Ivl, Trp63 and Hrnr.	1,10	2,00
TCTP_MOUSE	Translationally controlled tumor protein (Tpt1)		Implicated in cell growth, acute allergic response, and apoptosis (Fiucci et al., 2003).	Eef1b2, Bcl2l1, Eef1g, Rpl8, Eef2, Rps25, Gnb2l1, Rps3, Rps14 and Rplp2.	0,77	1,77*
sp|Q61495|	Desmoglein-1-alpha (Dsg1a)		Component of desmosomes present in the upper epidermis(Kljuic and Christiano, 2003).	Pkp3, Pkp1, Dsp, Jup, Pkp2, Pkp4, Klk5, Dsc3, Dsc1 and Dsc2.	1,47	2,03*
RBM3_MOUSE	RNA-binding protein 3 (Rbm3)		Increases protein synthesis at both physiological and mild hypothermic temperatures (Dresios et al., 2005).	Rpl4, Chtop, Pcbp1, Srsf1, Hnrnpk, Celf2, Srsf6, Snrpa, Celf1 and U2af2.	1,43	1,87
sp|O54724|	Caveolae-associated protein 1 (Ptrf)		Caveolae formation and organization (Couet et al., 1997).	Cav1, Ttf1, Polr1e, Polr1a, Nnmt, Polr1c, Taf1c, Tbp, Taf1b and Polr2l.	0,87	1,80*
NUCL_MOUSE	Nucleolin (Ncl)		Nucleolar protein of growing eukaryotic cells(Ginisty et al., 1999).	Fbl, Npm1, Wdr43, Nop58, Nop56, Wdr75, Nop14, Rps6, Utp6 and Wdr3.	1,23	1,54

Accession Number	Identifier	Known function in wound healing	Novel Identified	Interactions	Acute	Chronic
sp|Q9QXS1|	Plectin (Plec)		Anchors intermediate filaments to junctional complexes, the nuclear envelope and cytoplasmic(Wiche and Winter, 2011).	Itgb4, Col17a1, Fau, Gm9843, Itga6, Gnb2l1, Rps19, Rps3a1, Rpl26 and Cd151.	1,37	2,47
COF1_MOUSE	Cofilin-1 (Cfl1)		Regulates actin cytoskeleton dynamics and involved in cytokinesis and cell motility (Hotulainen et al., 2005).	Limk1, Actb, Limk2, Ssh1, Actg1, Ssh2, Wdr1, Ssh3, Cttn and Rhoa.	0,97	2,17
SYUG_MOUSE	Gamma-synuclein (Sncg)		Role in neurofilament network integrity (Buchman et al., 1998).	Uba2, Pfdn2, Sync, Atoh7, Fam78b, Mettl14, Bub1b, Pou4f2, Mmrn2 and Kcns3.	1,07	3,57*
RL22_MOUSE	Ribosomal protein L22 (Rpl22)		Encodes 60S ribosomal protein L22.	Rps6, Rpl30, Rpl26, Rps14, Rps8, Rpl10a, Rps13, Rps25, Rps3a1 and Rpl35a.	0,47	1,63*
sp|Q9D8Y0|	EF-hand domain-containing protein D2 (Efhd2)	Inflammation(Kroczek et al., 2010, Peled et al., 2018).		Arpc2, Arpc4, Actr2, Arpc3, Mapt, Ttll3, Trim67, Hspb7, Trim80 and Fbxo42.	0,73	1,87
PYGM_MOUSE	Glycogen phosphorylase, muscle form (Pygm)		Catalyzes the breakdown of glycogen to glucose-1-phosphate.	Gbe1, Agl, Phkg1, Pgm5, Pgm2, Ugp2, Phka1, Phkb, Amy1 and Pgm3.	1,73	0,83
sp|Q8CI43|	Myosin light chain 6B (Myl6b)		Regulatory light chain of myosin. Does not bind calcium.	Tpm2, Myh11, Tpm1, Myl12b, Tpm4, Mylk, Myl7, Acta2, Tln1 and Actg2.	3,20	1,27
sp|Q99PR8|	Heat shock protein beta-2 (Hspb2)		May regulate the kinase DMPK.	Mapk14, Akt1, Mapk11, Hspa1b, Hsp90aa1, Hsp90ab1, Mapk12, Mapkapk2, Mapk13 and Trp53.	3,10	1,17
sp|Q3MI48|	Junctional sarcoplasmic reticulum protein 1 (Jsrp1)		Involved in skeletal muscle excitation/contraction coupling (EC) (Yasuda et al., 2013).	Cacna1s, Rwdd2b, Ubn2, Srl, Ryr1, Atp2a1, Sypl2, Stac3, Casq1 and Klrg2.	2,87	0,77
sp|Q99MS7|	EH domain-binding protein 1-like protein 1 (Ehbp1l1)		Coordinates Rab8 and Bin1, plays a role in vesicle trafficking and involved in apical-directed transport in polarized epithelial cells (Nakajo et al., 2016).	Frmd8, Tigd3, Sssca1, Bin1, Cdc42ep2, Fam89b, Kcnk7, Map3k11 and Dpf2.	1,67	1,20
sp|Q91VX2|	Ubiquitin-associated protein 2 (Ubap2)		Encoded by UBap2 gene.	Zfr, Larp1b, Mrps36, Kcmf1, Phc3, Man1a2, Tbl1x, Cdyl, Pde4dip and mCG_125090.	1,87	1,10
OSTP_MOUSE	Osteopontin (Spp1)	Inflammation (Sodek et al., 2000, Weber and Cantor, 1996, Weber et al., 2012).		Cd44, Timp1, Il6, Fn1, Alb, Dmp1, tgb1, Mepe, Mmp7 and Fgf23.	3,33	1,27
sp|P49813|	Tropomodulin-1 (Tmod1)		Regulates filament length in skeletal muscle (Gokhin et al., 2015).	Neb, Tpm1, Tpm2, Ttn, Mybpc3, Tpm4, Tnnt2, Tnni2, Tnnt3 and Actn3.	5,30	1,50

Accession Number	Identifier	Known function in wound healing	Novel Identified	Interactions	Acute	Chronic
TENN_MOUSE	Tenascin-N (Tnn)		Involved in neurite outgrowth and cell migration in hippocampal explants(Neidhardt et al., 2003).	Vcan, Bcan, Sdc4, Itga8, Itga9, Itgav, Tnr, Itgb6, Itgb1 and Itgb3.	2,57	0,83
TRDN_MOUSE	Triadin (Trdn)		Contributes to the regulation of lumenal Ca2+ release via the sarcoplasmic reticulum calcium release channels (Zhang et al., 1997).	Ryr2, Ryr1, Asph, Casq2, Fkbp1b, Ryr3, Jph2, Jph1, Cacna1s and Casq1.	6,43	1,10
JPH2_MOUSE	Junctophilin-2 (Jph2)		Contributes to the formation of junctional membrane complexes (JMCs) which link the plasma membrane with the endoplasmic or sarcoplasmic reticulum in excitable cells(Beavers et al., 2014, Golini et al., 2011). Provides a structural foundation for functional cross-talk between the cell surface and intracellular calcium release channels (Landstrom et al., 2014).	Trdn, Casq2, Ryr1, Ryr3, Trpc3, Cav3, Ryr2, Jph1, Jph3 and Cacna1s.	2,87	1,00
JPH1_MOUSE	Junctophilin-1 (Jph1)		Contributes to the formation of junctional membrane complexes (JMCs) which link the plasma membrane with the endoplasmic or sarcoplasmic reticulum in excitable cells (Golini et al., 2011).Provides a structural foundation for functional cross-talk between the cell surface and intracellular calcium release channels (Landstrom et al., 2014).	Ryr1, Ryr3, Casq2, Jph3, Trdn, Sypl2, Jph2, Mtm1, Zc3h12c and Myo3b.	2,47	0,80
sp|Q8BWB1|	Synaptopodin 2-like protein (Synpo2l)		Accelerate nucleation of actin filament formation and to induce actin bundling (Chalovich and Schroeter, 2010).	Ankrd1, Myom2, Myoz1, Myoz2, Nrap, Cmya5, Smpx, Ttn, Ldb3 and Trdn.	1,93	0,80
sp|Q70KF4|	Cardiomyopathy-associated protein 5 (Cmya5)		Involved in compartmentalisation of protein kinase A (PKA).	Ttn, Ldb3, Actn2, Ckmt2, Myom2, Dtnbp1, Obscn, Myoz2, Tcap and Smpx.	1,73	0,97
LDB3_MOUSE	LIM domain-binding protein 3 (Ldb3)		Role in the interaction between the 58 muscular Z-line and α-actinin-2 (Yamashita et al., 2014).	Actn2, Myoz2, Ttn, Myot, Csrp3, Myl1, Tcap, Mypn, Actn3 and Tnni3.	2,03	0,97
BIN1_MOUSE	Myc box-dependent-interacting protein 1 (Bin1)		Regulation of synaptic vesicle endocytosis (Wu et al., 2009).	Dnm2, Wasl, Picalm, Dnm1, Dnm3, Sh3gl2, Eps15, Amph, Actr2 and Sh3gl3.	1,73	0,93
sp|Q9WUZ7|	SH3-binding domain glutamic acid-rich protein (Sh3bgr)		Forms a part of the SH3BGR family.	Psmg1, Wrb, Ripply3, Kcnj6, Hmgn1, Brwd1, Egfr, Bace2, Xkr6 and Emc3.	3,13	0,70

Accession Number	Identifier	Known function in wound healing	Novel Identified	Interactions	Acute	Chronic
sp|P70670|	Nascent polypeptide-associated complex subunit alpha (Naca)		Regulates the expression of genes involved in the development of myotubes (Berger et al., 2012).	Btf3, Btf3l4, Rpl7, Rpl19, Rpl32, Rpl4, Rps27a, Rps17, Rpl8 and Smyd1.	2,43	0,93
H10_MOUSE	Histone H1.0 (H1f0)		Condensation of nucleosome chains into higher-order structures (Brown et al., 2006).	H1fx, Asf1a, Trp53, Hmgb1, Cdk2, Dffb, Hmgb2, Hist1h1e, Hist1h1b and Hist1h1d.	2,33	1,37
sp|D3Z1D3|	ENSMUSG00000071540		RIKEN cDNA 3425401B19 gene.	Dyrk1a, Dyrk1b, Dcaf7, ENSMUSG00000066607, Ercc6, Suds3, Ercc8, Ghr, Fnta and Dalrd3.	2,77	1,13
TPM1_MOUSE	Tropomyosin alpha-1 chain (Tpm1)		Regulates myosin-actin interactions during muscle contraction and stabilizing cytoskeleton actin filaments in non-muscle cells (Singer et al., 2000).	Actn2, Tnnt2, Tnni1, Myh6, Tnni3, Tnnt3, Myl2, Myl3 and Acta2.	2,33	1,13
sp|Q91YE8|	Synaptopodin-2 (Synpo2)		Actin-binding and actin-bundling activity (Luo, 2004).	Kiaa0922, Tigd4, Rnf150, Ociad2, Ddit4l, Arfip1, Bag3, Scgn, Lias and Etfdh.	2,77	0,97
sp|Q8CI51|	PDZ and LIM domain protein 5 (Pdlim5)		Contributes to heart development by scaffolding PKC to the Z-disk region.	Vcl, Rwdd2b, Prkce, Sorbs2, Cacna1b, Actn1, Id2, Tpm2, Tpm1 and Acta2.	2,83	1,17
sp|Q9QZ47|	Troponin T (Tnnt3)		Contraction of striated skeletal muscles (Wei and Jin, 2016).	Tnni2, Tnnc2, Myl1, Actn3, Tnni1, Tpm2, Mybpc2, Tpm1, Tnni3 and Actn2.	2,87	1,13
H2AZ_MOUSE	Histone H2A.Z (H2afz)		Role in transcription regulation, DNA repair, DNA replication and chromosomal stability (Farris et al., 2005).	H3f3a, Hist2h3c2, Cdk1, Hist1h4j, H2afb2, Ruvbl1, Sirt1, Hist2h2ab, Kdm1a and Cenpa.	5,93	2,00
sp|K1C15_SHEEP|	Keratin 15 (KRT15)		Expressed in basal keratinocytes (Waseem et al., 1999).	APCDD1L, TELO2, CCDC101, SYNM, LGR6, LGR5, DNAJC15, LRIG1, KRT5, KRT77.	1,77	3,13
sp|Q923D2|	Flavin reductase (NADPH) (Blvrb)		Catalyzes the NADPH-dependent reduction of a variety of flavins via broad specificity oxidoreductase (Cunningham et al., 2000).	Hmox2, Hmox1, Blvra, Acp5, Rfk, Acp2, Bscl2, Ugt1a7c, Ugt2b1 and Ugt1a6b.	1,93	3,17
NFH_MOUSE	Neurofilament heavy polypeptide (Nefh)		Maintain neuronal calibre (Yuan et al., 2012).	Mapk14, Cdk5, Mapk11, Mapk13, Mapk12, Prph, Mbp, Calca, Nefl and Rbfox3.	2,03	2,47
RS14_MOUSE	Ribosomal protein S14 (Rps14)		Encode for the 40S ribosomal protein S14.	Rpl8, Rps5, Rps3, Rps25, Rps11, Rps15a, Rpl23, Rpl3, Rpl7 and Rpl5.	1,67	2,00
sp|P70232|	Neural cell adhesion molecule L1-like protein (Chl1)		Increases neuronal migration toward extracellular matrix proteins through endocytosis and MAP kinase signalling (Thelen et al., 2002).	Cntn6, Nrp1, Itgb1, Itga1, Itga2, Stip1, Ptpra, Dcx, St8sia3 and Gdnf.	2,63	2,07

Accession Number	Identifier	Known function in wound healing	Novel Identified	Interactions	Acute	Chronic
IGJ_MOUSE	Immunoglobulin J chain (Igj)		Links two monomer units of either IgM or IgA (Randall et al., 1992).	Fcamr, Ambp, Pigr, Ighv1-73, Cd79b, Cd79a, Iglc2, Piga, Syk and Pigm.	2,47	1,43
HORN_MOUSE	Hornerin (Hrnr)		Apart of the epidermal cornified cell envelopes (Henry et al., 2011).	Serpinb3b, Serpinb3c, Cap1, Dpp7, Ctsa, Padi2, Serpinb3a, Fabp5, Serpina3m and Ctsg.	2,80	1,63
sp|TRY1_BOVIN|	Bos taurus cationic trypsin (PRSS1)			ENSBTAG00000026119, ENSBTAG00000011995, ENSBTAG00000024245, SPINK1, SERPINA5, ALB, PTI, KRT1, KRT2 and AMBP.	1,73	1,63
NFM_MOUSE	Neurofilament medium polypeptide (Nefm)		Involved in the maintenance of neuronal calibre (Yuan et al., 2012).	Nefl, Prph, Mapk14, Mapk11, Mapk13, Mapk12, Nes, Vim, Des and Tubb3.	1,87	2,40
RL28_MOUSE	Ribosomal protein L28 (Rpl28)		Encodes for the 60S ribosomal protein L28.	Rpl19, Rpl18, Rpl8, Rpl26, Rpl34, Rpl10a, Rpl37a, Rpl36a, Rpl13 and Rpl5.	1,80	2,40
sp|A2AMM0|	Caveolae-associated protein 4 (Murc)		Controls the morphology of formed caveolae in cardiomyocytes (Ogata et al., 2008).	Cav3, Trim54, Dact1, Mybph, Cav1, Sestd1, Cav2, Lrrc17, Tnnc2 and Csrp3.	1,80	1,67
H15_MOUSE	Histone H1.5 (Hist1h1b)		Regulates individual gene transcription.	Ubn1, Asf1a, Hist1h1a, Hmgb2, H1f0, Hist1h1e, Hmgb1, Hist1h1d, Hira and Trp53.	3,53	1,67
RL14_MOUSE	Ribosomal protein L14 (Rpl14)		Encode for the 60S ribosomal protein L14.	Rps8, Rps11, Rpl35a, Rps3a1, Rpl8, Rpl26, Rps3, Rps13, Rps19 and Rps14.	2,33	3,20
ATR_MOUSE	Serine/threonine-protein kinase ATR (Atr)		Regulates DNA damage response mechanism (Goodarzi et al., 2003).	Chek1, Atrip, Topbp1, Rad17, Chek2, Blm, Mre11a, Wrn, Rad50 and Fancm.	2,63	1,27
sp|K1C9_HUMAN|	Keratin, type I cytoskeletal 9 (KRT9)		Keratin filament assembly.	KRT1, KRT7, KRT6B, KRT6A, KRT8, KRT4, KRT72, KRT5, KRT6C and KRT3.	1,83	2,17
sp|Q8VEE1|	LIM and cysteine-rich domains protein 1 (Lmcd1)		Role in the development of cardiac hypertrophy (Bian et al., 2010).	Gata6, Taf6l, Pcnx, Sgsm2, Lbh, Sbspon, Tsc22d3, Prpf38a, Ppp2r5e and Dlx2.	2,23	1,27
sp|K1C10_HUMAN|	KRT10	Re-epithelialization (Nuutila et al., 2012).		KRT1, KRT77, KRT5, KRT2, KRT16, PRSS1, KRT8, KRT7, KRT72 and KRT4.	1,70	2,07
H14_MOUSE	Histone H1.4 (Hist1h1e)		Regulates individual gene transcription.	Asf1a, Hist1h1d, Hist1h1a, Ubn1, H1f0, Cbx3, Hist1h1b, Hmgb2, Hist2h3c2 and Hist1h4j.	3,23	1,63

Accession Number	Identifier	Known function in wound healing	Novel Identified	Interactions	Acute	Chronic
H11_MOUSE	Histone H1.1 (Hist1h1a)		Regulates individual gene transcription.	Asf1a, Hist1h1b, Hist1h1e, Hmgb2, Hist1h1d, Hmgb1, Ubn1, H1f0, Hist1h1c and Hmga2.	3,53	2,03
sp|K2C1_HUMAN|	Keratin, type II cytoskeletal 1 (KRT1)		Regulates the activity of kinases (Chuang and Huang, 2007).	KRT10, KRT5, KRT2, KRT77, KRT9, PRSS1, KRT15, KRT13 and KRT17.	3,13	1,83
sp|Q69ZR2|	E3 ubiquitin-protein ligase HECTD1 (Hectd1)		Transfers the ubiquitin to targeted substrates.	Ubr4, Trip12, Ubr2, Ubr1, Ube2, Ube2z, Ube2a, Ube2o, Hectd3 and Ube2u.	1,77	2,63

Footnote: The table above displays proteins detected in both wild-type C57BL6/J mice treated with saline (Acute wound) and B6.cg-lepob/J (ob/ob), treated with NEP high (chronic wound). **Abbreviations:** refer to *Appendix D* for list of Abbreviations.

Chapter 7 : Conclusion, Future Perspectives and Limitations

Non-healing diabetic foot ulcers are characterised by the hindered progression from the inflammatory stage to the proliferative stage of healing resulting in a chronic inflammatory state (Landén et al., 2016, Zhao et al., 2016). The impairment in the progression of these wounds is not yet well understood. There are many animal models available that have contributed greatly to our understanding of wound healing, however none of these models are able to replicate the phenotype of human wound chronicity observed in non-healing diabetic foot ulcerations. Currently, many therapeutic approaches fail in clinical settings. A need for new models that are able to recapitulate/mimic the features of patient non-healing diabetic wounds will provide a greater understanding of dysfunctions occurring during the early phases of healing. This will greatly inform decisions on treatment strategies so that they can be clinically beneficial for patients.

Given results showing elevated NEP activity in the ulcer margins of diabetic patient foot ulceration compared to non-diabetic patients (Antezana et al., 2002) this study investigated the use of NEP in an animal wound model using B6.Cg-Lepob/J (ob/ob) to create a wound that tries to resemble the phenotype of non-healing diabetic wounds in patients. In addition, this study compared the impaired healing dynamics of this newly developed chronic wound model to that of a standard acute wound (C57BL/6J).

It was demonstrated that the administration of a high NEP concentration (1.02 mg/µL) in the ulcer margins of wounds created on the dorsal surface of B6.Cg-Lepob/J (ob/ob) resulted in similar features to that of patient diabetic wounds – delayed onset inflammation (day 2), high MMP-9 expression, delayed wound closure, hindered angiogenesis, re-epithelialization and granulation tissue formation. Specifically, when comparing the acute wounds to the chronic wounds, the chronic wounds displayed greater MMP-9 expression (day 0, 2 and 7), significantly lower wound contraction, no re-epithelialization, granulation tissue formation and angiogenesis occurring indicating that wound healing has been successfully hindered.

Proteomic analysis of the acute and chronic wounds indicated significant differences in the expression of proteins (Stefin-1, Stefin-3, Microtubule- associated protein 1B, Band 4.1-like protein 2, Caveolae-associated protein 1 and Gamma-synuclein) between chronic and acute wounds that have not been previously described to be directly implicated in wound healing. These proteins' functions were identified, and they could have downstream interactions that might play a role in healing. Two proteins known to be directly involved in wound healing (Alpha-1-acid glycoprotein 1 in inflammation and Nidogen-1 in proliferation and remodelling)

also differed. The overexpression of these proteins in chronic wounds could be attributed to either a positive feedback loop (elevated protein levels but downstream functions are impaired) or delayed onset healing (proteins have already been downregulated in acute group but remain elevated in chronic groups thereby delaying the onset of healing). Research needs to still be conducted on where exactly the dysregulation originates from.

Due to the small volume of wound fluid collected from each animal, wound fluid had to be pooled together for cytokine analysis limiting the establishment of variability in the cytokine levels amongst mice in each group, making statistical significance difficult to obtain. In future studies this will not change but this limitation can be overcome by increasing the number of animals per group so that at least 3 pooled samples are available for each treatment group. The chronic wounds were not directly compared to chronic patient wounds but rather literature was used as a guide to define characteristics of patient chronic wounds. The chronic wound induced in this study was monitored up to 7 days and not for a longer duration therefore it remains to be investigated to what extent does this method mimic a chronic wound with delayed healing or no healing.

In conclusion, high NEP administration in the wound edges of obese pre-diabetic mice resulted in a chronic wound model that better mimics human diabetic chronic wounds than lower NEP concentrations or saline administration. High NEP administration resulted in significantly lower wound closure that could be explained by higher MMP-9, lower cytokine content in wound fluid and differences in several proteins identified by proteomic analysis, however further work needs to be conducted to investigate to what extent this method mimics a chronic wound with delayed healing or no healing over greater time points.

Chapter 8 : References

AHMED, A. S., LI, J., ABDUL, A. M., AHMED, M., OSTENSON, C. G., SALO, P. T., HEWITT, C., HART, D. A. & ACKERMANN, P. W. 2017. Compromised Neurotrophic and Angiogenic Regenerative Capability during Tendon Healing in a Rat Model of Type-II Diabetes. *PLoS One,* 12**,** e0170748.

ALEXIADOU, K. & DOUPIS, J. 2012. Management of diabetic foot ulcers. *Diabetes therapy : research, treatment and education of diabetes and related disorders,* 3**,** 4-4.

ANTEZANA, M., SULLIVAN, S. R., USUI, M., GIBRAN, N., SPENNY, M., LARSEN, J., ANSEL, J., BUNNETT, N. & OLERUD, J. 2002. Neutral endopeptidase activity is increased in the skin of subjects with diabetic ulcers. *J Invest Dermatol,* 119**,** 1400-4.

ATABAY, K. D., YILDIZ, M. T., AVSAR, T., KARABAY, A. & KILIÇ, T. 2015. Knockdown of Pin1 leads to reduced angiogenic potential and tumorigenicity in glioblastoma cells. *Oncology letters,* 10**,** 2385-2389.

ATRI, C., GUERFALI, F. Z. & LAOUINI, D. 2018. Role of Human Macrophage Polarization in Inflammation during Infectious Diseases. *International journal of molecular sciences,* 19**,** 1801.

BAO, P., KODRA, A., TOMIC-CANIC, M., GOLINKO, M. S., EHRLICH, H. P. & BREM, H. 2009. The role of vascular endothelial growth factor in wound healing. *Journal of Surgical Research,* 153**,** 347-358.

BARANOWSKY, A., MOKKAPATI, S., BECHTEL, M., KRUGEL, J., MIOSGE, N., WICKENHAUSER, C., SMYTH, N. & NISCHT, R. 2010. Impaired wound healing in mice lacking the basement membrane protein nidogen 1. *Matrix Biol,* 29**,** 15-21.

BEAVERS, D. L., LANDSTROM, A. P., CHIANG, D. Y. & WEHRENS, X. H. T. 2014. Emerging roles of junctophilin-2 in the heart and implications for cardiac diseases. *Cardiovascular Research,* 103**,** 198-205.

BEN-BARUCH, A., BENGALI, K. M., BIRAGYN, A., JOHNSTON, J. J., WANG, J.-M., KIM, J., CHUNTHARAPAI, A., MICHIEL, D. F., OPPENHEIM, J. J. & KELVIN, D. J. 1995. Interleukin-8 receptor the role of the carboxyl terminus in signal transduction. *Journal of Biological Chemistry,* 270**,** 9121-9128.

BERGER, F., BERKHOLZ, J., BREUSTEDT, T., PLOEN, D. & MUNZ, B. 2012. Skeletal muscle-specific variant of nascent polypeptide associated complex alpha (skNAC): implications for a specific role in mammalian myoblast differentiation. *European journal of cell biology,* 91**,** 150-155.

BERLANGA-ACOSTA, J., SCHULTZ, G. S., LÓPEZ-MOLA, E., GUILLEN-NIETO, G., GARCÍA-SIVERIO, M. & HERRERA-MARTÍNEZ, L. 2013. Glucose toxic effects on granulation tissue productive cells: the diabetics' impaired healing. *BioMed research international,* 2013.

BHOWMICK, N. A., NEILSON, E. G. & MOSES, H. L. 2004. Stromal fibroblasts in cancer initiation and progression. *Nature,* 432**,** 332-337.

BIAN, Z. Y., HUANG, H., JIANG, H., SHEN, D. F., YAN, L., ZHU, L. H., WANG, L., CAO, F., LIU, C., TANG, Q. Z. & LI, H. 2010. LIM and cysteine-rich domains 1 regulates cardiac hypertrophy by targeting calcineurin/nuclear factor of activated T cells signaling. *Hypertension,* 55**,** 257-63.

BICKEL, M. 1993. The role of interleukin-8 in inflammation and mechanisms of regulation. *J Periodontol,* 64**,** 456-60.

BILODEAU, M., MACRAE, T., GABOURY, L., LAVERDURE, J. P., HARDY, M. P., MAYOTTE, N., PARADIS, V., HARTON, S., PERREAULT, C. & SAUVAGEAU, G. 2009. Analysis of blood stem cell activity and cystatin gene expression in a mouse model presenting a chromosomal deletion encompassing Csta and Stfa2l1. *PLoS One,* 4**,** e7500.

BLOOM, G. S., LUCA, F. C. & VALLEE, R. B. 1985. Microtubule-associated protein 1B: identification of a major component of the neuronal cytoskeleton. *Proceedings of the National Academy of Sciences,* 82**,** 5404.

BODNAR, R. J. 2013. Epidermal growth factor and epidermal growth factor receptor: the Yin and Yang in the treatment of cutaneous wounds and cancer. *Advances in wound care,* 2**,** 24-29.

BOU-GHARIOS, G., ABRAHAM, D. & DE CROMBRUGGHE, B. 2020. Type I collagen structure, synthesis, and regulation. *Principles of bone biology.* Elsevier.

BROWN, D. T., IZARD, T. & MISTELI, T. 2006. Mapping the interaction surface of linker histone H10 with the nucleosome of native chromatin in vivo. *Nature Structural & Molecular Biology,* 13**,** 250-255.

BUCHMAN, V. L., ADU, J., PINON, L. G., NINKINA, N. N. & DAVIES, A. M. 1998. Persyn, a member of the synuclein family, influences neurofilament network integrity. *Nat Neurosci,* 1**,** 101-3.

BURSSENS, P., STEYAERT, A., FORSYTH, R., VAN OVOST, E. J., DEPAEPE, Y. & VERDONK, R. 2005. Exogenously administered substance P and neutral endopeptidase inhibitors stimulate fibroblast proliferation, angiogenesis and collagen organization during Achilles tendon healing. *Foot Ankle Int,* 26**,** 832-9.

CANALIS, E. 2008. Platelet-Derived Growth Factor and the Skeleton. *Principles of Bone Biology.* Elsevier.

CANO SANCHEZ, M., LANCEL, S., BOULANGER, E. & NEVIERE, R. 2018. Targeting Oxidative Stress and Mitochondrial Dysfunction in the Treatment of Impaired Wound Healing: A Systematic Review. *Antioxidants (Basel, Switzerland),* 7**,** 98.

CAPOZZA, F., COMBS, T. P., COHEN, A. W., CHO, Y. R., PARK, S. Y., SCHUBERT, W., WILLIAMS, T. M., BRASAEMLE, D. L., JELICKS, L. A., SCHERER, P. E., KIM, J. K. & LISANTI, M. P. 2005. Caveolin-3 knockout mice show increased adiposity and whole body insulin resistance, with ligand-induced insulin receptor instability in skeletal muscle. *Am J Physiol Cell Physiol,* 288**,** C1317-31.

CARLSON, S. M., MOORE, K. E., SANKARAN, S. M., REYNOIRD, N., ELIAS, J. E. & GOZANI, O. 2015. A proteomic strategy identifies lysine methylation of splicing factor snRNP70 by the SETMAR enzyme. *Journal of Biological Chemistry,* 290**,** 12040-12047.

CHALOVICH, J. M. & SCHROETER, M. M. 2010. Synaptopodin family of natively unfolded, actin binding proteins: physical properties and potential biological functions. *Biophysical reviews,* 2**,** 181-189.

CHEN, J. S., LONGAKER, M. T. & GURTNER, G. C. 2013. Murine models of human wound healing. *Methods Mol Biol,* 1037**,** 265-74.

CHENG, F. & ERIKSSON, J. E. 2017. Intermediate filaments and the regulation of cell motility during regeneration and wound healing. *Cold Spring Harbor perspectives in biology,* 9**,** a022046.

CHENG, F., SHEN, Y., MOHANASUNDARAM, P., LINDSTROM, M., IVASKA, J., NY, T. & ERIKSSON, J. E. 2016. Vimentin coordinates fibroblast proliferation and keratinocyte differentiation in wound healing via TGF-beta-Slug signaling. *Proc Natl Acad Sci U S A,* 113**,** E4320-7.

CHO, H.-Y., MORGAN, D. L., BAUER, A. K. & KLEEBERGER, S. R. 2007. Signal transduction pathways of tumor necrosis factor–mediated lung injury induced by ozone in mice. *American journal of respiratory and critical care medicine,* 175**,** 829-839.

CHO, N., SHAW, J., KARURANGA, S., HUANG, Y., DA ROCHA FERNANDES, J., OHLROGGE, A. & MALANDA, B. 2018. IDF Diabetes Atlas: Global estimates of diabetes prevalence for 2017 and projections for 2045. *Diabetes research and clinical practice,* 138**,** 271-281.

CHUANG, N. N. & HUANG, C. C. 2007. Interaction of integrin beta1 with cytokeratin 1 in neuroblastoma NMB7 cells. *Biochem Soc Trans,* 35**,** 1292-4.

COLEMAN, D. L. 1978. Obese and diabetes: two mutant genes causing diabetes-obesity syndromes in mice. *Diabetologia,* 14**,** 141-8.

COUET, J., LI, S., OKAMOTO, T., IKEZU, T. & LISANTI, M. P. 1997. Identification of peptide and protein ligands for the caveolin-scaffolding domain Implications for the interaction of caveolin with caveolae-associated proteins. *Journal of Biological Chemistry,* 272**,** 6525-6533.

CUNNINGHAM, O., GORE, M. G. & MANTLE, T. J. 2000. Initial-rate kinetics of the flavin reductase reaction catalysed by human biliverdin-IXbeta reductase (BVR-B). *Biochem J,* 345 Pt 2**,** 393-9.

DELGADO, A. V., MCMANUS, A. T. & CHAMBERS, J. P. 2003. Production of tumor necrosis factor-alpha, interleukin 1-beta, interleukin 2, and interleukin 6 by rat leukocyte subpopulations after exposure to substance P. *Neuropeptides,* 37**,** 355-61.

DEMIDOVA-RICE, T. N., HAMBLIN, M. R. & HERMAN, I. M. 2012. Acute and impaired wound healing: pathophysiology and current methods for drug delivery, part 1: normal and chronic wounds: biology, causes, and approaches to care. *Adv Skin Wound Care,* 25**,** 304-14.

DIEGELMANN, R. F. & EVANS, M. C. 2004. Wound healing: an overview of acute, fibrotic and delayed healing. *Front Biosci,* 9**,** 283-9.

DRESIOS, J., ASCHRAFI, A., OWENS, G. C., VANDERKLISH, P. W., EDELMAN, G. M. & MAURO, V. P. 2005. Cold stress-induced protein Rbm3 binds 60S ribosomal subunits, alters microRNA levels, and enhances global protein synthesis. *Proceedings of the National Academy of Sciences,* 102**,** 1865-1870.

ELLIOT, S., WIKRAMANAYAKE, T. C., JOZIC, I. & TOMIC-CANIC, M. 2018. A Modeling Conundrum: Murine Models for Cutaneous Wound Healing. *J Invest Dermatol,* 138**,** 736-740.

ELSASSER, S., GALI, R. R., SCHWICKART, M., LARSEN, C. N., LEGGETT, D. S., MÜLLER, B., FENG, M. T., TÜBING, F., DITTMAR, G. A. G. & FINLEY, D. 2002. Proteasome subunit Rpn1 binds ubiquitin-like protein domains. *Nature Cell Biology,* 4**,** 725-730.

EMING, S. A., KRIEG, T. & DAVIDSON, J. M. 2007. Inflammation in wound repair: molecular and cellular mechanisms. *Journal of Investigative Dermatology,* 127**,** 514-525.

FANG, R. C., KRYGER, Z. B., BUCK, D. W., 2ND, DE LA GARZA, M., GALIANO, R. D. & MUSTOE, T. A. 2010. Limitations of the db/db mouse in translational wound healing research: Is the NONcNZO10 polygenic mouse model superior? *Wound Repair Regen,* 18**,** 605-13.

FARRIS, S. D., RUBIO, E. D., MOON, J. J., GOMBERT, W. M., NELSON, B. H. & KRUMM, A. 2005. Transcription-induced chromatin remodeling at the c-myc gene involves the local exchange of histone H2A.Z. *J Biol Chem,* 280**,** 25298-303.

FINNSON, K. W., MCLEAN, S., DI GUGLIELMO, G. M. & PHILIP, A. 2013. Dynamics of transforming growth factor beta signaling in wound healing and scarring. *Advances in wound care,* 2**,** 195-214.

FIUCCI, G., LESPAGNOL, A., STUMPTNER-CUVELETTE, P., BEAUCOURT, S., DUFLAUT, D., SUSINI, L., AMSON, R. & TELERMAN, A. 2003. Genomic organization and expression of mouse Tpt1 gene☆. *Genomics,* 81**,** 570-578.

FOURNIER, T., MEDJOUBI, N. N. & PORQUET, D. 2000. Alpha-1-acid glycoprotein. *Biochim Biophys Acta,* 1482**,** 157-71.

FOX, A. H. & LAMOND, A. I. 2010. Paraspeckles. *Cold Spring Harbor perspectives in biology,* 2**,** a000687.

FRYKBERG, R. G. 1998. Diabetic foot ulcers: current concepts. *J Foot Ankle Surg,* 37**,** 440-6.

FRYKBERG, R. G. & BANKS, J. 2015. Challenges in the treatment of chronic wounds. *Advances in wound care,* 4**,** 560-582.

FU, X. L., DING, H., MIAO, W. W., MAO, C. X., ZHAN, M. Q. & CHEN, H. L. 2019. Global recurrence rates in diabetic foot ulcers: A systematic review and meta-analysis. *Diabetes Metab Res Rev***,** e3160.

FUJIWARA, N. & KOBAYASHI, K. 2005. Macrophages in inflammation. *Curr Drug Targets Inflamm Allergy,* 4**,** 281-6.

GALEANO, M., TORRE, V., DEODATO, B., CAMPO, G. M., COLONNA, M., STURIALE, A., SQUADRITO, F., CAVALLARI, V., CUCINOTTA, D., BUEMI, M. & ALTAVILLA, D. 2001. Raxofelast, a hydrophilic vitamin E-like antioxidant, stimulates wound healing in genetically diabetic mice. *Surgery,* 129**,** 467-77.

GARGIULO, S., GRECO, A., GRAMANZINI, M., ESPOSITO, S., AFFUSO, A., BRUNETTI, A. & VESCE, G. 2012. Mice anesthesia, analgesia, and care, Part I: anesthetic considerations in preclinical research. *ILAR journal,* 53**,** E55-E69.

GARZA, A. E., POJOGA, L. H., MOIZE, B., HAFIZ, W. M., OPSASNICK, L. A., SIDDIQUI, W. T., HORENSTEIN, M., ADLER, G. K., WILLIAMS, G. H. & KHALIL, R. A. 2015. Critical role of striatin in blood pressure and vascular responses to dietary sodium intake. *Hypertension,* 66**,** 674-680.

GENOVA, R. M., MEYER, K. J., ANDERSON, M. G., HARPER, M. M. & PIEPER, A. A. 2018. Neprilysin inhibition promotes corneal wound healing. *Sci Rep,* 8**,** 14385.

GIBRAN, N. S., JANG, Y. C., ISIK, F. F., GREENHALGH, D. G., MUFFLEY, L. A., UNDERWOOD, R. A., USUI, M. L., LARSEN, J., SMITH, D. G., BUNNETT, N., ANSEL, J. C. & OLERUD, J. E. 2002. Diminished neuropeptide levels contribute to the impaired cutaneous healing response associated with diabetes mellitus. *J Surg Res,* 108**,** 122-8.

GINISTY, H., SICARD, H., ROGER, B. & BOUVET, P. 1999. Structure and functions of nucleolin. *Journal of Cell Science,* 112**,** 761-772.

GOH, S.-Y. & COOPER, M. E. 2008. The Role of Advanced Glycation End Products in Progression and Complications of Diabetes. *The Journal of Clinical Endocrinology & Metabolism,* 93**,** 1143-1152.

GOKHIN, D. S., OCHALA, J., DOMENIGHETTI, A. A. & FOWLER, V. M. 2015. Tropomodulin 1 directly controls thin filament length in both wild-type and tropomodulin 4-deficient skeletal muscle. *Development,* 142**,** 4351-4362.

GOLINI, L., CHOUABE, C., BERTHIER, C., CUSIMANO, V., FORNARO, M., BONVALLET, R., FORMOSO, L., GIACOMELLO, E., JACQUEMOND, V. & SORRENTINO, V. 2011. Junctophilin 1 and 2 proteins interact with the L-type Ca2+ channel dihydropyridine receptors (DHPRs) in skeletal muscle. *The Journal of biological chemistry,* 286**,** 43717-43725.

GONZALEZ, A. C. D. O., COSTA, T. F., ANDRADE, Z. D. A. & MEDRADO, A. R. A. P. 2016. Wound healing - A literature review. *Anais brasileiros de dermatologia,* 91**,** 614-620.

GOODARZI, A. A., BLOCK, W. D. & LEES-MILLER, S. P. 2003. The role of ATM and ATR in DNA damage-induced cell cycle control. *Progress in cell cycle research,* 5**,** 393-411.

GURTNER, G. C., WERNER, S., BARRANDON, Y. & LONGAKER, M. T. 2008. Wound repair and regeneration. *Nature,* 453**,** 314.

HAN, J. W., SIN, M. Y. & YOON, Y.-S. 2013. Cell therapy for diabetic neuropathy using adult stem or progenitor cells. *Diabetes & metabolism journal,* 37**,** 91-105.

HENRY, J., HSU, C. Y., HAFTEK, M., NACHAT, R., DE KONING, H. D., GARDINAL-GALERA, I., HITOMI, K., BALICA, S., JEAN-DECOSTER, C., SCHMITT, A. M., PAUL, C., SERRE, G. & SIMON, M. 2011. Hornerin is a component of the epidermal cornified cell envelopes. *Faseb j,* 25**,** 1567-76.

HOFFMANN, M. H. & GRIFFITHS, H. R. 2018. The dual role of Reactive Oxygen Species in autoimmune and inflammatory diseases: evidence from preclinical models. *Free Radic Biol Med,* 125**,** 62-71.

HOTULAINEN, P., PAUNOLA, E., VARTIAINEN, M. K. & LAPPALAINEN, P. 2005. Actin-depolymerizing Factor and Cofilin-1 Play Overlapping Roles in Promoting Rapid F-Actin Depolymerization in Mammalian Nonmuscle Cells. *Molecular Biology of the Cell,* 16**,** 649-664.

JIANG, F., ZHANG, Y. & DUSTING, G. J. 2011. NADPH oxidase-mediated redox signaling: roles in cellular stress response, stress tolerance, and tissue repair. *Pharmacol Rev,* 63**,** 218-42.

JUNG, N., YU, J., UM, J., DUBON, M. J. & PARK, K. S. 2016. Substance P modulates properties of normal and diabetic dermal fibroblasts. *Tissue Eng Regen Med,* 13**,** 155-161.

KACZOCHA, M., VIVIECA, S., SUN, J., GLASER, S. T. & DEUTSCH, D. G. 2012. Fatty acid-binding proteins transport N-acylethanolamines to nuclear receptors and are targets of endocannabinoid transport inhibitors. *J Biol Chem,* 287**,** 3415-24.

KALLURI, R. & ZEISBERG, M. 2006. Fibroblasts in cancer. *Nature Reviews Cancer,* 6**,** 392-401.

KANT, V., GOPAL, A., KUMAR, D., BAG, S., KURADE, N. P., KUMAR, A., TANDAN, S. K. & KUMAR, D. 2013. Topically applied substance P enhanced healing of open excision wound in rats. *Eur J Pharmacol,* 715**,** 345-53.

KANT, V., KUMAR, D., KUMAR, D., PRASAD, R., GOPAL, A., PATHAK, N. N., KUMAR, P. & TANDAN, S. K. 2015. Topical application of substance P promotes wound healing in streptozotocin-induced diabetic rats. *Cytokine,* 73**,** 144-55.

KANT, V., KUMAR, D., PRASAD, R., GOPAL, A., PATHAK, N. N., KUMAR, P. & TANDAN, S. K. 2017. Combined effect of substance P and curcumin on cutaneous wound healing in diabetic rats. *J Surg Res,* 212**,** 130-145.

KEAYS, D. A. 2007. Neuronal migration: unraveling the molecular pathway with humans, mice, and a fungus. *Mamm Genome,* 18**,** 425-30.

KIM, J. E., LEE, J. H., KIM, S. H. & JUNG, Y. 2018. Skin Regeneration with Self-Assembled Peptide Hydrogels Conjugated with Substance P in a Diabetic Rat Model. *Tissue Eng Part A,* 24**,** 21-33.

KLEIBER, M. 1975. Metabolic turnover rate: a physiological meaning of the metabolic rate per unit body weight. *J Theor Biol,* 53**,** 199-204.

KLJUIC, A. & CHRISTIANO, A. M. 2003. A novel mouse desmosomal cadherin family member, desmoglein 1γ. *Experimental Dermatology,* 12**,** 20-29.

KOBIELAK, A. & BODDUPALLY, K. 2014. Junctions and Inflammation in the Skin. *Cell Communication & Adhesion,* 21**,** 141-147.

KROCZEK, C., LANG, C., BRACHS, S., GROHMANN, M., DÜTTING, S., SCHWEIZER, A., NITSCHKE, L., FELLER, S. M., JÄCK, H.-M. & MIELENZ, D. 2010. Swiprosin-1/EFhd2 controls B cell receptor signaling through the assembly of the B cell receptor, Syk, and phospholipase C γ2 in membrane rafts. *The Journal of Immunology,* 184**,** 3665-3676.

LANDÉN, N. X., LI, D. & STÅHLE, M. 2016. Transition from inflammation to proliferation: a critical step during wound healing. *Cellular and molecular life sciences : CMLS,* 73**,** 3861-3885.

LANDSTROM, A. P., BEAVERS, D. L. & WEHRENS, X. H. T. 2014. The junctophilin family of proteins: from bench to bedside. *Trends in molecular medicine,* 20**,** 353-362.

LANG, K., SCHMID, F. X. & FISCHER, G. 1987. Catalysis of protein folding by prolyl isomerase. *Nature,* 329**,** 268-70.

LAROUCHE, J., SHEORAN, S., MARUYAMA, K. & M. MARTINO, M. 2018. Immune Regulation of Skin Wound Healing: Mechanisms and Novel Therapeutic Targets. *Advances in Wound Care,* 7.

LASSELIN, J. & CAPURON, L. 2014. Chronic low-grade inflammation in metabolic disorders: relevance for behavioral symptoms. *Neuroimmunomodulation,* 21**,** 95-101.

LEAL, E. C., CARVALHO, E., TELLECHEA, A., KAFANAS, A., TECILAZICH, F., KEARNEY, C., KUCHIBHOTLA, S., AUSTER, M. E., KOKKOTOU, E., MOONEY, D. J., LOGERFO, F. W., PRADHAN-NABZDYK, L. & VEVES, A. 2015. Substance P promotes wound healing in diabetes by modulating inflammation and macrophage phenotype. *The American journal of pathology,* 185**,** 1638-1648.

LEBERT, D., SQUIRRELL, J. M., FREISINGER, C., RINDY, J., GOLENBERG, N., FRECENTESE, G., GIBSON, A., ELICEIRI, K. W. & HUTTENLOCHER, A. 2018. Damage-induced reactive oxygen species regulate vimentin and dynamic collagen-based projections to mediate wound repair. *Elife,* 7**,** e30703.

LEE, M., ROY, N., MOGFORD, J., SCHIEMANN, W. & MUSTOE, T. 2004. Fibulin-5 promotes wound healing in vivo. *Journal of the American College of Surgeons,* 199**,** 403-10.

LEITER, E. H., STROBEL, M., O'NEILL, A., SCHULTZ, D., SCHILE, A. & REIFSNYDER, P. C. 2013. Comparison of Two New Mouse Models of Polygenic Type 2 Diabetes at the Jackson Laboratory, NONcNZO10Lt/J and TALLYHO/JngJ. *Journal of Diabetes Research,* 2013**,** 7.

LEPÄNTALO, M., APELQVIST, J., SETACCI, C., RICCO, J. B., DE DONATO, G., BECKER, F., ROBERT-EBADI, H., CAO, P., ECKSTEIN, H. H., DE RANGO, P., DIEHM, N., SCHMIDLI, J., TERAA, M., MOLL, F. L., DICK, F. & DAVIES, A. H. 2011. Chapter V: Diabetic Foot. *European Journal of Vascular and Endovascular Surgery,* 42**,** S60-S74.

LI, J., CHEN, J. & KIRSNER, R. 2007. Pathophysiology of acute wound healing. *Clin Dermatol,* 25**,** 9-18.

LIN, Z. Q., KONDO, T., ISHIDA, Y., TAKAYASU, T. & MUKAIDA, N. 2003. Essential involvement of IL-6 in the skin wound-healing process as evidenced by delayed wound healing in IL-6-deficient mice. *J Leukoc Biol,* 73**,** 713-21.

LIU, J. Y., HU, J. H., ZHU, Q. G., LI, F. Q. & SUN, H. J. 2006. Substance P receptor expression in human skin keratinocytes and fibroblasts. *Br J Dermatol,* 155**,** 657-62.

LIU, Y., MIN, D., BOLTON, T., NUBE, V., TWIGG, S. M., YUE, D. K. & MCLENNAN, S. V. 2009. Increased matrix metalloproteinase-9 predicts poor wound healing in diabetic foot ulcers. *Diabetes Care,* 32**,** 117-9.

LOBMANN, R., AMBROSCH, A., SCHULTZ, G., WALDMANN, K., SCHIWECK, S. & LEHNERT, H. 2002. Expression of matrix-metalloproteinases and their inhibitors in the wounds of diabetic and non-diabetic patients. *Diabetologia,* 45**,** 1011-1016.

LONGMATE, W. M., MONICHAN, R., CHU, M.-L., TSUDA, T., MAHONEY, M. G. & DIPERSIO, C. M. 2014. Reduced fibulin-2 contributes to loss of basement membrane integrity and skin blistering in mice lacking integrin α3β1 in the epidermis. *The Journal of investigative dermatology,* 134**,** 1609-1617.

LORENZON, E., COLLADEL, R., ANDREUZZI, E., MARASTONI, S., TODARO, F., SCHIAPPACASSI, M., LIGRESTI, G., COLOMBATTI, A. & MONGIAT, M. 2012. MULTIMERIN2 impairs tumor angiogenesis and growth by interfering with VEGF-A/VEGFR2 pathway. *Oncogene,* 31**,** 3136-47.

LU, R., WANG, H., LIANG, Z., KU, L., O'DONNELL, W. T., LI, W., WARREN, S. T. & FENG, Y. 2004. The fragile X protein controls microtubule-associated protein 1B translation and microtubule stability in brain neuron development. *Proceedings of the National Academy of Sciences,* 101**,** 15201-15206.

LUKAČÍNOVÁ, A., HUBKOVÁ, B., RÁCZ, O. & NIŠTIAR, F. 2013. Animal models for study of diabetes mellitus. *Diabetes mellitus-insights and perspectives***,** 229-54.

LUO, J.-H. 2004. SYNPO2 (synaptopodin 2). *Atlas of Genetics and Cytogenetics in Oncology and Haematology*.

MACKELLAR, M. & VIGERUST, D. J. 2016. Role of Haptoglobin in Health and Disease: A Focus on Diabetes. *Clinical Diabetes,* 34**,** 148-157.

MASHAGHI, A., MARMALIDOU, A., TEHRANI, M., GRACE, P. M., POTHOULAKIS, C. & DANA, R. 2016. Neuropeptide substance P and the immune response. *Cell Mol Life Sci,* 73**,** 4249-4264.

MAST, B. A. & SCHULTZ, G. S. 1996. Interactions of cytokines, growth factors, and proteases in acute and chronic wounds. *Wound Repair Regen,* 4**,** 411-20.

MATIAS, M. A., SAUNUS, J. M., IVANOVSKI, S., WALSH, L. J. & FARAH, C. S. 2011. Accelerated wound healing phenotype in Interleukin 12/23 deficient mice. *Journal of inflammation (London, England),* 8**,** 39-39.

MCCARTY, S. M. & PERCIVAL, S. L. 2013. Proteases and Delayed Wound Healing. *Advances in wound care,* 2**,** 438-447.

MUANGMAN, P., SPENNY, M. L., TAMURA, R. N. & GIBRAN, N. S. 2003. Fatty acids and glucose increase neutral endopeptidase activity in human microvascular endothelial cells. *Shock,* 19**,** 508-12.

MUANGMAN, P., TAMURA, R. N. & GIBRAN, N. S. 2005. Antioxidants inhibit fatty acid and glucose-mediated induction of neutral endopeptidase gene expression in human microvascular endothelial cells. *J Am Coll Surg,* 200**,** 208-15.

NAKAJO, A., YOSHIMURA, S.-I., TOGAWA, H., KUNII, M., IWANO, T., IZUMI, A., NOGUCHI, Y., WATANABE, A., GOTO, A. & SATO, T. 2016. EHBP1L1 coordinates Rab8 and Bin1 to regulate apical-directed transport in polarized epithelial cells. *J Cell Biol,* 212**,** 297-306.

NEIDHARDT, J., FEHR, S., KUTSCHE, M., LÖHLER, J. & SCHACHNER, M. 2003. Tenascin-N: characterization of a novel member of the tenascin family that mediates neurite repulsion from hippocampal explants. *Molecular and Cellular Neuroscience,* 23**,** 193-209.

NI, T., LIU, Y., PENG, Y., LI, M., FANG, Y. & YAO, M. 2016. Substance P induces inflammatory responses involving NF-κB in genetically diabetic mice skin fibroblasts co-cultured with macrophages. *American journal of translational research,* 8**,** 2179-2188.

NOCH, E. K. & KHALILI, K. 2013. The role of AEG-1/MTDH/LYRIC in the pathogenesis of central nervous system disease. *Advances in cancer research,* 120**,** 159-192.

NUNAN, R., HARDING, K. G. & MARTIN, P. 2014. Clinical challenges of chronic wounds: searching for an optimal animal model to recapitulate their complexity. *Disease models & mechanisms,* 7**,** 1205-1213.

NUUTILA, K., SILTANEN, A., PEURA, M., BIZIK, J., KAARTINEN, I., KUOKKANEN, H., NIEMINEN, T., HARJULA, A., AARNIO, P. & VUOLA, J. 2012. Human skin transcriptome during superficial cutaneous wound healing. *Wound Repair and Regeneration,* 20**,** 830-839.

O'CONNOR, T. M., O'CONNELL, J., O'BRIEN, D. I., GOODE, T., BREDIN, C. P. & SHANAHAN, F. 2004. The role of substance P in inflammatory disease. *Journal of cellular physiology,* 201**,** 167-180.

OGATA, T., UEYAMA, T., ISODONO, K., TAGAWA, M., TAKEHARA, N., KAWASHIMA, T., HARADA, K., TAKAHASHI, T., SHIOI, T., MATSUBARA, H. & OH, H. 2008. MURC, a muscle-restricted coiled-coil protein that modulates the Rho/ROCK pathway, induces cardiac dysfunction and conduction disturbance. *Mol Cell Biol,* 28**,** 3424-36.

OHNUMA, K., UCHIYAMA, M., YAMOCHI, T., NISHIBASHI, K., HOSONO, O., TAKAHASHI, N., KINA, S., TANAKA, H., LIN, X., DANG, N. H. & MORIMOTO, C. 2007. Caveolin-1 triggers T-cell activation via CD26 in association with CARMA1. *J Biol Chem,* 282**,** 10117-31.

OKONKWO, U. A. & DIPIETRO, L. A. 2017. Diabetes and Wound Angiogenesis. *International journal of molecular sciences,* 18**,** 1419.

OLERUD, J. E., USUI, M. L., SECKIN, D., CHIU, D. S., HAYCOX, C. L., SONG, I. S., ANSEL, J. C. & BUNNETT, N. W. 1999. Neutral endopeptidase expression and distribution in human skin and wounds. *J Invest Dermatol,* 112**,** 873-81.

OLINS, A. L., RHODES, G., WELCH, D. B. M., ZWERGER, M. & OLINS, D. E. 2010. Lamin B receptor: multi-tasking at the nuclear envelope. *Nucleus (Austin, Tex.),* 1**,** 53-70.

OLMOS, Y. & CARLTON, J. G. 2016. The ESCRT machinery: new roles at new holes. *Current Opinion in Cell Biology,* 38**,** 1-11.

ORNITZ, D. M. & ITOH, N. 2015. The fibroblast growth factor signaling pathway. *Wiley Interdisciplinary Reviews: Developmental Biology,* 4**,** 215-266.

OWEN, J. & MOHAMADZADEH, M. 2013. Macrophages and chemokines as mediators of angiogenesis. *Frontiers in physiology,* 4**,** 159.

PARK, J. H., KIM, S., HONG, H. S. & SON, Y. 2016. Substance P promotes diabetic wound healing by modulating inflammation and restoring cellular activity of mesenchymal stem cells. *Wound Repair Regen,* 24**,** 337-48.

PELED, M., DRAGOVICH, M. A., ADAM, K., STRAZZA, M., TOCHEVA, A. S., VEGA, I. E. & MOR, A. 2018. EF Hand Domain Family Member D2 Is Required for T Cell Cytotoxicity. *J Immunol,* 201**,** 2824-2831.

PERIAYAH, M. H., HALIM, A. S. & MAT SAAD, A. Z. 2017. Mechanism Action of Platelets and Crucial Blood Coagulation Pathways in Hemostasis. *International journal of hematology-oncology and stem cell research,* 11**,** 319-327.

PERNOW, B. 1983. Substance P. *Pharmacol Rev,* 35**,** 85-141.

PRADHAN, L., CAI, X., WU, S., ANDERSEN, N. D., MARTIN, M., MALEK, J., GUTHRIE, P., VEVES, A. & LOGERFO, F. W. 2011. Gene expression of pro-inflammatory cytokines and neuropeptides in diabetic wound healing. *The Journal of surgical research,* 167**,** 336-342.

PRADHAN, L., NABZDYK, C., ANDERSEN, N. D., LOGERFO, F. W. & VEVES, A. 2009. Inflammation and neuropeptides: the connection in diabetic wound healing. *Expert reviews in molecular medicine,* 11**,** e2-e2.

RANDALL, T. D., BREWER, J. W. & CORLEY, R. B. 1992. Direct evidence that J chain regulates the polymeric structure of IgM in antibody-secreting B cells. *J Biol Chem,* 267**,** 18002-7.

REISS, M. J., HAN, Y.-P., GARCIA, E., GOLDBERG, M., YU, H. & GARNER, W. L. 2010. Matrix metalloproteinase-9 delays wound healing in a murine wound model. *Surgery,* 147**,** 295-302.

ROTH, W., KUMAR, V., BEER, H.-D., RICHTER, M., WOHLENBERG, C., REUTER, U., THIERING, S., STARATSCHEK-JOX, A., HOFMANN, A., KREUSCH, F., SCHULTZE, J. L., VOGL, T., ROTH, J., REICHELT, J., HAUSSER, I. & MAGIN, T. M. 2012. Keratin 1 maintains skin integrity and participates in an inflammatory network in skin through interleukin-18. *Journal of Cell Science,* 125**,** 5269-5279.

RUHANEN, H., BORRIE, S., SZABADKAI, G., TYYNISMAA, H., JONES, A. W., KANG, D., TAANMAN, J. W. & YASUKAWA, T. 2010. Mitochondrial single-stranded DNA binding protein is required for maintenance of mitochondrial DNA and 7S DNA but is not required for mitochondrial nucleoid organisation. *Biochim Biophys Acta,* 1803**,** 931-9.

SASAKI, S., MORI, D., TOYO-OKA, K., CHEN, A., GARRETT-BEAL, L., MURAMATSU, M., MIYAGAWA, S., HIRAIWA, N., YOSHIKI, A., WYNSHAW-BORIS, A. & HIROTSUNE, S. 2005. Complete loss of Ndel1 results in neuronal migration defects and early embryonic lethality. *Mol Cell Biol,* 25**,** 7812-27.

SCOTT, J. R., TAMURA, R. N., MUANGMAN, P., ISIK, F. F., XIE, C. & GIBRAN, N. S. 2008. Topical substance P increases inflammatory cell density in genetically diabetic murine wounds. *Wound Repair Regen,* 16**,** 529-33.

SHAW, T. J. & MARTIN, P. 2009. Wound repair at a glance. *Journal of Cell Science,* 122**,** 3209-3213.

SHI, J., BARAKAT, M., CHEN, D. & CHEN, L. 2018. Bicellular Tight Junctions and Wound Healing. *International journal of molecular sciences,* 19**,** 3862.

SHU, B., XIE, J. L., XU, Y. B., LAI, W., HUANG, Y., MAO, R. X., LIU, X. S. & QI, S. H. 2015. Effects of skin-derived precursors on wound healing of denervated skin in a nude mouse model. *Int J Clin Exp Pathol,* 8**,** 2660-9.

SINGER, J. M., HERMANN, G. J. & SHAW, J. M. 2000. Suppressors of mdm20 in yeast identify new alleles of ACT1 and TPM1 predicted to enhance actin-tropomyosin interactions. *Genetics,* 156**,** 523-534.

SINGH, V. P., BALI, A., SINGH, N. & JAGGI, A. S. 2014. Advanced glycation end products and diabetic complications. *The Korean journal of physiology & pharmacology : official journal of the Korean Physiological Society and the Korean Society of Pharmacology,* 18**,** 1-14.

SIRA, J. & EYRE, L. 2016. Physiology of haemostasis. *Anaesthesia & Intensive Care Medicine,* 17**,** 79-82.

SKIDGEL, R. A., ENGELBRECHT, S., JOHNSON, A. R. & ERDOS, E. G. 1984. Hydrolysis of substance p and neurotensin by converting enzyme and neutral endopeptidase. *Peptides,* 5**,** 769-76.

SODEK, J., GANSS, B. & MCKEE, M. 2000. Osteopontin. *Critical Reviews in Oral Biology & Medicine,* 11**,** 279-303.

SPENNY, M. L., MUANGMAN, P., SULLIVAN, S. R., BUNNETT, N. W., ANSEL, J. C., OLERUD, J. E. & GIBRAN, N. S. 2002. Neutral endopeptidase inhibition in diabetic wound repair. *Wound Repair Regen,* 10**,** 295-301.

STAPELS, D. A. C., GEISBRECHT, B. V. & ROOIJAKKERS, S. H. M. 2015. Neutrophil serine proteases in antibacterial defense. *Current opinion in microbiology,* 23**,** 42-48.

SU, Y., PELZ, C., HUANG, T., TORKENCZY, K., WANG, X., CHERRY, A., DANIEL, C., LIANG, J., NAN, X., DAI, M.-S., ADEY, A., IMPEY, S. & SEARS, R. 2018. Post-translational modification localizes MYC to the nuclear pore basket to regulate a subset of target genes involved in cellular responses to environmental signals. *Genes & Development,* 32.

SZKLARCZYK, D., GABLE, A. L., LYON, D., JUNGE, A., WYDER, S., HUERTA-CEPAS, J., SIMONOVIC, M., DONCHEVA, N. T., MORRIS, J. H., BORK, P., JENSEN, L. J. & MERING, C. V. 2019. STRING v11: protein-protein association networks with increased coverage, supporting functional discovery in genome-wide experimental datasets. *Nucleic Acids Res,* 47**,** D607-d613.

TANABE, K., LIU, Z., PATEL, S., DOBLE, B. W., LI, L., CRAS-MENEUR, C., MARTINEZ, S. C., WELLING, C. M., WHITE, M. F., BERNAL-MIZRACHI, E., WOODGETT, J. R. & PERMUTT, M. A. 2008. Genetic deficiency of glycogen synthase kinase-3beta corrects diabetes in mouse models of insulin resistance. *PLoS Biol,* 6**,** e37.

TAO, H., BERNO, A. J., COX, D. R. & FRAZER, K. A. 2007. In vitro human keratinocyte migration rates are associated with SNPs in the KRT1 interval. *PloS one,* 2**,** e697.

THELEN, K., KEDAR, V., PANICKER, A. K., SCHMID, R.-S., MIDKIFF, B. R. & MANESS, P. F. 2002. The Neural Cell Adhesion Molecule L1 Potentiates Integrin-Dependent Cell Migration to Extracellular Matrix Proteins. *The Journal of Neuroscience,* 22**,** 4918-4931.

TURNER, A. J., ISAAC, R. E. & COATES, D. 2001. The neprilysin (NEP) family of zinc metalloendopeptidases: genomics and function. *Bioessays,* 23**,** 261-9.

UM, J., YU, J. & PARK, K.-S. 2017. Substance P accelerates wound healing in type 2 diabetic mice through endothelial progenitor cell mobilization and Yes-associated protein activation. *Molecular medicine reports,* 15**,** 3035-3040.

VAN DIJK, W., DO CARMO, S., RASSART, E., DAHLBÄCK, B. & SODETZ, J. M. 2013. The plasma lipocalins α1-acid glycoprotein, apolipoprotein D, apolipoprotein M and complement protein C8γ. *Madame Curie Bioscience Database [Internet].* Landes Bioscience.

VAN DIJK, W., POS, O., VAN DER STELT, M. E., MOSHAGE, H. J., YAP, S. H., DENTE, L., BAUMANN, P. & EAP, C. B. 1991. Inflammation-induced changes in expression and glycosylation of genetic variants of alpha 1-acid glycoprotein. Studies with human sera, primary cultures of human hepatocytes and transgenic mice. *The Biochemical journal,* 276 (Pt 2)**,** 343-347.

VELNAR, T., BAILEY, T. & SMRKOLJ, V. 2009. The wound healing process: an overview of the cellular and molecular mechanisms. *Journal of International Medical Research,* 37**,** 1528-1542.

VENTECLEF, N., JAKOBSSON, T., STEFFENSEN, K. R. & TREUTER, E. 2011. Metabolic nuclear receptor signaling and the inflammatory acute phase response. *Trends in Endocrinology & Metabolism,* 22**,** 333-343.

VINCENT, A. M., RUSSELL, J. W., LOW, P. & FELDMAN, E. L. 2004. Oxidative stress in the pathogenesis of diabetic neuropathy. *Endocr Rev,* 25**,** 612-28.

VLASSARA, H. & URIBARRI, J. 2014. Advanced glycation end products (AGE) and diabetes: cause, effect, or both? *Current diabetes reports,* 14**,** 453-453.

WALKER, J. L., BLEAKEN, B. M., ROMISHER, A. R., ALNWIBIT, A. A. & MENKO, A. S. 2018. In wound repair vimentin mediates the transition of mesenchymal leader cells to a myofibroblast phenotype. *Mol Biol Cell,* 29**,** 1555-1570.

WANG, Q., MUFFLEY, L. A., HALL, K., CHASE, M. & GIBRAN, N. S. 2009. Elevated glucose and fatty acid levels impair substance P-induced dermal microvascular endothelial cell migration and proliferation in an agarose gel model system. *Shock,* 32**,** 491-7.

WASEEM, A., DOGAN, B., TIDMAN, N., ALAM, Y., PURKIS, P., JACKSON, S., LALLI, A., MACHESNEY, M. & LEIGH, I. M. 1999. Keratin 15 expression in stratified epithelia: downregulation in activated keratinocytes. *J Invest Dermatol,* 112**,** 362-9.

WASSELL, J. 2000. Haptoglobin: function and polymorphism. *Clinical laboratory,* 46**,** 547-552.

WEBER, A., WASILIEW, P. & KRACHT, M. 2010. Interleukin-1 (IL-1) pathway. *Sci Signal,* 3**,** cm1.

WEBER, C. E., LI, N. Y., WAI, P. Y. & KUO, P. C. 2012. Epithelial-Mesenchymal Transition, TGF-β, and Osteopontin in Wound Healing and Tissue Remodeling After Injury. *Journal of Burn Care & Research,* 33**,** 311-318.

WEBER, G. F. & CANTOR, H. 1996. The immunology of Eta-1/osteopontin. *Cytokine Growth Factor Rev,* 7**,** 241-8.

WEI, B. & JIN, J.-P. 2016. TNNT1, TNNT2, and TNNT3: Isoform genes, regulation, and structure–function relationships. *Gene,* 582**,** 1-13.

WICHE, G. & WINTER, L. 2011. Plectin isoforms as organizers of intermediate filament cytoarchitecture. *Bioarchitecture,* 1**,** 14-20.

WIEMAN, T. J. 2005. Principles of management: the diabetic foot. *The American journal of surgery,* 190**,** 295-299.

WU, Y., MATSUI, H. & TOMIZAWA, K. 2009. Amphiphysin I and regulation of synaptic vesicle endocytosis. *Acta medica Okayama,* 63**,** 305-323.

XU, X. R., CARRIM, N., NEVES, M. A. D., MCKEOWN, T., STRATTON, T. W., COELHO, R. M. P., LEI, X., CHEN, P., XU, J., DAI, X., LI, B. X. & NI, H. 2016. Platelets and platelet adhesion molecules: novel mechanisms of thrombosis and anti-thrombotic therapies. *Thrombosis journal,* 14**,** 29-29.

YABE, D., NAKAMURA, T., KANAZAWA, N., TASHIRO, K. & HONJO, T. 1997. Calumenin, a Ca2+-binding protein retained in the endoplasmic reticulum with a novel carboxyl-terminal sequence, HDEF. *Journal of Biological Chemistry,* 272**,** 18232-18239.

YAMASHITA, Y., MATSUURA, T., KUROSAKI, T., AMAKUSA, Y., KINOSHITA, M., IBI, T., SAHASHI, K. & OHNO, K. 2014. LDB3 splicing abnormalities are specific to skeletal muscles of patients with myotonic dystrophy type 1 and alter its PKC binding affinity. *Neurobiology of disease,* 69**,** 200-205.

YANG, L., DI, G., QI, X., QU, M., WANG, Y., DUAN, H., DANIELSON, P., XIE, L. & ZHOU, Q. 2014. Substance P promotes diabetic corneal epithelial wound healing through molecular mechanisms mediated via the neurokinin-1 receptor. *Diabetes,* 63**,** 4262-74.

YASUDA, T., DELBONO, O., WANG, Z.-M., MESSI, M. L., GIRARD, T., URWYLER, A., TREVES, S. & ZORZATO, F. 2013. JP-45/JSRP1 Variants Affect Skeletal Muscle Excitation–Contraction Coupling by Decreasing the Sensitivity of the Dihydropyridine Receptor. *Human Mutation,* 34**,** 184-190.

YOUNAN, G., OGAWA, R., RAMIREZ, M., HELM, D., DASTOURI, P. & ORGILL, D. P. 2010. Analysis of nerve and neuropeptide patterns in vacuum-assisted closure-treated diabetic murine wounds. *Plast Reconstr Surg,* 126**,** 87-96.

YOUNG, A. & MCNAUGHT, C.-E. 2011. The physiology of wound healing. *Surgery (Oxford),* 29**,** 475-479.

YUAN, A., RAO, M. V., VEERANNA & NIXON, R. A. 2012. Neurofilaments at a glance. *Journal of cell science,* 125**,** 3257-3263.

ZHANG, L., KELLEY, J., SCHMEISSER, G., KOBAYASHI, Y. M. & JONES, L. R. 1997. Complex formation between junctin, triadin, calsequestrin, and the ryanodine receptor proteins of the cardiac junctional sarcoplasmic reticulum membrane. *Journal of Biological Chemistry,* 272**,** 23389-23397.

ZHANG, P., LU, J., JING, Y., TANG, S., ZHU, D. & BI, Y. 2016. Global Epidemiology of Diabetic Foot Ulceration: A Systematic Review and Meta-Analysis. *Annals of medicine,* 49**,** 1-21.

ZHAO, R., LIANG, H., CLARKE, E., JACKSON, C. & XUE, M. 2016. Inflammation in chronic wounds. *International journal of molecular sciences,* 17**,** 2085.

ZHONG, J., GONG, Q. & MIMA, A. 2017. Inflammatory regulation in diabetes and metabolic dysfunction. *Journal of diabetes research,* 2017.

ZHU, F.-B., FANG, X.-J., LIU, D.-W., SHAO, Y., ZHANG, H.-Y., PENG, Y., ZHONG, Q.-L., LI, Y.-T. & LIU, D.-M. 2016. Substance P combined with epidermal stem cells promotes wound healing and nerve regeneration in diabetes mellitus. *Neural regeneration research,* 11**,** 493-501.

ZHU, F. B., LIU, D. W., ZHANG, H. Y., XU, J. C., PENG, Y., ZHONG, Q. L. & LI, Y. T. 2012. [Effect of substance P combined with epidermal stem cells on wound healing and nerve regeneration in rats with diabetes mellitus]. *Zhonghua Shao Shang Za Zhi,* 28**,** 25-31.

ZILBERMAN, M. 2011. *Active implants and scaffolds for tissue regeneration*, Springer.

Chapter 9 : Appendices

Appendix A: Ethics Approval letter

UNIVERSITEIT•STELLENBOSCH•UNIVERSITY
jou kennisvennoot • your knowledge partner

Approved
Protocol

Date: 30 – June – 2017

PI Name: Van De Vyver, Mari M

Protocol #: SU-ACUD17-00016

Title: Development of a chronic wound model using B6.Cg-Lepob/J obese diabetic and C57BL/6J wild-type control mice: Characterizing cellular changes that impair regenerative potential of wound-derived fibroblasts and endogenous mesenchymal stem cells.

Dear Mari Van De Vyver, the Response to Modification, was reviewed on 23-June-2017 by the Research Ethics Committee: Animal Care and Use via committee review procedures and was approved. Please note that this clearance is only valid for a period of twelve months. Ethics clearance of protocols spanning more than one year must be renewed annually through submission of a progress report, up to a maximum of three years.

Applicants are reminded that they are expected to comply with accepted standards for the use of animals in research and teaching as reflected in the South African National Standards 10386: 2008. The SANS 10386: 2008 document is available on the Division for Research Developments website www.sun.ac.za/research.

As provided for in the Veterinary and Para-Veterinary Professions Act, 1982. It is the principal investigator's responsibility to ensure that all study participants are registered with or have been authorised by the South African Veterinary Council (SAVC) to perform the procedures on animals, or will be performing the procedures under the direct and continuous supervision of a SAVC-registered veterinary professional or SAVC-registered para-veterinary professional, who are acting within the scope of practice for their profession.

Please remember to use your protocol number, SU-ACUD17-00016 on any documents or correspondence with the REC: ACU concerning your research protocol. Please note that the REC: ACU has the prerogative and authority to ask further questions, seek additional information, require further modifications or monitor the conduct of your research. Any event not consistent with routine expected outcomes that results in any unexpected animal welfare issue (death, disease, or prolonged distress) or human health risks (zoonotic disease or exposure, injuries) must be reported to the committee, by creating an Adverse Event submission within the system.

We wish you the best as you conduct your research. If you have any questions or need further help, please contact the REC: ACU secretariat at wabeukes@sun.ac.za or 021 808 9003.

Sincerely, REC: ACU Secretariat

Research Ethics Committee: Animal Care and Use

UNIVERSITEIT
STELLENBOSCH
UNIVERSITY

Amendment Approval

Date: 15 June 2018

PI Name: Dr.
Mari Van de
Vyver Protocol
#:3857
Title: Development of a chronic wound model using B6.Cg-Lepob/J obese diabetic and C57BL/6J wild-type control mice: Characterizing cellular changes that impair regenerative potential of wound-derived fibroblasts and endogenous mesenchymal stem cells.

Dear Mari Van de Vyver ,

The Development of a chronic wound model using B6.Cg-Lepob/J obese diabetic and C57BL/6J wild-type control mice: Characterizing cellular changes that impair regenerative potential of wound-derived fibroblasts and endogenous mesenchymal stem cells - amendment. , was reviewed on 13 June 2018 by the Research Ethics Committee: Animal Care and Use via committee review procedures and was approved. Please note that this clearance is only valid for a period of twelve months. Ethics clearance of protocols spanning more than one year must be renewed annually through submission of a progress report, up to a maximum of three years.

New Co-workers:

Kiara Boodhoo (MSc student) and Dr Dalene de Swardt (Postdoc)

Applicants are reminded that they are expected to comply with accepted standards for the use of animals in research and teaching as reflected in the South African National Standards 10386: 2008. The SANS 10386: 2008 document is available on the Division for Research Developments website www.sun.ac.za/research.

As provided for in the Veterinary and Para-Veterinary Professions Act, 1982. It is the principal investigator's responsibility to ensure that all study participants are registered with or have been authorised by the South African Veterinary Council (SAVC) to perform the procedures on animals, or will be performing the procedures under the direct and continuous supervision of a SAVC-registered veterinary professional or SAVC-registered para-veterinary professional, who are acting within the scope of practice for their profession.

Please remember to use your protocol number 3857 on any documents or correspondence with the REC: ACU concerning your research protocol.

Please note that the REC: ACU has the prerogative and authority to ask further questions, seek additional information, require further modifications or monitor the conduct of your research.

Any event not consistent with routine expected outcomes that results in any unexpected animal welfare issue (death, disease, or prolonged distress) or human health risks (zoonotic disease or exposure, injuries) must be reported to the committee, by creating an Adverse Event submission within the system.

We wish you the best as you conduct your research.

If you have any questions or need further help, please contact the REC: ACU Secretariat

at wabeukes@sun.ac.za or 021 808 9003. Sincerely,

Winston Beukes REC: ACU Secretariat
Research Ethics Committee: Animal Care and Use

Appendix B: Animal Wellness monitoring sheet

FMHS Animal Research Facility **Health and Welfare Monitoring Sheet**

Cage ID:	**Group description:**	
	email:	**tel:**
Researcher:	**email:**	**tel:**
Protocol #:		

Date	Time	Appearance	Behaviour	Cage	Comments	Initials
			:			

Appearance	**1**: well-groomed; bright facial expresion; no discharges; no lesions; normal posture/breathing **2**: coat slightly rough; subtle discharges/lesions; dull facial expression; mild hunching; abnormal breathing **3**: staring coat; obvious discharges/lesions; facial bulge/squinting; hunched posture; breathing difficulty
Behaviour	**1**. Alert; curious; active; interactive with cage mates; normal gait **2**: less active; isolated from cage mates; less responsive; abnormal gait **3**: inactive; poorly responsive;
Cage	Cage is clean and dry; faecal pellets are normal; water and food available

Monitoring must be performed twice a day if a cage is scored "2" Veterinary staff must be alerted if a cage is scored "3"

Appendix C: Cytokine standard curves

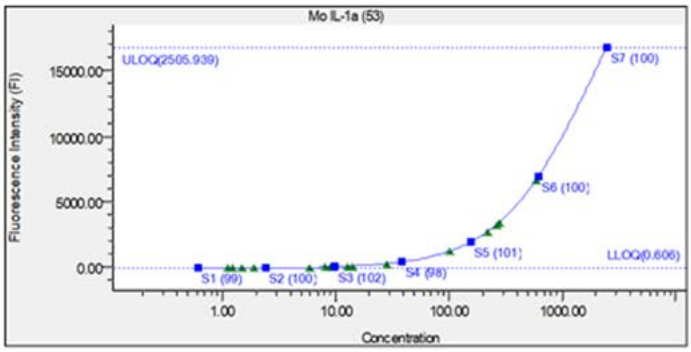

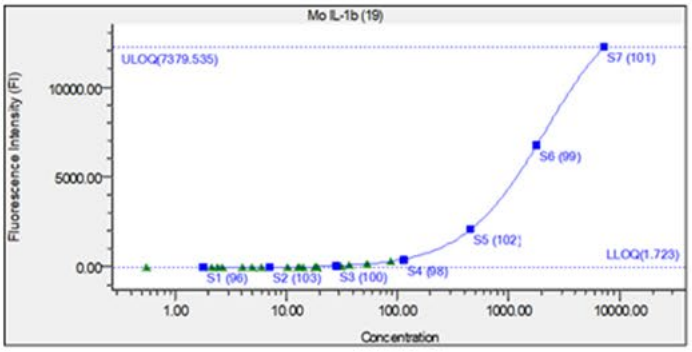

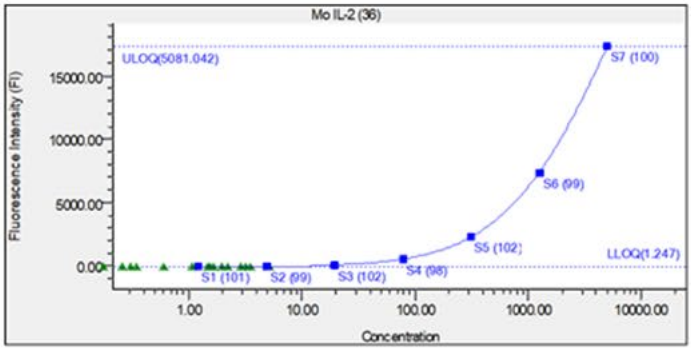

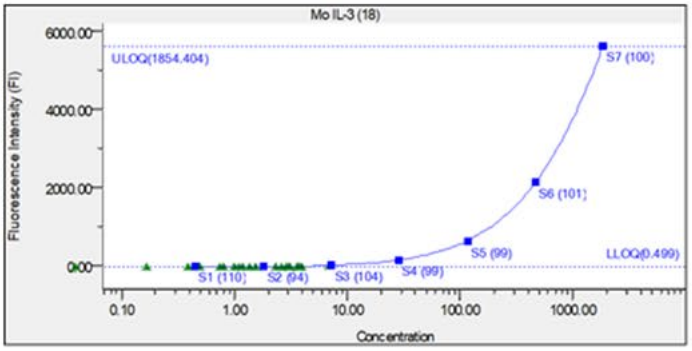

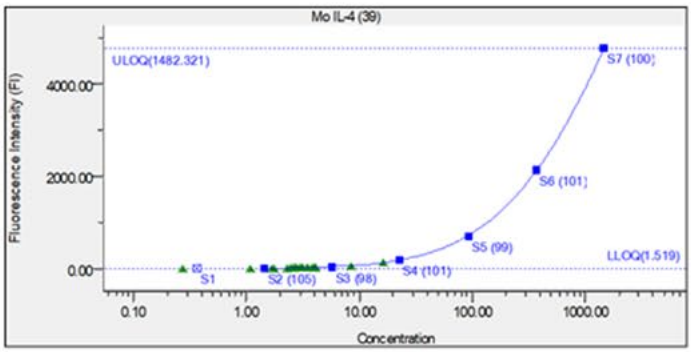

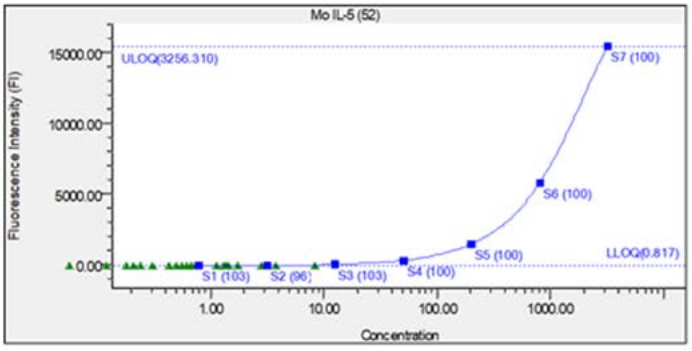

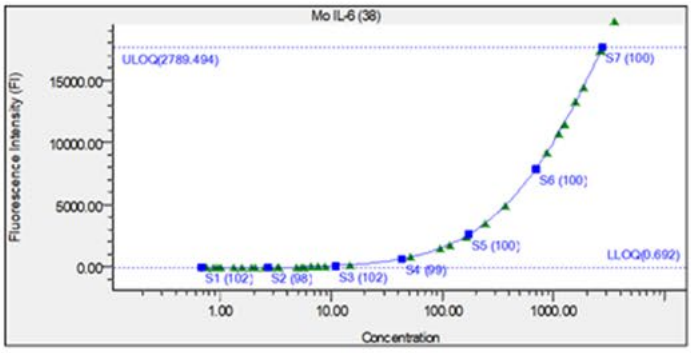

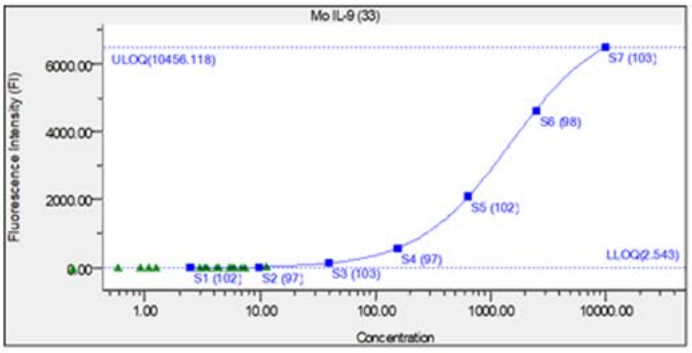

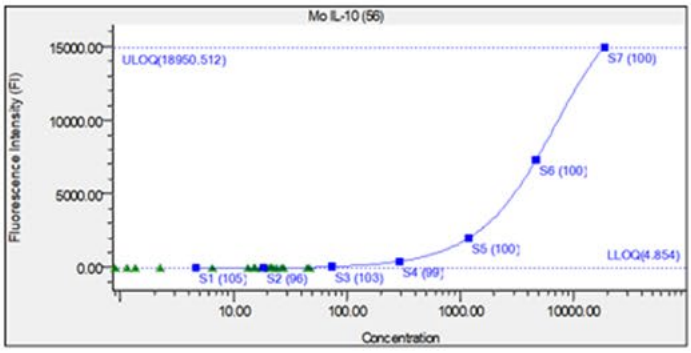

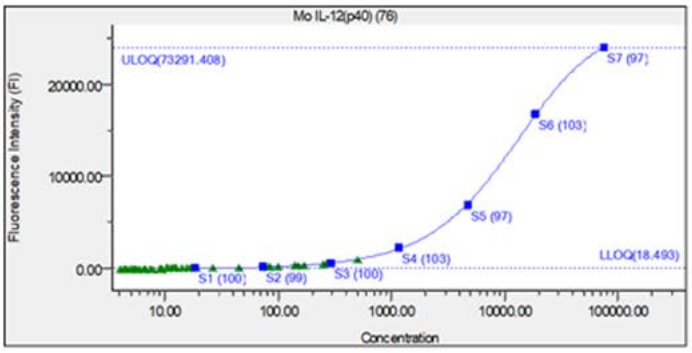

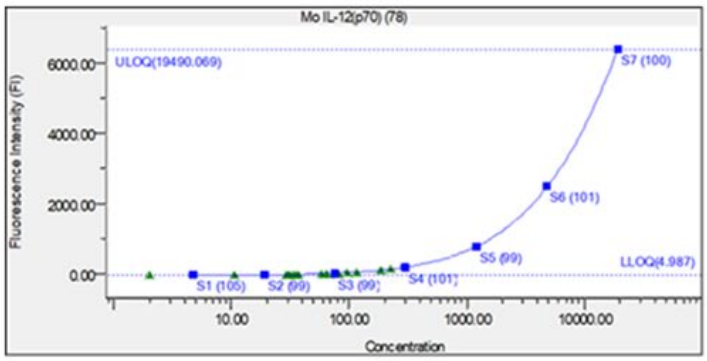

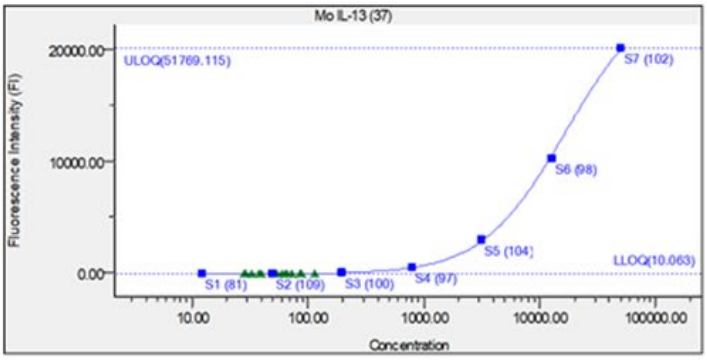

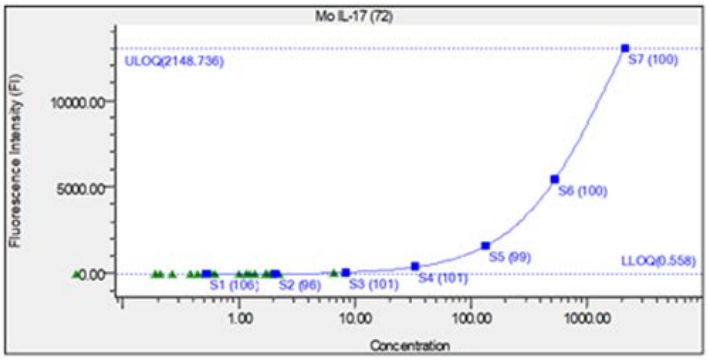

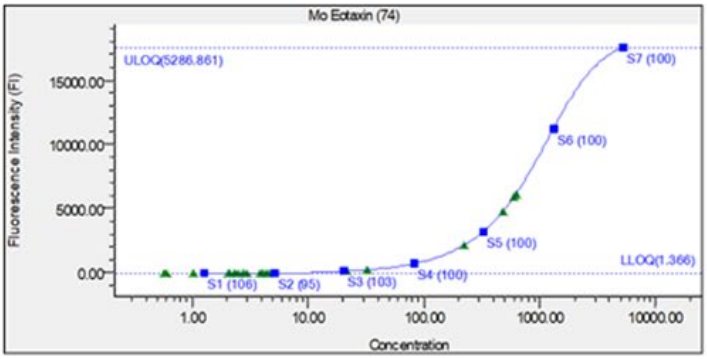

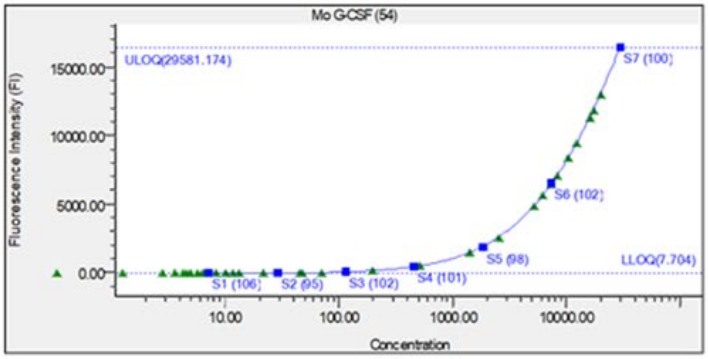

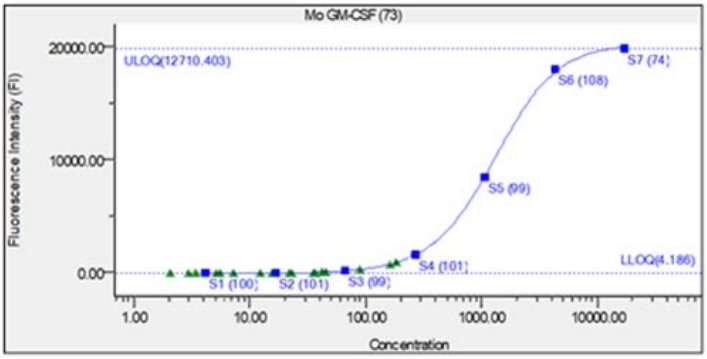

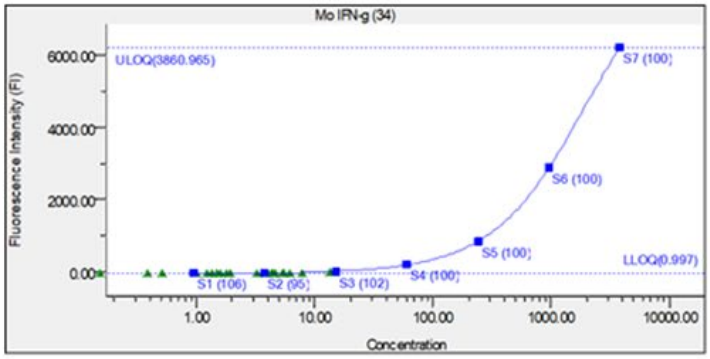

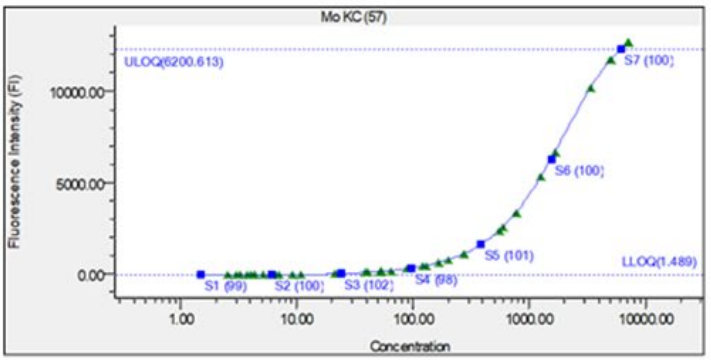

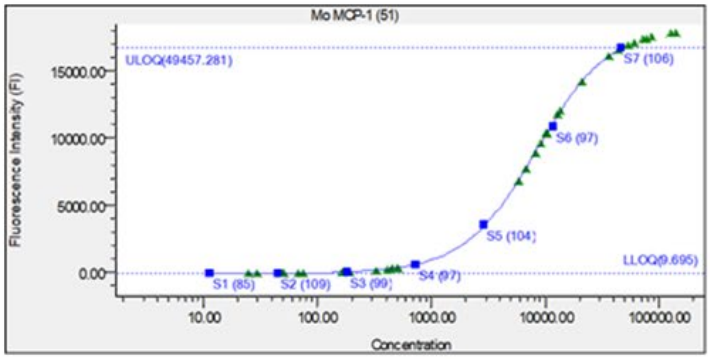

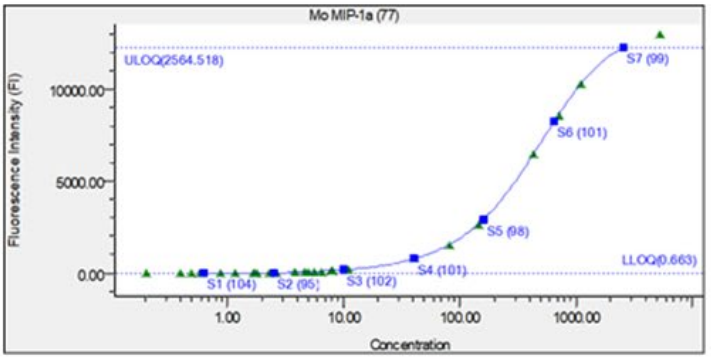

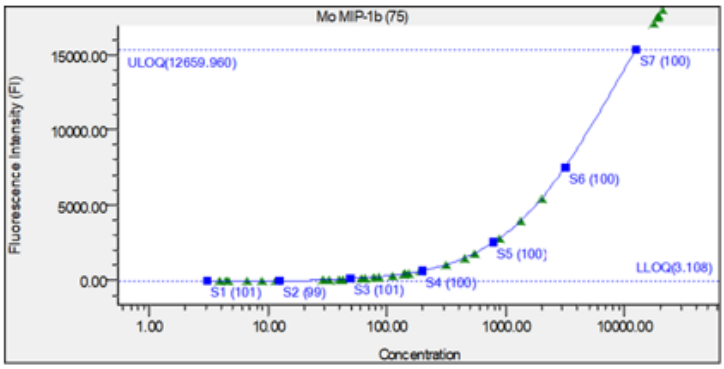

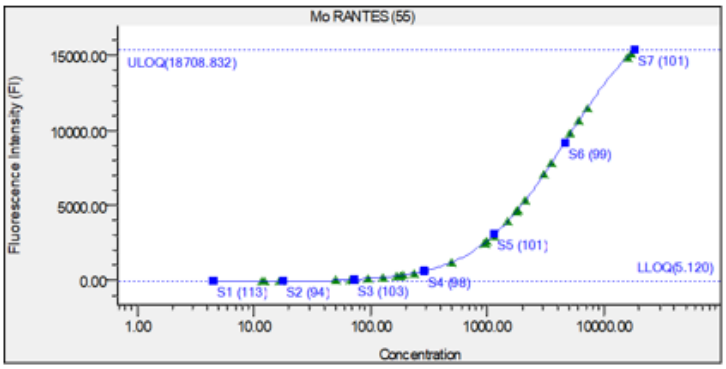

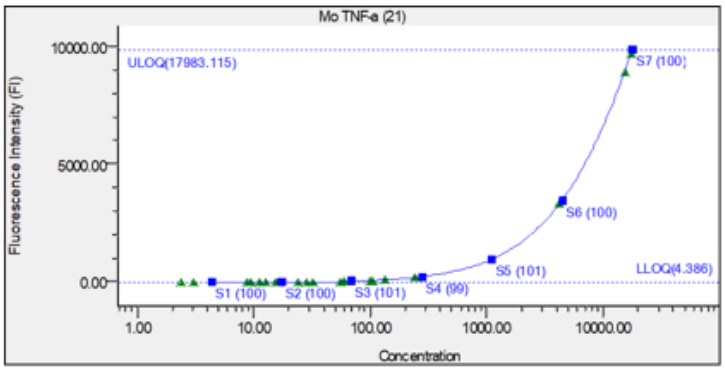

Appendix D: Abbreviations for Table 6.1

A2m: Alpha-2-macroglobulin-P

Abca13: ATP-binding cassette

Abhd5: 1-acylglycerol-3-phosphate O-acyltransferase

Acly: ATP-citrate synthase

Acp2: Acid phosphatase 2

Acp5: Tartrate-resistant acid phosphatase type 5

Acta2: Actin, aortic smooth muscle

Actb: Actin, cytoplasmic 1

Actg1: Actin, cytoplasmic 2

Actg2: Actin, gamma-enteric smooth muscle

Actn: Alpha-actinin

Actr: Actin-related protein

Adipoq: Adiponectin

AGE: Advanced glycation end-products

Agl: Amylo-1,6-glucosidase

Ahctf1: Protein ELYS

Ahsg: Alpha-2-HS-glycoprotein

Akt1: RAC-alpha serine/threonine-protein kinase

Alb: Serum albumin

Ambp: Protein AMBP, Inter-alpha-trypsin inhibitor inhibits trypsin

Amph: Amphiphysin

Amy: Amylase

Ankrd1: Ankyrin repeat domain-containing protein 1

APCDD1L: Adenomatosis polyposis coli down-regulated 1-like

Apoa1: Apolipoprotein A-I

Arfip1: ADP-ribosylation factor interacting protein 1

Arpc:	Actin-related protein 2/3 complex subunit
Asf1a:	Histone chaperone ASF1A
Asph:	Aspartyl/asparaginyl beta-hydroxylase
Atoh:	Protein atonal homolog
Atp2a1:	Sarcoplasmic/endoplasmic reticulum calcium ATPase 1
Atrip:	ATR-interacting protein
Bace2:	Beta-secretase 2
Bag3:	BAG family molecular chaperone regulator 3
Banf1:	Barrier-to-autointegration factor
BC100530:	MCG130175, isoform CRA_b
BC117090:	cDNA sequence BC1179090
Bcan:	Brevican core protein
Bcl2l1:	Bcl-2-like protein 1
Bin1:	Myc box-dependent-interacting protein 1
Blm:	Bloom syndrome protein homolog
Blvra:	Biliverdin reductase A
Brwd1:	Bromodomain and WD repeat-containing protein 1
Bscl2:	Seipin
Btf3:	Transcription factor BTF3
Btf3l4:	Basic transcription factor 3-like 4
Bub1b:	Mitotic checkpoint serine/threonine-protein kinase BUB1 beta
C3:	Complement C3
Cacna1b:	Voltage-dependent N-type calcium channel subunit alpha-1B
Cacna1s:	Voltage-dependent L-type calcium channel subunit alpha-1S
Calca:	Calcitonin
Cap1:	Adenylyl cyclase-associated protein 1
Cask:	Peripheral plasma membrane protein CASK

Casp:	Caspase
Casq:	Calsequestrin
Casq1:	Calsequestrin-1
Cav:	Caveolin
Cbx:	Chromobox protein homolog
CCDC101:	Uncharacterized protein; Coiled-coil domain containing 101
Ccdc58:	Coiled-coil domain containing 58
Cd151:	CD151 antigen
Cd163:	Scavenger receptor cysteine-rich type 1 protein M130
Cd44:	CD44 antigen
Cd79a:	B-cell antigen receptor complex-associated protein alpha chain
Cd79b:	B-cell antigen receptor complex-associated protein beta chain
Cdc42ep2:	Cdc42 effector protein 2
Cdc5l:	Cell division cycle 5-like protein
Cdh2:	Cadherin-2
Cdk:	Cyclin-dependent kinase
Cdyl:	Chromodomain Y-like protein
Celf:	CUGBP Elav-like family member
Cenpa:	Histone H3-like centromeric protein A
Chek1:	Serine/threonine-protein kinase Chk1
Chek2:	Serine/threonine-protein kinase Chk2
Chmp4b:	Charged multivesicular body protein 4b.
Chmp5:	Charged multivesicular body protein 5
Chtop:	Chromatin target of PRMT1 protein
Cidec:	Cell death activator CIDE-3
Ciz1:	CDKN1A interacting zinc finger protein 1
Ckmt2:	Creatine kinase S-type

Cldn:	Claudin
Clip1:	CAP-Gly domain-containing linker protein 1
Cmya5:	Cardiomyopathy-associated protein 5
Cntn6:	Contactin-6
Col17a1:	Collagen alpha-1(XVII) chain
Col1a1:	Collagen alpha-1(I) chain
Col1a2:	Collagen alpha-2(I) chain
Col6a1:	Collagen alpha-1(VI) chain
Cpsf6:	Cleavage and polyadenylation specificity factor subunit 6
Crtap:	Cartilage-associated protein
Csrp3:	Cysteine and glycine-rich protein 3
Csta1:	Cystatin-A
Ctnna1:	Catenin alpha-1
Ctsa:	Lysosomal protective protein
Ctsg:	Cathepsin G
Cttn:	Src substrate cortactin
Cttnbp2:	Cortactin-binding protein 2
Cttnbp2nl:	CTTNBP2 N-terminal-like protein
Cyfip1:	Cytoplasmic FMR1-interacting protein 1
Cyp24a1:	1,25-dihydroxyvitamin D(3) 24-hydroxylase, mitochondrial
Cyp51:	Lanosterol 14-alpha demethylase
Dact1:	Dapper homolog 1
Dad1:	Dolichyl-diphosphooligosaccharide--protein glycosyltransferase subunit
Dag2:	Disks large homolog 2
Dalrd3:	DALR anticodon-binding domain-containing protein 3
Dcaf7:	DDB1- and CUL4-associated factor 7
Dcx:	Neuronal migration protein doublecortin

Ddit4l:	DNA damage-inducible transcript 4-like protein
Ddost:	Dolichyl-diphosphooligosaccharide--protein glycosyltransferase
Des:	Desmin
Dffb:	DNA fragmentation factor subunit beta
Dhx5:	Pre-mRNA-splicing factor ATP-dependent RNA helicase DHX15
Dhx9:	ATP-dependent RNA helicase A
Dig4:	Disks large homolog 4
Dlx2:	Homeobox protein DLX-2;
Dmp1:	Dentin matrix acidic phosphoprotein 1
DNAJC15:	DnaJ (Hsp40) homolog, subfamily C, member 15
Dnm:	Dynamin
Dpf2:	Zinc finger protein ubi-d4
Dpp7:	Dipeptidyl peptidase 2
Drosha:	Ribonuclease 3
Dsc:	Desmocollin
Dsg1a:	Desmoglein-1-alpha
Dsp:	Desmoplakin
Dtnbp1:	Dysbindin
Dut:	Deoxyuridine triphosphatase, isoform CRA_b
Dync1h1:	Cytoplasmic dynein 1 heavy chain 1
Dync1i1:	Cytoplasmic dynein 1 intermediate chain 1
Dynll2:	Dynein light chain 2, cytoplasmic
Dyrk1:	Dual specificity tyrosine-phosphorylation-regulated kinase 1
E4f1:	Transcription factor E4F1
Eef1:	Elongation factor 1
Egfr:	Epidermal growth factor receptor
Eln:	Elastin

Emc3: ER membrane protein complex subunit 3

Emd: Emerin

Emp2: Epithelial membrane protein 2

ENSBTAG00000011995: Chymotrypsinogen A

ENSBTAG00000024245: Cationic trypsin Alpha-trypsin chain 1 Alpha-trypsin chain 2

ENSBTAG00000026119: Uncharacterized protein

ENSMUSG00000066607: UPF0583 protein C15orf59 homolog

Epb4.1: Protein 4.1

Epb4.1l: Band 4.1-like protein

Epb4.1l2: Band 4.1-like protein 2

Epb4.1l3: Band 4.1-like protein 3

Eps15: Epidermal growth factor receptor substrate 15

Ercc: Excision repair cross-complementing rodent repair deficiency

Etfdh: Electron transfer flavoprotein-ubiquinone oxidoreductase

Fabp5: Fatty acid-binding protein, epidermal

Fam78b: Protein FAM78B

Fam89b: Leucine repeat adapter protein 25

Fancm: Fanconi anemia group M protein homolog

Fau: Ubiquitin-like protein FUBI

FblL: rRNA 2'-O-methyltransferase fibrillarin

Fbxo: F-box only protein

Fcamr: High affinity immunoglobulin alpha and immunoglobulin mu Fc receptor

Fga: Fibrinogen alpha chain

Fgb: Fibrinogen beta chain

Fgf: Fibroblast growth factor

Fgg: Fibrinogen gamma chain

Fkbp1a: Peptidyl-prolyl cis-trans isomerase FKBP1A

Fkbp1b:	Peptidyl-prolyl cis-trans isomerase FKBP1B
Fmr1:	Synaptic functional regulator
Fn1:	Fibrinogen alpha chain
Fnta:	Protein farnesyltransferase/geranylgeranyltransferase type-1 subunit alpha
Frmd8:	FERM domain containing 8
Fstl1:	Follistatin-related protein 1
Fth1:	Ferritin heavy chain
Fuca1:	Tissue alpha-L-fucosidase
Fus:	RNA-binding protein FUS
Gan:	Gigaxonin
Gata6:	Transcription factor GATA-6
Gbe1:	1,4-alpha-glucan-branching enzyme
Gdnf:	Glial cell line-derived neurotrophic factor
Ghr:	Growth hormone receptor
Gja1:	Gap junction alpha-1 protein
Gm4758:	Predicted gene 4758
Gm5416:	Predicted gene 5416
Gm5483:	MCG130182, isoform CRA_a
Gm5689:	Predicted gene 5689
Gm8186:	Small nuclear ribonucleoprotein G
Gm9843:	Predicted gene 9843
Gnb2l1:	Receptor of activated protein C kinase 1
Grn:	Granulins
Gsk3b:	Glycogen synthase kinase-3 beta
H1f0:	Histone H1.0
H1fx:	H1 histone family, member X
H2afb2:	H2A histone family, member B2

H3f3a: Histone H3.3

Hba-a1: Hemoglobin subunit alpha

Hbb-bs: Hemoglobin

Hectd3: E3 ubiquitin-protein ligase HECTD3

Hipk2: Homeodomain-interacting protein kinase 2

Hira: Protein HIRA

Hist1h1a: Histone H1.1

Hist1h1b: Histone H1.5

Hist1h1c: Histone H1.2

Hist1h1d: Histone H1.3

Hist1h1e: Histone H1.4

Hist1h4j: Histone cluster 1, H4j

Hist2h2ab: Histone H2A type 2-B

Hist2h3c2: Histone H3.2

Hmga2: High mobility group protein HMGI-C

Hmgb1: High mobility group protein B1

Hmgb2: High mobility group protein B2

Hmgn1: Non-histone chromosomal protein HMG-14

Hmox: Heme oxygenase

Hnrnpa1: Heterogeneous nuclear ribonucleoprotein A1

Hnrnpa2b1: Heterogeneous nuclear ribonucleoproteins A2/B1

Hnrnph1: Heterogeneous nuclear ribonucleoprotein H

Hnrnph2: Heterogeneous nuclear ribonucleoprotein H2

Hnrnpk: Heterogeneous nuclear ribonucleoprotein K

Hp: Haptoglobin

Hrnr: Hornerin

Hsd17b7: 3-keto-steroid reductase

Hsp90aa1: Heat shock protein HSP 90-alpha

Hsp90ab1: Heat shock protein HSP 90-beta

Hsp90b1: Endoplasmin

Hspa1b: Heat shock 70 kDa protein 1B

Hspa5: 78 kDa glucose-regulated protein

Hspb7: Heat shock protein family, member 7

Id2: DNA-binding protein inhibitor ID-2

Ighv1-73: Immunoglobulin heavy variable 1-73

Iglc2: Ig lambda-2 chain C region; Immunoglobulin lambda constant 2

IL: Interleukin

Irf3: Interferon regulatory factor 3

Itga: Integrin alpha

Itgav: Integrin alpha-V

Itgb: Integrin beta

Ivl: Involucrin

Jph: Junctophilin

Jup: Junction plakoglobin

Kcmf1: E3 ubiquitin-protein ligase KCMF1

Kcnj6: G protein-activated inward rectifier potassium channel 2

Kcnk7: Potassium channel subfamily K member 7

Kcns3: Potassium voltage-gated channel subfamily S member 3

Kdm1a: Lysine-specific histone demethylase 1A

Kiaa0922: Transmembrane protein 131-like

Klk5: Kallikrein related-peptidase 5

Klrg2: Killer cell lectin-like receptor subfamily G

Krt: Keratin

Lama: Laminin subunit alpha

Lamb:	Laminin subunit beta
Lamc:	Laminin subunit gamma
Larp1b:	La ribonucleoprotein domain family, member 1B
Lbh:	Protein LBH
Ldb3:	LIM domain-binding protein 3
Lemd3:	Inner nuclear membrane protein Man1
Lepre1:	Prolyl 3-hydroxylase 1
Leprel2:	Prolyl 3-hydroxylase 3
LGR:	Leucine-rich repeat containing G protein-coupled receptor
Lias:	Lipoyl synthase
Limk:	LIM domain kinase
Lipe:	Hormone-sensitive lipase
Lmnb1:	Lamin B1
Lor:	Loricrin
Loxl1:	Lysyl oxidase homolog 1
Lpar6:	Lysophosphatidic acid receptor 6
Lrg1:	Leucine-rich alpha-2-glycoprotein 1
LRIG1:	Leucine-rich repeats and immunoglobulin-like domains 1
Lrrc17:	Leucine-rich repeat-containing protein 17
Ltf:	Lactotransferrin
Man1a2:	Mannosyl-oligosaccharide 1,2-alpha-mannosidase IB
Map1b:	Microtubule-associated protein 1B
Map1lc3a:	Microtubule-associated proteins 1A/1B light chain 3A
Map2:	Microtubule-associated protein 2
Map3k11:	Mitogen-activated protein kinase kinase kinase 11
Mapk:	Mitogen-activated protein kinase
Mapkapk:	MAP kinase-activated protein kinase

Mapre3: Microtubule-associated protein RP/EB family member 3

Mapt: Microtubule-associated protein tau

Mbp: Myelin basic protein

mCG_125090: La ribonucleoprotein domain family, member 1B

mCG_130165: RIKEN cDNA 2010005H15 gene

mCG_130165: RIKEN cDNA 2010005H15 gene

Mepe: Matrix extracellular phosphoglycoprotein with ASARM motif

Mettl14: N6-adenosine-methyltransferase non-catalytic subunit

Mfap: Microfibrillar-associated protein

Mllt4: Afadin

MMP: Matrix metalloprotease

Mmrn: Multimerin

Mob4: MOB-like protein phocein

Mre11a: Double-strand break repair protein MRE11

Mrps: Mitochondrial ribosomal protein S

Mst4: Serine/threonine-protein kinase 26

Mthfd1: C-1-tetrahydrofolate synthase, cytoplasmic

Mtm1: Myotubularin

Mybpc2: Myosin-binding protein C

Mybpc3: Myosin-binding protein C

Mybph: Myosin-binding protein H

Myh11: Myosin-11

Myl1: Myosin light chain 1/3

Myl12b: Myosin regulatory light chain 12B

Myl7: Myosin, light polypeptide 7

Mylk: Myosin light chain kinase

Myo3b: Myosin-IIIb

Myom: Myomesin

Myot: Myotilin

Myoz: Myozenin

Mypn: Myopalladin

Nckap1l: Nck-associated protein 1-like

Nde1: Nuclear distribution protein nudE homolog 1

Ndel1: Nuclear distribution protein nudE-like 1

Neb: Nebulin

Nefl: Neurofilament light polypeptide

Nenf: Neudesin

Nes: Nestin

Nhp2: H/ACA ribonucleoprotein complex subunit 2

Nid1: Nidogen-1

Nip7: 60S ribosome subunit biogenesis protein NIP7 homolog

Nlgn: Neuroligin

Nnmt: Nicotinamide N-methyltransferase

Nono: Non-POU domain-containing octamer-binding protein

Nop: Nucleolar protein

Npm1: Nucleophosmin

Nrap: Nebulin-related-anchoring protein

Nrp1: Neuropilin-1

Nrxn: Neurexin

Nucb1: Nucleobindin-1Fga:

Nuf2: Kinetochore protein Nuf2

Obscn: Obscurin

Ociad2: OCIA domain containing 2

Ocln: Occludin

Orm:	Alpha-1-acid glycoprotein
Ost4:	Dolichyl-diphosphooligosaccharide--protein glycosyltransferase subunit 4
Ostc:	Oligosaccharyltransferase complex subunit
P4hb:	Protein disulfide-isomerase
Padi2:	Protein-arginine deiminase type-2
Pafah1b1:	Platelet-activating factor acetylhydrolase IB subunit alpha
Pcbp1:	Poly(rC)-binding protein 1
Pcnx:	Pecanex-like protein 1
Pcsk9:	Proprotein convertase subtilisin/kexin type 9
Pcx:	Pyruvate carboxylase, mitochondrial
Pde4dip:	Myomegalin
Pdia4:	Protein disulfide-isomerase A4
Pdia6:	Protein disulfide-isomerase A6
Peo1:	Twinkle protein, mitochondrial
Pfdn:	Prefoldin subunit
Pgm2:	Phosphoglucomutase-1
Pgm3:	Phosphoacetylglucosamine mutase
Pgm5:	Phosphoglucomutase-like protein 5
Phc3:	Polyhomeotic-like protein 3
Phk:	Phosphorylase b kinase regulatory subunit
Phkg1:	Phosphorylase b kinase gamma catalytic chain
Picalm:	Phosphatidylinositol-binding clathrin assembly protein
Piga:	N-acetylglucosaminyl-phosphatidylinositol biosynthetic protein
Pigm:	GPI mannosyltransferase 1
Pigr:	Polymeric immunoglobulin receptor
Pip4k2a:	Phosphatidylinositol 5-phosphate 4-kinase type-2 alpha
Pip4k2b:	Phosphatidylinositol 5-phosphate 4-kinase type-2 beta

Pip4k2c: Phosphatidylinositol 5-phosphate 4-kinase type-2 gamma

Pkp: Plakophilin

Plk1: Serine/threonine-protein kinase PLK1

Pnpla2: Patatin-like phospholipase domain-containing protein 2

Polg: DNA polymerase subunit gamma-1

Polg2: DNA polymerase subunit gamma-2

Polr1a: DNA-directed RNA polymerase I subunit RPA1

Polr1c: DNA-directed RNA polymerases I and III subunit RPAC1

Polr1e: DNA-directed RNA polymerase I subunit RPA49

Polr2l: DNA-directed RNA polymerases I, II, and III subunit RPABC5

Polrmt: DNA-directed RNA polymerase, mitochondrial

Pou4f2: POU domain, class 4, transcription factor 2

Ppard: Peroxisome proliferator-activated receptor delta

Ppp2r1a: Serine/threonine-protein phosphatase 2A 65 kDa regulatory subunit A

Ppp2r5e: Serine/threonine-protein phosphatase 2A

Ppp5c: Serine/threonine-protein phosphatase 5

Prkac: cAMP-dependent protein kinase catalytic subunit

Prkce: Protein kinase C epsilon type

Prkg: cGMP-dependent protein kinase

Prpf38a: Pre-mRNA-splicing factor 38A

Prph: Peripherin

Psmg1: Proteasome assembly chaperone 1

PTI: Bos taurus spleen trypsin inhibitor

Ptpra: Receptor-type tyrosine-protein phosphatase alpha

Ptrf: Caveolae-associated protein 1

Pygb: Glycogen phosphorylase

Rad17: Cell cycle checkpoint protein RAD17

Rad50: DNA repair protein RAD50; Component of the MRN complex

Rasal2: RAS protein activator like 2

Rbfox3: RNA binding protein fox-1 homolog 3

Rbm14: RNA-binding protein 14;

Retn: Resistin

Rfk: Riboflavin kinase

Rhoa: Transforming protein RhoA

Ripply3: Protein ripply3

Rnf150: Ring finger protein 150

Rpl: Ribosomal protein L

Rplp: Ribosomal protein P

Rpn: Dolichyl-diphosphooligosaccharide--protein glycosyltransferase subunit

Rps: Ribosomal protein S

Rptn: Repetin

Ruvbl1: RuvB-like 1

Rwdd2b: RWD domain containing 2B

Rwdd2b: RWD domain containing 2B

Rxra: Retinoic acid receptor RXR-alpha

Ryr: Ryanodine receptor

Sbspon: Somatomedin-B and thrombospondin type-1 domain-containing protein

Scgn: Secretagogin

Sdc4: Syndecan-4

Sec61a1: Protein transport protein Sec61 subunit alpha isoform 1

Sec61g: Protein transport protein Sec61 subunit gamma

Serpina3m: Serine (or cysteine) peptidase inhibitor, clade A, member 3M

SERPINA5: Plasma serine protease inhibitor

Serpinb3a: Serine (or cysteine) peptidase inhibitor, clade B (ovalbumin), member 3A

Serpinb3b: Serine (or cysteine) peptidase inhibitor, clade B (ovalbumin), member 3B

Serpinb3c: Serine (or cysteine) peptidase inhibitor, clade B, member 3C

Serpinh1: Serpin H1

Sestd1: SEC14 domain and spectrin repeat-containing protein 1

Sfpq: Splicing factor, proline- and glutamine-rich

Sgol1: Shugoshin 1

Sgsm2: Small G protein signaling modulator 2

Sh3gl2: Endophilin-A1

Sh3gl3: Endophilin-A3

Sirt1: NAD-dependent protein deacetylase sirtuin-1

Slc1a2: Excitatory amino acid transporter 2

Slmap: Sarcolemmal membrane-associated protein

Smpx: Small muscular protein

Smyd1: Histone-lysine N-methyltransferase Smyd1

Sncg: Gamma-synuclein

Snd1: Staphylococcal nuclease domain-containing protein 1

Snrnp70: U1 small nuclear ribonucleoprotein 70 kDa

Snrp: U1 small nuclear ribonucleoprotein

Snrpa: U1 small nuclear ribonucleoprotein A

Snrpd: Small nuclear ribonucleoprotein Sm D

Snrpd: Small nuclear ribonucleoprotein-associated protein B

Snrpe: Small nuclear ribonucleoprotein E

Snrpf: Small nuclear ribonucleoprotein F

Sorbs2: Sorbin and SH3 domain-containing protein 2

SPINK1: Serine protease inhibitor Kazal-type 1

Sprr3: Small proline-rich protein 3

Sprtn: SprT-like domain-containing protein Spartan

Sqle:	Squalene monooxygenase
Src:	Neuronal proto-oncogene tyrosine-protein kinase Src
Srl:	Sarcalumenin
Srsf:	Serine/arginine-rich splicing factor
Ssh:	Protein phosphatase Slingshot homolog
Ssr4:	Translocon-associated protein subunit delta
Sssca1:	Sjogren's syndrome/scleroderma autoantigen 1 homolog
St8sia3:	Sia-alpha-2,3-Gal-beta-1,4-GlcNAc-R-alpha 2,8-sialyltransferase
Stac3:	SH3 and cysteine-rich domain-containing protein 3
Staf2l1:	Stefin-2
Staf3:	Stefin-3
Stfa1:	Stefin-1
Stip1:	Stress-induced-phosphoprotein 1
Stk:	Serine/threonine-protein kinase
Strip:	Striatin-interacting protein
Stt3a:	Dolichyl-diphosphooligosaccharide--protein glycosyltransferase subunit STT3A
Stt3b:	Dolichyl-diphosphooligosaccharide--protein glycosyltransferase subunit STT3B
Suds3:	Sin3 histone deacetylase corepressor complex component SDS3
Sun2:	SUN domain-containing protein 2
Syk:	Tyrosine-protein kinase SYK
Sync:	Syncoilin
SYNM:	Synemin
Sypl2:	Synaptophysin-like protein 2
Taf1:	TATA box-binding protein-associated factor RNA polymerase I subunit
Taf6l:	TAF6-like RNA polymerase II p300

Tatdn1:	Putative deoxyribonuclease TATDN1
Tbl1x:	F-box-like/WD repeat-containing protein TBL1X
Tbp:	TATA-box-binding protein
Tcap:	Telethonin
TELO2:	Telomere maintenance 2
Tfam:	Transcription factor A, mitochondrial
Tgm1:	Protein-glutamine gamma-glutamyltransferase K
Tigd:	Tigger transposable element derived 3
Timp:	Metalloproteinase inhibitor
Tln1:	Talin-1
Tnnc2:	Troponin C, skeletal muscle
Tnni1:	Troponin I, slow skeletal muscle
Tnni2:	Troponin I, fast skeletal muscle
Tnni3:	Troponin I
Tnni3:	Troponin I, cardiac muscle
Tnnt2:	Troponin T, cardiac muscle
Tnnt3:	Troponin T, fast skeletal muscle
Tnr:	Tenascin-R
Topbp1:	DNA topoisomerase 2-binding protein 1
Tpm1:	Tropomyosin alpha-1 chain
Tpm2:	Tropomyosin beta chain
Tpm4:	Tropomyosin alpha-4 chain
Tpt1:	Translationally controlled tumor protein
Trdn:	Triadin
Trim:	Tripartite motif-containing
Trim54:	Tripartite motif-containing protein 54
Trip12:	E3 ubiquitin-protein ligase TRIP12

Trp53: Cellular tumor antigen p53

Trp53inp1: Tumor protein p53-inducible nuclear protein 1

Trp63: Tumor protein 63

Trpc3: Short transient receptor potential channel 3

Trtr: Transthyretin

Tsc22d3: TSC22 domain family protein 3

Tspyl5: Testis-specific Y-encoded-like protein 5

Ttf1: Transcription termination factor 1

Ttll3: Tubulin monoglycylase TTLL3

Ttn: Titin

Ttr: Transthyretin

Tubb3: Tubulin beta-3 chain

Tusc3: Tumor suppressor candidate 3

U2af2: Splicing factor U2AF 65 kDa subunit

Uba: SUMO-activating enzyme subunit

Ube2: Ubiquitin-conjugating enzyme E2 B

Ube2a: Ubiquitin-conjugating enzyme E2 A

Ube2o: (E3-independent) E2 ubiquitin-conjugating enzyme UBE2O

Ube2u: Ubiquitin-conjugating enzyme E2U

Ube2z: Ubiquitin-conjugating enzyme E2 Z

Ubn: Ubinuclein

Ubr: E3 ubiquitin-protein ligase UBR

Ugp2: UTP--glucose-1-phosphate uridylyltransferase

Ugt1a6b: UDP-glucuronosyltransferase

Ugt1a7c: UDP-glucuronosyltransferase 1-7C

Ugt2b1: UDP-glucuronosyltransferase

Utp6: U3 small nucleolar RNA-associated protein 6 homolog

Vcan:	Versican core protein
Vcl:	Vinculin
Vim:	Vimentin
Vps:	Vacuolar protein sorting-associated protein
Vta1:	Vacuolar protein sorting-associated protein VTA1 homolog
Vtn:	Vitronectin
Wasl:	Neural Wiskott-Aldrich syndrome protein
Wdr:	WD repeat-containing protein
Wrb:	Tail-anchored protein insertion receptor WRB
Wrn:	Werner syndrome ATP-dependent helicase homolog
Wwtr1:	WW domain-containing transcription regulator protein 1
Xkr6:	XK-related protein 6
Zc3h12c:	Probable ribonuclease ZC3H12C
Zcrb1:	Zinc finger CCHC-type and RNA binding motif 1
Zfr:	Zinc finger RNA-binding protein
Zw10:	Centromere/kinetochore protein zw10 homolog